ABSTRACT

Title of Document:	A HIERARCHICAL FRAMEWORK FOR STATISTICAL MODEL VALIDATION OF ENGINEERED SYSTEMS.
	Byungchang Jung, Doctor of Philosophy, 2011
Directed By:	Dr. Byeng D. Youn
	Assistant Professor, Department of Mechanical Engineering

As the role of computational models has increased, the accuracy of computational results has been of great concern to engineering decision-makers. To address a growing concern about the predictive capability of the computational models, this dissertation proposed a generic model validation framework with four research objectives as: Objective 1 — to develop a hierarchical framework for statistical model validation that is applicable to various computational models of engineered products (or systems); Objective 2 — to advance a model calibration technique that can facilitate to improve predictive capability of computational models in a statistical manner; Objective 3 — to build a validity check engine of a computational model

with limited experimental data; and Objective 4 — to demonstrate the feasibility and effectiveness of the proposed validation framework with five engineering problems requiring different experimental resources and predictive computational models: (a) cellular phone, (b) tire tread block, (c) thermal challenge problem, (d) constrained-layer damping structure and (e) energy harvesting device.

The validation framework consists of three activities: validation planning (top-down), validation execution (bottom-up) and virtual qualification. The validation planning activity requires knowledge about physics-of-failure (PoF) mechanisms and/or system performances of interest. The knowledge facilitates to decompose an engineered system into subsystems and/or components such that PoF mechanisms or system performances of interest can be decomposed accordingly. The validation planning activity takes a top-down approach and identifies vital tests and predictive computational models of which contain both known and unknown model input variable(s). On the other hand, the validation execution activity takes a bottom-up approach, which improves the predictive capability of the computational models from the lowest level to the highest using the statistical calibration technique. This technique compares experimental results with predicted ones from the computational model to determine the best statistical distributions of unknown random variables while maximizing the likelihood function. As the predictive capability of a computational model at a lower hierarchical level is improved, this enhanced model can be fused into the model at a higher hierarchical level. The validation execution activity is then continued for the model at the higher hierarchical level. After the statistical model calibration, a validity of the calibrated model should be assessed;

therefore, a hypothesis test for validity check method was developed to measure and evaluate the degree of mismatch between predicted and observed results while considering the uncertainty caused by limited experimental data. Should the model become valid, the virtual qualification can be executed in a statistical sense for new product developments. With five case studies, this dissertation demonstrates that the validation framework is applicable to diverse classes of engineering problems for improving the predictive capability of the computational models, assessing the fidelity of the computational models, and assisting rational decision making on new design alternatives in the product development process.

A HIERARCHICAL FRAMEWORK FOR STATISTICAL MODEL VALIDATION
OF ENGINEERED SYSTEMS

By

Byungchang Jung

Dissertation submitted to the Faculty of the Graduate School of the
University of Maryland, College Park, in partial fulfillment
of the requirements for the degree of
Doctor of Philosophy
2011

Advisory Committee:

Assistant Professor Byeng D. Youn, Chair, Advisor

Professor Bongtae Han, Co-advisor
Associate Professor Jeffrey Herrmann
Associate Professor Linda Schmidt
Professor Rance Cleaveland

Acknowledgements

Throughout my PhD study I have had many opportunities to collaborate with a wide range of people. These interactions have been the most rewarding part of my research. Although I cannot possibly thank everyone individually in writing, I would like to express my gratitude to a few of them who have been particularly helpful and inspiring.

I would first and foremost like to express my deep and sincere thanks to my advisor, Dr. Byeng D. Youn, with a deep sense of gratitude. He patiently guided me through my PhD studies, continuously challenging me to set my sights higher and never accepting less than my best efforts. This thesis would not have been possible without his wisdom, knowledge and commitment.

Next, I would like to express my deep gratitude to Dr. Bongtae Han who has graciously acted as a co-advisor on my thesis. I am extremely thankful for his support, encouragement and the direction that he has provided during my study. I am also indebted to all my dissertation committee members, Dr. Linda Schmidt, Dr. Jeffrey Herrmann, and Dr. Rance Cleaveland. Their insightful guidance and valuable comments are indispensable to the accomplishment of this dissertation.

Third, I would like to express my deepest thanks to my lab mates, Dr. Soobum Lee, Dr. Zhimin Xi, Dr. Pingfeng Wang, Dr. Chao Hu, and Ms. Lulu Wang, for their lively discussion and support whenever I was in need. Innumerous days and nights with them in the lab has made my time in graduate school a very enjoyable one. I also would like to express my sincere thanks to Mr. Moonhwan Chang and other

members of Korean Graduate Students Organization in mechanical engineering for their help and friendship during my PhD.

Finally, I wish to extend my special and sincere thanks to my parents, a sister and a brother for their constant love, support and confidence in me. My most heartfelt thanks go to my fiancé, Soyoung. For her unwavering love, and encouragement, I will be always in debt.

Table of Contents

List of Tables

List of Figures

x

Nomenclature

a_0	=	*material parameter of a fractional derivative model*
a_1	=	*material parameter of a fractional derivative model*
$\mathbf{b}$	=	*design variable vector*
b_1	=	*length of constraining layer in top & bottom panels*
b_2	=	*thickness of a damping layer*
b_3	=	*thickness of a constraining layer*
b_4	=	*length of constraining layer in left & right panels*
c	=	*speed of sound*
c_1	=	*material parameter of a fractional derivative model*
D	=	*critical value*
D_z	=	*electric displacement tensor*
d	=	*piezoelectric matrix*
d_J	=	*joint area metric*
d_C	=	*cross entropy metric*
$\mathbf{E}$	=	*expectation operator*
E	=	*elastic modulus*
E_z	=	*electric field tensor*
E_1^*	=	*random complex modulus*
E^*	=	*complex modulus*
E'	=	*storage modulus*

E''	=	*loss modulus*
e	=	*prediction (model) error*
F	=	*cumulative distribution function*
f	=	*probability density function*
f_c	=	*frequency*
$f_c a$	=	*reduced frequency*
G	=	*constraint function*
G^t	=	*target constraint value*
H_0	=	*null hypothesis*
H_1	=	*thickness of a damping layer*
H_2	=	*thickness of a constraining layer*
i	=	*number of experimental data*
$\mathbf{K}$	=	*global stiffness matrix of a beam FE model*
k	=	*thermal conductivity*
L	=	*likelihood function*
L	=	*length of solid slab*
$\mathbf{M}$	=	*global mass matrix of a beam FE model*
N	=	*number of random variables*
p	=	*probability*
p_f	=	*marginal failure probability*
p_0	=	*sea-level standard atmospheric pressure*
q	=	*heat flux in a thermal challenge problem*

R	=	specific gas constant
R^t	=	target reliability value
r	=	radiated power from the structure
S	=	cumulative distribution function of samples
$S*$	=	strain tensor
s^E	=	strain compliance matrix
T	=	temperature
$T*$	=	stress tensor
T_f	=	marginal temperature
U_m	=	area metric
$\mathbf{u}$	=	complex eigenvector of a beam FE model
u	=	cumulative density
w	=	density of damping and constraining layers
$\mathbf{X}$	=	Known model variable vector
Y	=	Observed (experimental) response
$\hat{Y}$	=	Predicted (simulated) response
$\mathbf{y}$	=	random response vector
y	=	component of a random response (or experiment)
$\mathbf{Z}$	=	augmented variable vector
α	=	significance level
$\alpha(T)$	=	shift factor
β	=	material parameter of a fractional derivative model

γ	=	correlation coefficient
δ	=	random field
ε	=	observation (experimental) error
ε^T	=	permittivity matrix
$\tilde{\varepsilon}$	=	strain
ε_E^*	=	error in a complex modulus
ζ	=	controllable variable
ζ^c	=	sound pressure
η_k	=	modal loss factor of the k-th mode of a beam FE model
$\mathbf{\Theta}$	=	calibration parameter vector
$\mathbf{\theta}$	=	Unknown model variable vector
λ^c	=	complex eigenvalue of a beam FE model
μ	=	mean
μ_f	=	friction coefficient
ν	=	coefficient of important signature in random field
ξ	=	parameter of a regression model
ξ_t	=	width of beam structure
Π	=	performance function of structural-acoustic system
ρ	=	density
ρC_p	=	volumetric heat capacity
ς	=	mechanical damping ratio
$\tilde{\sigma}$	=	stress

σ	=	*standard deviation*
υ	=	*pressure exponential parameter*
Φ	=	*objective function*
ϕ	=	*significnat signature in random field*
φ	=	*contact pressure*
ψ_k	=	*natural frequency of the k-th mode of beam FE model*
Ω	=	*length of a constrained-layer*

Abbreviations

C

CDF: Cumulative Distribution Function

D

DDO: Deterministic Design Optimization

DoI: Degree of Invalid

E

EDR: Eigenvector Dimension Reduction

EH: Energy Harvesting

F

FE: Finite Element

G

GoF: Goodness-of-fit

I

IC: Integrated Circuit

M

MCS: Monte Carlo Simulation

P

PDF: Probability Density Function

PoF: Physics of Failure

PoI: Performance of Interest

R

RBDO: Reliability-based Design Optimization

U

UP: Uncertainty Propagation

V

V&V: Verification and Validation

Chapter 1: Introduction

1.1 Background and Motivation

Technological advances and increasing customer expectations have resulted in new products appearing on the market at an ever-increasing pace. In a traditional product development process, repeated activities of prototyping and testing bring a product closer to a final specification by improving its performance and reliability. This cost-intensive, time-consuming product development process, however, can be a barrier to speed, a key factor in a competitive market environment. As engineered products become more complex and the product life-cycles get shorter, virtual testing has become more important for cost-effective product evaluation and design. Figure 1 shows the role of virtual product testing in the product development process.

Virtual testing can reduce required tests and save time and cost on product development. A grand challenge is to build reliable computational models with high accuracy (or predictive capability). Model validation is thus essential for development of computational models with high accuracy [1]. However, although there is increasing consistency in the formal definition of the model-validation process, there is still open discussion about the steps of the process, which can vary depending on the nature of engineering problems. This can be explained with the following four primary reasons. First, computational models become invalid due to various sources of variability and/or uncertainty in manufacturing tolerances, operational conditions, material properties, and experimental error. However, there is no model validation framework that accounts for the sources of variability and/or

uncertainty. Second, the sources of variability and/or uncertainty are not well understood due to limited resources (e.g., time, budget, facility). Therefore their statistical models are unknown. Third, experiments required for the validity evaluation of a computational model are limited. The proposed dissertation research is thus designed to develop a generic framework for statistical model validation that tackles the addressed challenges aforementioned.
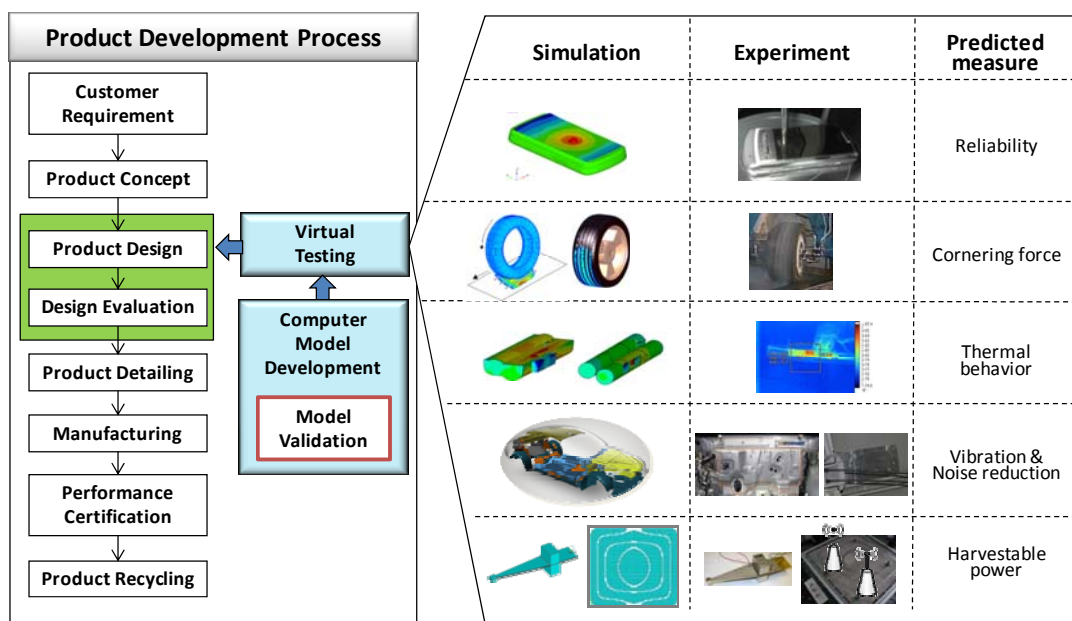
Fig. 1. Virtual testing in a product development process

1.2 Research Objectives and Scopes

The proposed research involves four research objectives as below.

<u>Objective 1 – A generic framework development for statistical model validation</u>

This framework facilitates dealing with different sources of variability and/or uncertainty in a computational model. The framework will be formed with three activities: (1) top-down model validation planning, (2) bottom-up model validation

2

execution and (3) virtual qualification. Specific techniques and guidelines are also proposed for each activity.

Objective 2 – Integration of a statistical approach to model calibration and validation

Model calibration is an essential step in an overall validation process to improve the predictive capability of computational models. In a deterministic sense, model calibration involves the adjustment of a few model variables to maximize the agreement between the predicted (or computational) and observed (or experimental) outputs. However, the deterministic approach is not appropriate because it does not account for variability and/or uncertainty in mathematical and computational models, manufacturing processes, and operational conditions. A statistical approach must be developed to model the various sources of variability and/or uncertainty, to analyze the variability and/or uncertainty propagation (UP) through computational models, and to improve the predictive capability of the models through statistical calibration and validation. Advanced statistical techniques (e.g., uncertainty propagation, statistical calibration and validity check techniques) must be integrated with computational model calibration and validation.

Objective 3 – A validity check engine of a computational model

The validity check still remains a challenge in a two-fold sense. First, when few sets of experimental data are collected at different operating conditions, it is beneficial to integrate the evidence from all the observations into a single measure of overall mismatch. Second, the small sample size of experiments will produce another layer of uncertainty in a validity check metric, of which the effect on model validity must

be carefully understood. The hypothesis test for validity check is thus proposed to solve these challenges by considering the effect of limited experimental data.

1.3 Dissertation Overview

The dissertation is organized as follows. Chapter 2 reviews the current state of knowledge in the related research topics including model verification, model validation, model calibration and uncertainty propagation analysis. Chapter 3 presents the proposed researches with three research thrusts as (1) a hierarchical framework for statistical model validation, (2) an advanced technique for statistical model calibration, and (3) a hypothesis test method for validity check. In Chapter 4, five engineering problems (cellular phone, tire tread block, thermal challenge problem, constrained-layer damping structure, and energy harvesting device) are employed to demonstrate the proposed validation framework and techniques. Finally, Chapter 5 discusses the contributions of this dissertation and potential future research directions. The challenges, objectives and expected benefits of the proposed researches are summarized in Table 1.

Table 1 Challenges, objectives and benefits of the proposed dissertation work

Challenges	• No generic framework for statistical model validation of engineered systems • Variability and/or uncertainty in a model validation process • Unknown random input variables in a computational model • Limited resources for validation experiments
Objectives	• Development of a generic framework for statistical model validation • Development of a technique for statistical model calibration • Development of a practical validity check engine • Feasibility demonstration of the proposed validation framework with various engineering problems
Expected benefits	• Standard guideline for statistical model validation with definitions, procedures, statistical techniques and case studies • Development of computational models with high accuracy by considering the sources of variability and/or uncertainty in a physical system • Practical solution of validity check that fully utilizes limited experimental data in determining fidelity of computational models • Increase of a confidence level on computational models and reduction of confliction between predicted and experimental results • Extended role of computational models in designing robust and reliable engineering products • Significant saving of cost and time in building valid computational models • Rational decision making on new design alternatives in the product development process

Chapter 2: Literature Review

This chapter provides the related state of knowledge of the research topics within the scope of this dissertation. The review is presented in the following five sections: In Sections 2.1 and 2.2, researches on model verification and validation (V&V) and statistical model calibration are reviewed. Section 2.3 presents the literatures of uncertainty propagation analysis. Finally, studies on constrained-layer damping structure and energy harvesting are summarized in Sections 2.4 and 2.5.

2.1 Model Verification and Validation

As the role of computational models has increased, the accuracy of the computational results becomes important to analysts who make decisions based on these predicted results. For decades, researchers have sought to improve the accuracy of computational models through the process of the model verification and validation (V&V), which helps ensure that the models accurately represent the real-world systems (or products). Among various works on model verification and validation (V&V), the survey articles that have been introduced by various engineering groups such as the American Institute of Aeronautics and Astronautics (AIAA) [1], the American Society of Mechanical Engineers (ASME) [2], the Department of Energy Laboratories (Sandia [3], Loss Alamos [4], and Lawrence Livermore [5]) and Institute for Computational Engineering and Sciences (ICES) [6] explain the state-of-the-art concepts, terminologies, processes and techniques on model in detail. In their works, the verification is briefly defined as the assessment of the accuracy of a computational model implementation; and, the validation is the assessment of the

accuracy of computational results by comparison with experimental data [1]. The important concepts for model V&V addressed in those references are summarized below.

- Model development

The processes of model V&V start from modeling of engineered systems. The ASME guideline [2] well described the three types of models in computational solid mechanics from general to specific: (1) conceptual model, (2) mathematical model, and (3) computational model. After identifying the physical system, the conceptual model, the collection of assumptions and descriptions of physical processes representing the mechanics behavior of the physical system, can be defined. With the conceptual model defined, analysts can define the mathematical model the mathematical equation, boundary and initial condition, and modeling data needed to describe the conceptual model. The computational model is the numerical implementation of the mathematical model, usually in the form of spatial/temporal discretization, numerical algorithm and convergence criteria. Generally, the results of the computational model are compared to available experimental data for model validation.

- Model verification

In ASME guideline [2], the model verification is defined as "the process of determining that a computational model accurately represents the underlying mathematical model and its solution". Figure 2 briefly shows the main components and activities in model V&V [4,7].
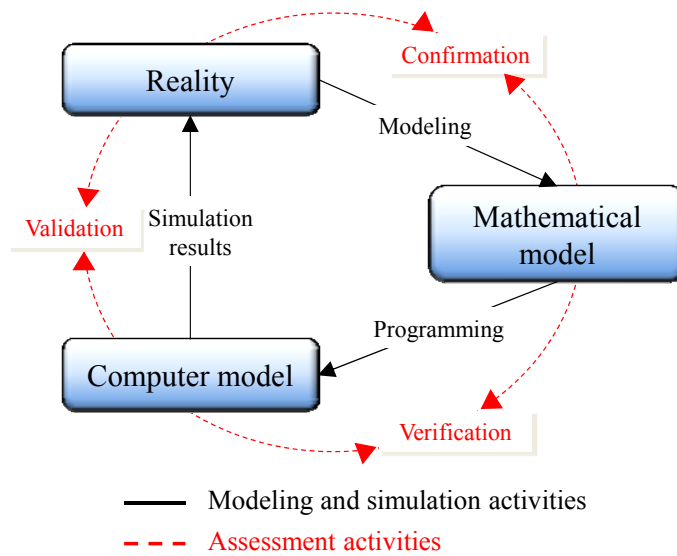
Fig. 2. Simplified view of the model V&V process

The verification deals with the relationship between the mathematical model and its programmed implementation in the code (the computational model). The verification is mainly conducted by comparing numerical solutions of the mathematical model to highly accurate benchmark solutions. The use of benchmark solutions in the verification is called "testing" in software engineering community [8]. The verification generally can be divided into two activities: (1) code verification and (2) calculation verification [3,9]. The major goal of the code verification is to confirm that the mathematical model (computer software) is working as intended. Two activities are usually considered for the code verification: (1) software quality assurance (SQA) and (2) numerical algorithm verification. The SQA activity identifies and eliminates programming and implementation errors within the mathematical model. The SQA activity ensures that the code is reliable (implemented correctly) and produces repeatable results on specified computer hardware, operating systems and compilers. The code developer should perform the

8

SQA by running all relevant verification problems provided with the software using configuration management and static (or dynamic) software quality testing. The numerical algorithm verification concerns the correctness of the numerical algorithms that are implemented in the code [4]. In this activity, test problems with known (analytical) or highly accurate (benchmark) solutions are devised and compared to solutions obtained from the code. The calculation verification is to evaluate the accuracy of the discrete solution of the mathematical model by estimating the numerical errors due to discretization approximations. The insufficient spatial or temporal discretization, insufficient convergence tolerance, incorrect input options, and finite precision arithmetic can be identified using the calculation verification. It is relatively popular to perform code-to-code comparisons as a means of the calculation verification in the absence of sufficient verification evidence from other sources.

- Model validation

As shown in Fig. 2, the model validation deals with the relationship between the computational results from the computational model and reality, i.e., experimental results. The model validation is defined as the process of determining the degree to which a model is an accurate representation of the real world from the perspective of the intended uses of the model [1,2]. The phrase "process of determining" emphasizes that the model validation is an on-going activity that concludes only when acceptable agreement between experiment and simulation is achieved. The phrase "degree to which" emphasizes that the simulation and the experimental results are uncertain. Finally, the phrase "intended uses of the model" emphasizes that the

validity of a model is defined over the domain of model form, input variables and predictive responses. In order to determine the degree of the validity quantitatively, a comparison between the experimental and computational results has to be performed with any validity check metric. Oberkampf et al. [10] developed a validity check metric based on the concept of statistical confidence intervals. Ferson et al. [11] used integrated area between the cumulative distribution functions (CDFs) of experimental and computational results as a validation measure, and Rebba et al. [12] used the distance metric based on the Anderson-Darling statistics.

- Model calibration

Different with a model validation activity which mainly assesses the confidence of computational results, model calibration is a process of maximizing the agreement of predicted results with respect to a set of experimental data through the adjustment of a set of physical input variables. In computational engineering society, model validation sometimes means an model calibration activity which involves the estimation or optimization of model input variables using experimental data from a system [7,13,14]. Oftentimes, model calibration may be a more appropriate process because of constraints in fiscal budgets and computer resources. However, the model calibration should be carefully exercised, because it directly impacts the confidences of the computational model. For the successful calibration, we should clearly understand the distinction between the calibration variable and tuning variable. The calibration variables have physically interpretable meaning; however, the tuning variable may be notional and of little or no meaning in the physical system.

- Uncertainty in model validation

Uncertainties in a computational model can be categorized as: (1) aleatory uncertainty, (2) epistemic uncertainty, and (3) prediction error [4]. The aleatory uncertainty (i.e., variability, inherent uncertainty), which always exists in physical systems, arises from an inherent randomness in an engineered system. The knowledge of experts cannot be expected to reduce this uncertainty although their knowledge may be useful in quantifying the uncertainty [15]. Thus, this type of uncertainty is sometimes referred to as irreducible uncertainty. Examples include variations in geometric or material properties, loading environment and assembly procedures. The epistemic uncertainty (i.e., reducible uncertainty) derives from a lack of knowledge about the true value of the model input variable. Obtaining more information will decrease the epistemic uncertainty and allow a better estimate of the true distribution; therefore, expert judgments may be useful in its reduction. Last, the prediction error creates a reproducible (i.e. deterministic) bias in the prediction and can be acknowledged (detected) or unacknowledged (undetected). Examples include inaccurate model form, physical parameters, implementation errors in the computational code and non-converged computational models.

- Key principles for the successful model validation

Important principles addressed several times in the references above are summarized below. These principles should be considered to build a valid computational model in the model validation process.

(1) Verification must precede validation.

(2) Validation is specific to a particular computational model for a particular intended use.

(3) An understanding of the variability (and uncertainty) sources in both simulation and experimental results is important for the success of model validation

(4) Independence between analysts and experimentalist should be maintained in obtaining both the predictive and experiment results. For example, the experimental results should not be revealed to the analysts until they have completed the simulations results. When experimental results are available to the analysts prior to establishing their simulation results, the human tendency is to 'tune' the model to the experimental results to produce a favorable comparison. This tendency decreases the level of confidence in the computational model to predict.

(5) The model validation requires close cooperation among analysts and experimentalists to make the mathematical and physical models consistent during the validation activities. Collaboration and shared expertise between researchers in industry/academia and simulation/experiment is another key to make the predictive model feasible.

- Validation challenge workshop

In the Validation Challenge Workshop [16] sponsored by the Sandia National Laboratory, many researchers suggested the state of the art approaches for the model calibration and validation, and applied their approaches to one of the devised three problems: (1) thermal challenge problem in the field of heat transfer [11, 16-22], (2) static frame problem [12,23,27], and (3) structural dynamics challenge problem [28-33]. Researchers utilized various technical approaches in solving the problems such

as Bayesian analysis, statistical inference, bootstrapping, Monte Carlo sampling, worst case scenario approach, etc. For the thermal challenge problem, some of the works purely focused on the model calibration and a prediction of the failure probability with the updated model, while others study validity of the computational model without the model calibration. The Bayesian calibration [34] is followed to calibrate the model parameters in Ref. [20,21]. A normal Markov Chain Monte Carlo and modular Markov Chain Monte Carlo are used to obtain posterior distribution. Xiong et al. [35] developed a maximum likelihood estimation approach for the model calibration with different formulations. Ferson et al. [11] developed the u-pooling method for the validation of thermal challenge problem. Hills et al. [19] use the first-order sensitivity analysis to account for model parameter uncertainty. For the static frame problem, the material property (the elastic modulus) was characterized using random field process. The marginal distribution for the material property was estimated by either parametric or non-parametric procedure. Pradlwarter et al. [27] and Rebba et al. [12] employed kernel density estimates and Polynomial Chaos expansion to approximate the marginal distribution, respectively. For the structural dynamics challenge problem, the model calibration mainly involved the usage of Karhunen-Loeve expansion. The stochastic term in the Karhunen-Loeve expansion are modeled using the Gaussian and log-normal distribution [22,31], polynomial chaos expansion [29], kernel density estimator [27,31,32], and empirical cumulative density function [22].

2.2 Statistical Model Calibration

To improve the predictive capability of a computational model, model calibration techniques have been developed in recent years. Model calibration adjusts a set of unknown model input variables associated with a computational model so that the agreement is maximized between the predicted (or simulated) and observed (or experimental) responses (or outputs). In a deterministic sense, model calibration is thought of as the adjustment of a few model input variables to minimize the discrepancy between the predicted and observed results. However, the deterministic approach is not appropriate since various uncertainties exist in material properties, loading condition, boundary condition, etc. Statistical model calibration, on the contrary, means refining the probability distributions of unknown input variables through comparison of the predicted and observed outputs [34]. Current statistical model calibration is mainly based on methods of moments [36], Bayesian statistics [18,20,25,37,40] and maximum likelihood estimation [35,41]. Statistical model calibration with Bayesian statics mainly focuses on the surrogate model (also called metamodel [42]), which replaces expensive computational models of engineered systems. In the computational engineering, it is common for computational models to take hours or days to run. For example, the finite element (FE) tire simulation may take days to execute a single run to predict the cornering or braking performance [13]. Because it generally becomes impossible to conduct enough simulation runs to thoroughly cover the entire input variable space for the design purpose, surrogate models such as polynomial function [43] and kriging model [44] have been developed with design of experiment techniques [45]. The drawback of simply using a fitted

14

metamodel is that it may ignore metamodel uncertainty, i.e., the uncertainty that results from not knowing the output of the expensive computational model except at a finite set of sampling points. One of the most popular approaches developed to solve this drawback is the response surface approximation approach using Gaussian process [46,47]. In that approach, the response surface is viewed as a realization of a Gaussian random process (GRB), and Bayesian methods are used to interpolate/extrapolate the response surface by calculating its posterior distribution given the sampling sites. Kennedy and O'Hagan [37] proposed the inferential ideas behind statistical model calibration with Bayesian statistics using Gaussian process model. They formulate a model for calibration that includes an observation (experimental) error term and a model discrepancy function. Both the observation error term and the model discrepancy function are also represented by a Gaussian process model. After that, they use a Bayesian approach to obtain a "posterior" estimate of the statistical parameters associated with the model input variables and model discrepancy function. Here the purpose of Bayesian updating is to reduce uncertainty in the parameters through the experimental data. In Bayesian approach, initial lack of knowledge of the unknown model parameters is represented by assigning prior distributions, and this lack of knowledge is revised by calibrating their distributions based on the experimental data through Bayesian analysis. One limitation of the Bayesian approach is that the calibration parameters are assumed to remain fixed, but unknown due to lack of knowledge. However, in reality, model input variables vary randomly due to manufacturing variation, variation in raw materials, variation in environmental or use conditions, etc. Another limitation of

Bayesian approach is that for complex engineered systems, Bayesian approach requires a large amount of computational efforts to update the parameters in the Gaussian process model [37]. In spite of these limitations, the Bayesian approach may be advantageous when very few experimental data are available, especially when a good prior knowledge is available to assign the informative prior distributions for model parameters. Youn et al. [48] and Xiong et al. [35] applied maximum likelihood based model calibration approach to the thermal challenge problem, and compared this approach with Bayesian model calibration approach. In contrast to Bayesian approach, the maximum likelihood based approach treats parameters as intrinsic random and estimates their distributional properties by comparing the simulation results with the experimental data.

2.3 Uncertainty Propagation Analysis

Uncertainty propagation (UP) analysis is an essential part of statistical model calibration. UP analysis refers to the determination of the uncertainty in analysis results that is propagated from uncertainties in the input variables of a computational model that arise because of the inherent randomness in physical systems (material properties, boundary condition, etc.), modeling idealizations, experimental variability, measurement inaccuracy and manufacturing tolerance. Existing UP analysis methods can be categorized into the four categories as: (1) the sampling method, (2) the expansion method, (3) the metamodeling method, and (4) the approximate integration method.

(1) The sampling method: The sampling method is the most comprehensive but expensive method to use for estimating moments and reliability of system responses.

16

It is often used to verify a probability density function (PDF) of system responses when alternative UP methods are employed. The sampling methods draw samples from the input parameter populations, evaluate the deterministic model using these samples, and then build a probability density function (PDF) of the responses. Monte Carlo Simulation (MCS) [49,50] is the most widely used sampling method but demands thousands of computational analyses. To relieve the computational burden, other sampling methods have been developed, such as quasi-MCS [51], importance sampling [52] and directional sampling [53].

(2) The expansion method: The expansion method is to estimate statistical moments of system responses with a small perturbation to simulate input uncertainty. This expansion method includes Taylor expansion [54], perturbation method [55], Neumann expansion method [56], etc. Taylor expansion and perturbation methods require high-order partial sensitivities to maintain good accuracy. The Neumann expansion method employs Neumann series expansion of the inverse of random matrices, which requires an enormous amount of computational effort. In summary, all expansion methods could become computationally inefficient or inaccurate when the number or the degree of input uncertainty is high. Moreover, since it requires high-order partial sensitivities of system responses, it may not be practical for large-scale engineering applications.

(3) The metamodeling method: There currently exist a number of metamodeling techniques, such as polynomial response surface model (PRSM), multivariate adaptive regression spline (MARS), radial basis function (RBF), kriging, neural networks, and support vector regression (SVR). Each technique has its own fitting

method. For example, PRSM are usually fitted with the (moving) least square method [45] and the kriging method is fitted with the search for the best linear unbiased predictor [57]. All of these techniques are capable of function approximation with different accuracy, robustness and computational efficiency levels. PRSM are not suitable for high dimensional problems because of a curse of dimensionality. MARS constructs response surface from a set of coefficients and basis functions from the regression data, which makes it suitable for problems with high input dimensions [58]. However, it normally cannot produce accurate results for nonlinear problems [59]. RBF is useful for multivariate scattered data interpolation [60]. However, it is unable to interpolate large sets of data in an efficient and numerically stable way and maintain a good level of accuracy at the same time [61]. In general the kriging models can produce accurate results for nonlinear problems but difficult to obtain and use because a global optimization process is applied to identify the maximum likelihood estimators [59]. Although neural networks are able to approximate very complex models well, they have the two disadvantages: (1) being a "black box" approach, and (2) having a computationally expensive training process [62]. It is well known that the accuracy of SVR depends on a good setting of meta-parameters and the kernel parameters where optimal parameter selection is complicated [63].

(4) The approximate integration method: The approximate integration method is a direct approach to estimate the probability density function (PDF) or statistical moments through numerical integration. Numerical integration can be done in the input uncertainty domain [64] or the output uncertainty domain [65]. Recently, the

18

dimension reduction method [64] has been proposed and is known to be a sensitivity-free method. In the univariate dimension reduction method, it uses an additive decomposition of the responses that simplifies one multi-dimensional integration to multiple one-dimensional integrations. Generally, it can provide accurate lower moment of system responses such as mean. However, it may produce a relatively large error for the second-order or higher moments of nonlinear system responses. In the general dimension reduction method [66], the theoretical error of univariate dimension reduction method can be reduced by considering multi-dimensional integrations. However, the computation effort is increased exponentially.

2.4 Constrained-layer Damping Structure

Adding a viscoelastic damping material to a structural surface is a typical way to reduce noise and vibration of structures [67]. For example, damping sheets on the body of passenger cars reduce noise and vibration in the cabin. Damping materials are also used in airplanes, launching vehicles, ships, and electric appliances. In these applications, it is important to optimize the layout and optimal location of the unconstrained/constrained-layer damping material to reduce vibration and noise of structures effectively. However, it is difficult to obtain a robust damping layout design, since the viscoelastic damping material possesses frequency- and temperature-dependent dynamic responses. In most cases surface damping treatments are exposed to an open air, so the damping material experiences a wide range of temperatures, which vary periodically and randomly. As a result, substantial variations in the damping material properties can be observed in the service life of the material and are expected to reduce the quality of damping performance against noise

and vibration. On the other hand, test data inherently contain experimental errors (e.g., experimental noise and measurement errors) due to difficulty in measuring the dynamic responses of the viscoelastic damping material. For example, the loss factor which is one of the material properties is highly sensitive to the boundary conditions of a measurement apparatus, resulting in significant experimental error. The loss factor estimation is known to be the least accurate among the modal parameters of a structure [68].

Many researchers have suggested different optimal design formulations for damping layout of structures [69-76]. These studies have primarily focused on designing a constrained-layer damping layout to maximize damping efficiency. Lee et al. proposed design optimization methods for constrained/unconstrained-layer damping layouts in structural noise and vibration problems, in which the frequency- and temperature-dependent dynamic responses of the viscoelastic damping material were considered [77,78]. In these works [69-78], the optimal damping layouts were obtained with no consideration of temperature variation and damping material uncertainty. Only a few researchers have acknowledged the importance of these factors to random damping characteristics in structural dynamic problems [79-82].

2.5 Energy Harvesting

The continual advances in wireless technology and low power electronics have allowed the deployment of small remote sensor networks for various applications including building automation, smart factory, structural health monitoring, environmental monitoring, and body area network. Current wireless devices must be designed to include electrochemical batteries as the power source. But the use of the

batteries can be troublesome due to their limited lifespan, especially when the replacement for inaccessible and remote location is required. Furthermore, the battery replacement costs \$80~\$500 including labor and it exceeds the price of a sensor [83]. This issue has initiated the rapid growth of the energy harvesting field as an ultimate solution to prolong the battery life or, ideally, eliminate the need of batteries for wireless sensors. The energy harvesting (EH) devices harvests electrical energy from the ambient energy sources surrounding the electronics such as sunlight, thermal gradient, human motion and body heat, vibration, and ambient RF energy [84,85]. While each of these sources of energy can be effectively used to power remote sensors, vibration energy has gained much attention due to its widespread availability.

Mechanical vibration energy can be converted to electrical energy using electrostatic, electromagnetic, or piezoelectric energy conversion. Among them, piezoelectricity is the ability of some materials to generate an electric potential in response to applied mechanical stress, and its energy conversion can be said to combine most of the advantages of both electromagnetic and electrostatic converters [86]. It has been studied to compare piezoelectric, electromagnetic, and electrostatic configurations as a means of harvesting energy from a variety of vibration sources. This study showed that piezoelectric material is the simplest and most practical way of conversion [87,89]. Piezoelectric material includes PZT (Lead zirconate titanate), ZnO (Zinc oxide), and PVDF (Polyvinylidene Difluoride), and PZT is known to possess the best conversion efficiency among them [89].

A typical energy harvesting (EH) device using piezoelectricity is a cantilever unimorph/bimorh and it generates AC voltage proportional to bending strain of the piezoelectric material. Glynne-Jones et al. [87] screen-printed PZT on a stainless steel plate to get power of 3W. Leland et al. manufactured a piezoelectric EH using PZT-5A4E, brass, and a mass made of tungsten [90]. They generated the power of 29.3W using vibration from human walking for 50 minutes. Roundy et al. manufactured a cantilever energy harvester using PZT and PVDF and performed design optimization to obtain high power output with the change of mass, length of cantilever beam, piezoelectric material thickness, and external resistance value [91]. Sodano et al. formulated a model of an energy harvesting system that consists of a cantilever beam with piezoelectric patches attached and experimentally verified it [92]. Chen et al. proposed the relationship between the deduced voltage and the mechanical strain in a cantilever bimorph micro transducer [93]. Elvin et al. [94] developed a self-powered damage detection unit for energy generation and storage using PVDF. The performance of the sensor was illustrated in terms of sensing and wirelessly communicating data about the damage state of a structure to a remote receiving unit.

The studies on the optimal shape of a cantilever energy harvester have been done and a rectangular and a trapezoidal shape of piezoelectric beam shape were mostly compared in terms of tolerable amplitude and output power under vibration, and a trapezoidal shape turned out to be more efficient because of a uniformly large strain at every point on the beam surface [87,95,96]. Zheng et al. suggested a topological optimum design to maximize energy conversion [97], but this design raised additional

manufacturing issue. The amount of power generated by piezoelectric EH devices has been evaluated in a number of researches. Umeda et al. conducted a study into the characteristics of energy storage by a Piezo-generator with a bridge rectifier and capacitor [98]. The piezo-generator consisted of a steel ball and a piezoelectric vibrator, a bridge rectifier and capacitor. To simulate the generation and storage mechanism they employed an equivalent circuit model, and showed that their prototype achieved a maximum efficiency of 35%. Sodano et al. studied the storage of electrical energy from energy harvesting devices in batteries and capacitors [99], and characterized a several commercial piezoelectric materials for energy harvesting applications [100,101]. Using EH devices developed above, some ambient vibration sources have been found and utilized for electric energy generation mainly from machinery and human movement (several vibration sources are well introduced in the references [86,96]). Granstrom et al. developed a piezoelectric polymer backpack strap which generated electrical energy from the oscillating tension in the strap during walking [102]. Leland et al. mounted an energy harvester on a wooden staircase and generated electricity from vibrations in the staircase to get around 30W [90]. Some case studies of energy harvesting from vehicle engine vibration and bridge vibration is found in a website [103]. Shoe-mounted energy harvester is another example of EH which utilized human movement; pressure by heel strikes [104,105].

The studies on the design of piezoelectric EH devices include the design of mechanical characteristics (shape, material, excitation, etc) and electric circuits. Some researchers have found that a trapezoidal cantilever shape is more efficient than a rectangular cantilever shape because of a uniformly large strain at every point on

the beam surface [87,95]. Shen et al. [108] experimentally compared the EH performance of three piezoelectric materials (PZT(Lead Zirconate Titanate), fiber, and polymer) and verified that PZT shows the best performance. Wideband vibration was considered for design of EH devices in [109-111]. Ottman et al. [112,113] studied the use of an adaptive step-down DC–DC converter to maximize the power output from a piezoelectric device. Recent researches on piezoelectric energy harvesting devices are well summarized in review articles [96,106,107].

Chapter 3: Proposed Research

3.1 Scope of Proposed Research

The objective of the research is to develop a generic framework for statistical model validation that facilitates to build computational models with highly predictive capability. The proposed research comprises of four research thrusts as: (1) a hierarchical framework for statistical model validation, (2) statistical model calibration, (3) hypothesis test for validity check and (4) feasibility demonstration of the proposed validation framework. Figure 3 summarizes the scope of the proposed research.
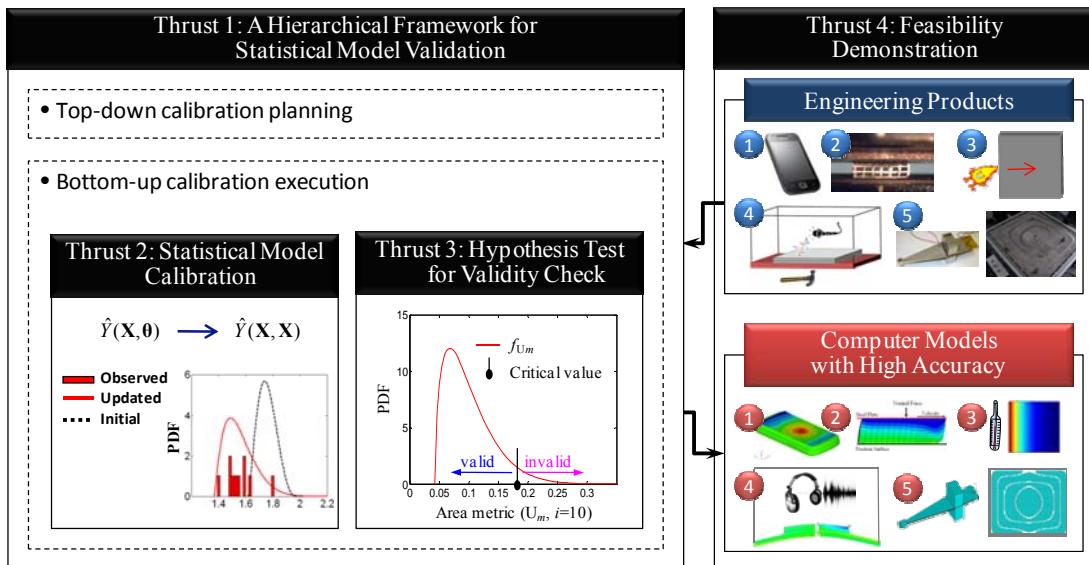
Fig. 3. The scope of the proposed research

Five engineering problems on the right box in Fig. 3 (cellular phone, tire tread block, thermal challenge problem, constrained-layer damping structure and energy harvesting device) are selected as case studies to demonstrate the feasibility of the proposed validation framework. Each engineering problem requires different

validation techniques depending on the characteristics of engineered systems, performances of interest (PoI), computational models (model form, input variable, and response), and experimental resources.

3.1.1 Thrust 1: A Hierarchical Framework for Statistical Model Validation

The objective of this research thrust is to develop a hierarchical framework for statistical model validation that will be conceptually defined with its formal procedure. The framework is composed of three model validation activities: (1) top-down model validation planning, (2) bottom-up model validation execution and (3) virtual qualification. In the model validation planning, engineers first define either the physics-of-failure (PoF) mechanisms or the performances of interest (PoI) of a system (or product). The system (top-level in a hierarchy) should be first decomposed into subsystems or components, of which valid computational models can predict behaviors of the PoF or PoI. Vital experiments and computational models along with both known and unknown model input variable(s) must be identified at each hierarchy. Subsequently, the model validation execution and virtual qualification will be planned. After the completion of the planning, the model validation execution takes a bottom-up approach. It consists of three tasks: (1) model variable characterization, (2) statistical model calibration, and (3) hypothesis test for validity check. Three tasks should be performed at any hierarchical level using the information of model input variables, computational models, and available experiments determined in the validation planning step. As the predictive model at a lower hierarchical level becomes valid, the valid model is fused into a model at a

higher hierarchical level. The validation execution is then continued for the model at the higher hierarchical level. If the computational model in a system level turns out to be valid, the virtual qualification will be triggered with the valid computational model of the system.

3.1.2 Thrust 2: Statistical Model Calibration

The objective of this research thrust is to develop an advanced technique of statistical model calibration. The technique can determine unknown model input variables by minimizing the discrepancy between predicted (or simulated) and observed (or experimental) results in a statistical sense. This research objective is attained by integrating the following techniques: (1) likelihood function as a calibration metric, (2) unconstrained optimization, (3) uncertainty propagation analysis.

3.1.3 Thrust 3: Hypothesis Test for Validity Check

The objective of this research thrust is to develop a method of assessing fidelity of a calibrated computational model in a statistical manner. This research objective can be attained by the proposed hypothesis test for validity check which evaluates null hypothesis—a calibrated model is valid—by comparing an area metric with a designated critical value. Type 1[1] and 2 errors[2] are employed to decide a rejection region which depends on the number of experimental data and degree of mismatch between predicted and experimental results. The null hypothesis can be rejected only

---

[1] Probability that we reject a computational model when it is valid

[2] Probability that we do not reject a computational model when it is invalid

when the area metric strongly suggests that the null hypothesis is false at an assigned significant level.

3.1.4 Thrust 4: Feasibility Demonstration

The objective of this research thrust is to demonstrate the procedure and feasibility of the proposed validation framework and techniques with five engineering products: (1) cellular phone, (2) tire tread block, (3) thermal challenge problem, (4) constrained-layer damping structure, and (5) energy harvesting device. To achieve this research objective, the computational models were carefully developed and investigated. Experimental data for the cellular phone, tire tread block and energy harvesting device were obtained with the assistance of experts in industry and academia. For the thermal challenge problem and constrained-layer damping structure, data and information from references were employed for the validation activity.

3.2 A Hierarchical Framework for Statistical Model Validation

A general model development process and the proposed model validation framework are explained in Sections 3.2.1 and 3.2.2, respectively.

3.2.1 Overview of Model Validation

Based on the model validation procedure proposed by the ASME Standard Committee [2] and Xiong et al. [35], the model validation activities has been devised with model calibration (or model updating), validity check and model refinement as depicted in Fig. 4.

In many engineering problems, especially if unknown model variables exist in a computational model, model improvement is a necessary step during the validation process to bring a model into better agreement with experimental responses. We can improve a model using two strategies: (1) to update the model through the model calibration and (2) to refine the model to change the model form.
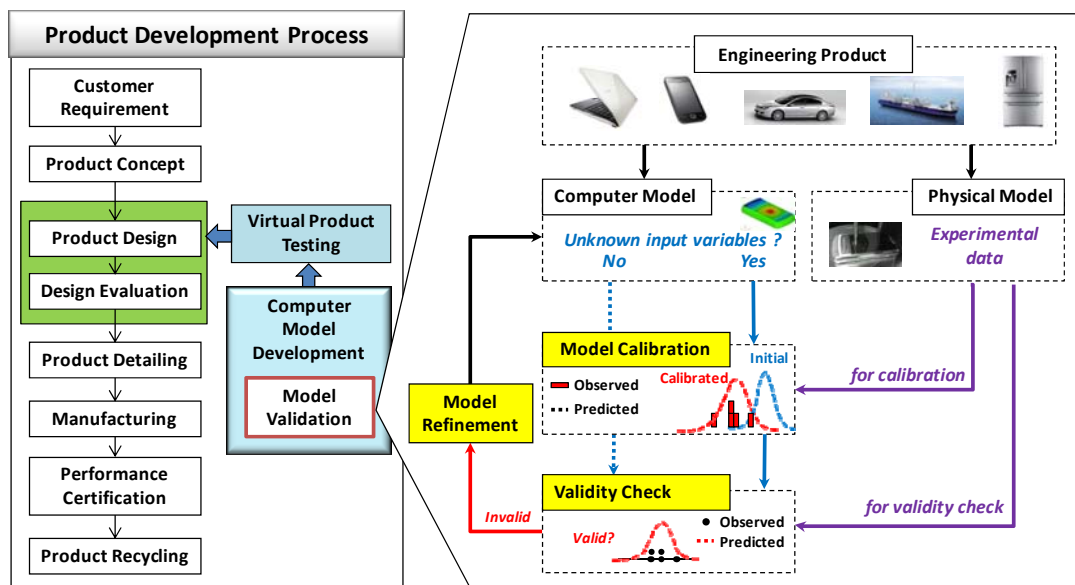
Fig. 4. Model validation procedure

Model calibration is the process of adjusting unknown model variables in the computational model to enhance the agreement with experimental data. Sensitivity analysis and optimization techniques can be employed to define critical unknown model variables and to calibrate the variables. The updated model must be validated with validation experimental data. This process is referred to as a validity check in this thesis. It is important to note that the experiments for model calibration should be designed and executed differently from the validation experiments, as shown in Fig. 4. The model should be refined if the agreement between experimental and simulation outcomes is unacceptable in the validity check. The feedback information

29

collected from sensitivity analysis, model calibration, and validity check should be used for model refinement. Model refinement can be applied to either the conceptual or mathematical model. This refinement reconsiders the physical process of system and changes the mathematical expressions to build a more realistic model that better represents the physics of the system. For example, model refinement can perform the following actions: (1) to reconsider the governing principles of physical system, subsystem or component of interest (e.g., a replacement of linear theory by a non-linear theory at the material, boundary and deformation sides), (2) to identify additional model variables, and (3) to refine a computational model with model verification activity (e.g., a removal of programming and implementation errors through Software Quality Assurance procedures, a verification of correctness of the numerical algorithms in the code through numerical algorithm verification, and an increase of mesh density through numerical error estimation). Extensive research on the model refinement (or model verification) is beyond the scope of this research, since it requires extensive consideration of the conceptual, mathematical, computational models, and software. Once the computational model is refined, the validation activities must be performed again as shown in Fig. 4. Generally, the model validation activity without model calibration (denoted in Fig. 4) is a desired approach because model refinement can fundamentally improve the predictive capability of a computational model and validity check with high-quality experimental data can confirm the accuracy of the computational results; however, the model refinement and validity check are often restricted by the available knowledge and resources (e.g., time, budget, man-power). Model calibration, on the

other hand, is a more practical and efficient method, so it is a more appropriate approach in industry. It is believed that the well-defined calibration planning and metric can help increase the predictive capability of the computational model. In this dissertation, the validation activity is thus defined as not merely a process of assessing the accuracy of a computational model, but also a process of improving the model accuracy through the model calibration. The statistical model calibration in Section 3.3, thus important, as well as practical, for the hierarchical model validation proposed.

Computational models of various engineered systems have different types of uncertain sources, random variables and predicted responses. For example, experimental data have inherent randomness in physical systems, measurement error, and statistical uncertainty due to the dearth of the data. Likewise, the responses of a computational model must be randomly represented as a result of inherent randomness in model parameters (e.g., material behavior, geometry and initial/loading/boundary conditions), model error (or prediction error), and statistical uncertainty. As explained in Section 2.3, uncertainties in a computational model can be categorized as aleatory uncertainty, epistemic uncertainty and prediction error. Aleatory uncertainty arises from inherent randomness in a system, and epistemic uncertainty stems from a lack of knowledge on a true value (e.g. lack of experimental data for variable quantification). The prediction error can be divided into a model error due to an inaccurate model form and an implementation error. Figure 5 summarizes techniques that tackle corresponding uncertain sources.

The variability of some model parameters can be characterized using experimental data, whereas the variability of the other variables cannot be estimated because explicitly related data do not exist. The former variables are referred to as known model variables, and the latter as unknown model variables. In addition, randomness is present in either a parametric form or a field (or process) form. Therefore, the random input variables in a computational model can be categorized as: (1) known random parameter variable, (2) unknown random parameter variable, (3) known random field variable, and (4) unknown random field variable as described in Fig. 6. The proposed validation framework provides a guideline to characterize all random variables with three techniques as shown in Fig. 6: (1) random parameter characterization, (2) random field characterization and (3) statistical model calibration.
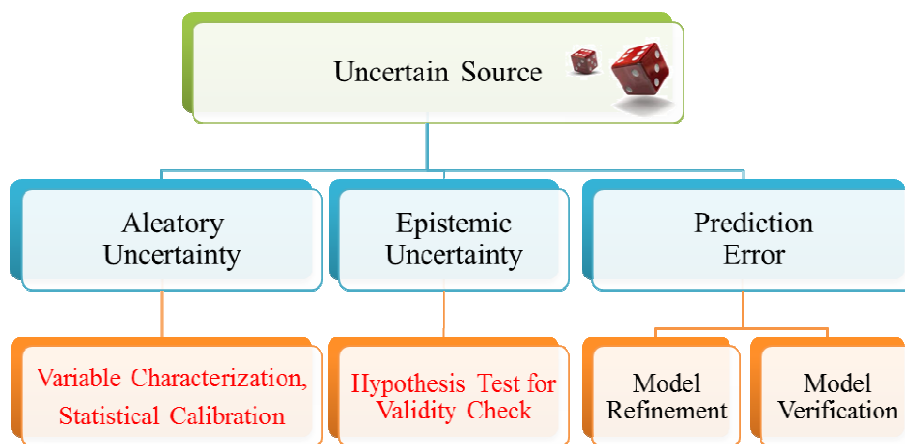
Fig. 5. Uncertain sources in a model and related validation activities
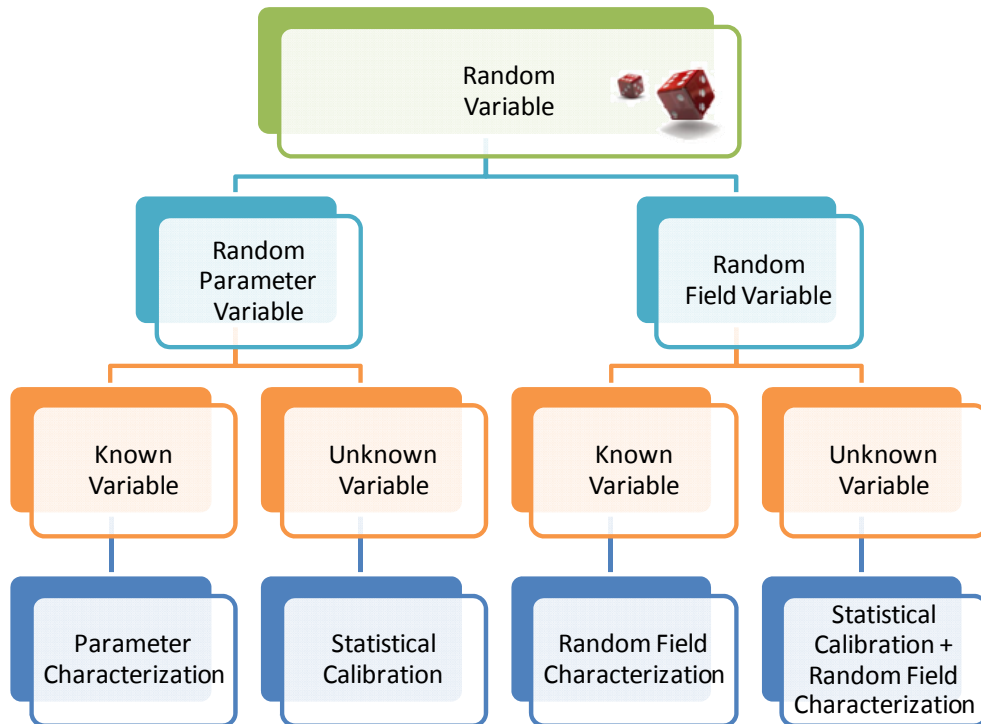
Fig. 6. Random variables in a model and related characterization technique

3.2.2 A Hierarchical Framework for Statistical Model Validation

Validating computational models of engineered products (or systems) is not trivial because the computational models contain many unknown model variables (e.g., material properties and boundary conditions). Model validation is even more difficult when the computational models involve more complicated mathematical formulations with many unknown model parameters. This difficulty underscores the need of a systematic approach to the computational model validation for an engineered system. This dissertation thus proposes a hierarchical framework for statistical model validation, which consists of three activities as shown in Fig. 7: (1) top-down model validation planning, (2) bottom-up model validation execution and (3) virtual

33

qualification. Details of the validation activities will be explained with a problem of a cellular phone system in the next subsections.
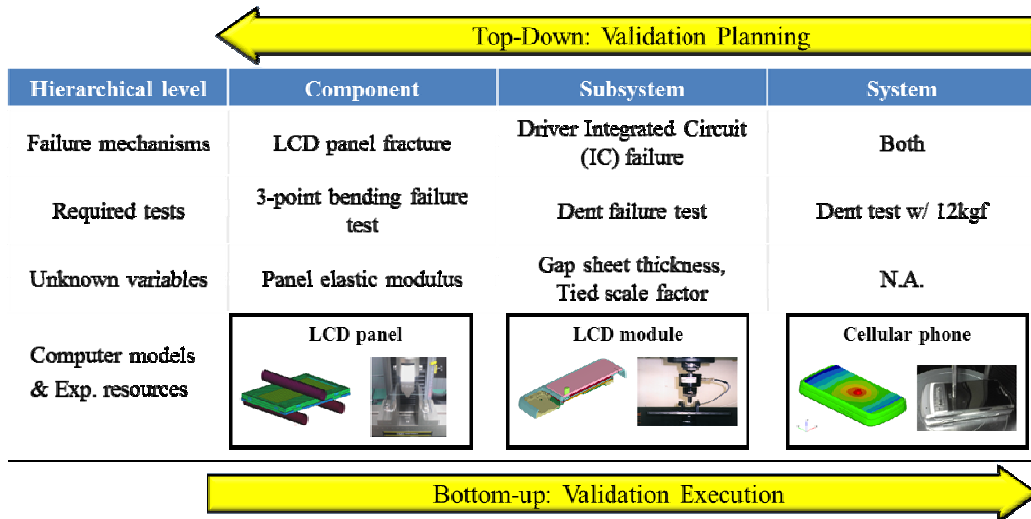
Fig. 7. The hierarchical model validation framework of cellular phone system

3.2.2.1 Model Validation Planning

The hierarchical model validation process begins with the model validation planning. The validation planning is a top-down activity. The planning is composed of three primary steps: (Step 1) the model decomposition planning, (Step 2) the model validation execution planning, and (Step 3) the virtual qualification planning.

(Step 1) Model decomposition planning: It includes system decomposition, resourcing and model variable classification. The first step is to define the Performance of Interests (PoIs) (or primary failure mechanisms) of an engineered system. Warranty reports or customer surveys are important for better understanding the PoIs (or primary failure mechanisms) of the system. Next, the system decomposition is planned based on ample understanding of the PoIs (or primary failure mechanisms) observed in the system (or top) level. A complex engineered

34

system will be physically divided into three, or more, progressively simpler tiers: subsystems and components. The available computational models and experimental resources should be summarized at each tier, and they are clearly defined and understood. Experts' opinion and available references helps identify vital computational models, experimental tests, and modeling details at any hierarchical level. Finally, the model input variables are defined, and unknown variable vectors are divided into $\boldsymbol{\theta}_{sy}$, $\boldsymbol{\theta}_{sb}$, and $\boldsymbol{\theta}_c$ as the system is decomposed into subsystems and, subsequently, components.

A predicted response given by a computational model of a system can be expressed as

$$\hat{Y}_{sy}(\mathbf{X}_{sy},\mathbf{X}_{sb},\mathbf{X}_c,\boldsymbol{\theta}_{sy},\boldsymbol{\theta}_{sb},\boldsymbol{\theta}_c,\boldsymbol{\zeta}) = Y_{sy}(\mathbf{X}_{sy},\mathbf{X}_{sb},\mathbf{X}_c,\boldsymbol{\theta}_{sy},\boldsymbol{\theta}_{sb},\boldsymbol{\theta}_c,\boldsymbol{\zeta}) + e_{sy} + \varepsilon_{sy} \qquad (1)$$

where $\hat{Y}$ and Y are predicted and observed (experimental) responses; $\mathbf{X}$ and $\boldsymbol{\theta}$ are the known and unknown variable vectors, respectively; $\boldsymbol{\zeta}$ is the controllable variable (e.g., operating conditions – environmental temperature or pressure of a product); e and ε are respectively the prediction error (model error and implementation error) and observation error (experimental error); the subscript sy, sb, and c mean 'system', 'subsystem', and 'component', respectively. The predicted responses in the computational model of a subsystem or component can be expressed as

$$\hat{Y}_{sb}(\mathbf{X}_{sb},\mathbf{X}_c,\boldsymbol{\theta}_c,\boldsymbol{\theta}_{sb},\boldsymbol{\zeta}) = Y_{sb}(\mathbf{X}_{sb},\mathbf{X}_c,\boldsymbol{\theta}_c,\boldsymbol{\theta}_{sb},\boldsymbol{\zeta}) + e_{sb} + \varepsilon_{sb} \qquad (2)$$

$$\hat{Y}_c(\mathbf{X}_c,\boldsymbol{\theta}_c,\boldsymbol{\zeta}) = Y_c(\mathbf{X}_c,\boldsymbol{\theta}_c,\boldsymbol{\zeta}) + e_c + \varepsilon_c \qquad (3)$$

To help understanding on this step 1, a case study of cellular phone system in Section 4.1.2 is invited. The objective of the case study is to develop a valid computational model that can be used to predict the reliability of a cellular phone

35

system against a dent test as shown in Fig. 8. The cellular phone system has two primary failure mechanisms related to the LCD module: LCD panel fracture and Driver Integrated Circuit (IC) failure in the LCD module, as shown in Fig. 7. The computational models that simulate the LCD failure in the cellular phone system include six unknown model variables ($\boldsymbol{\theta}$), such as material properties and interface conditions. To make the system model calibration affordable, the computational model of the cellular phone system was decomposed into subsystem(s) and component(s). This decomposition planning was designed to isolate the failure mechanisms (or PoI) and identify unknown model variables along the system hierarchy. First, separation of the LCD module (subsystem) from the cellular phone (system) isolated the Driver IC failure mechanism. A dent failure test (destructive testing) was performed to replicate the failure in the module. The dent simulation model was developed with LS-DYNA software, as shown in Fig. 9. Subsequently, the decomposition of the LCD panel (component) from the LCD module (subsystem) isolated the LCD panel failure mechanism. A 3-point bending failure test (destructive testing) was designed to replicate the LCD panel breakage. Correspondingly, the 3-point bending simulation model was developed using an explicit method in the LS-DYNA software, as shown in Fig. 10.

The cellular phone model includes many unknown model variables ($\boldsymbol{\theta}$), such as material properties and interface conditions. Figure 11 shows the configuration of the LCD module. Among many, six model variables were found to be unknown through expert knowledge about the computational model for the LCD module (subsystem). The six variables included four material properties (the light guide panel, chassis,

mold frame, and Driver IC) and two interface conditions (gap sheet thickness and tied

scale factor as an interface condition between layers 2 and 8). In the component level,

the elastic modulus of the LCD panel is defined as unknown variable.
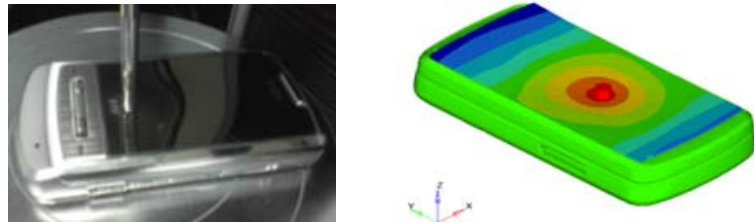
Fig. 8. Dent test and simulation for cellular phone system (system level)
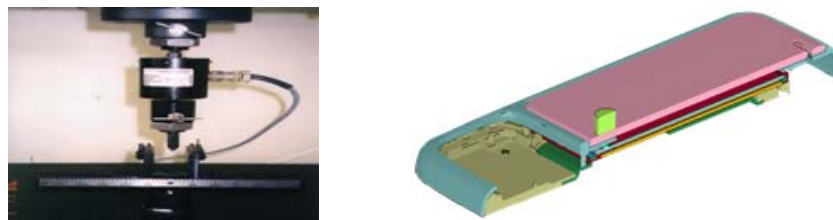
Fig. 9. Dent test and simulation for LCD module (subsystem level)
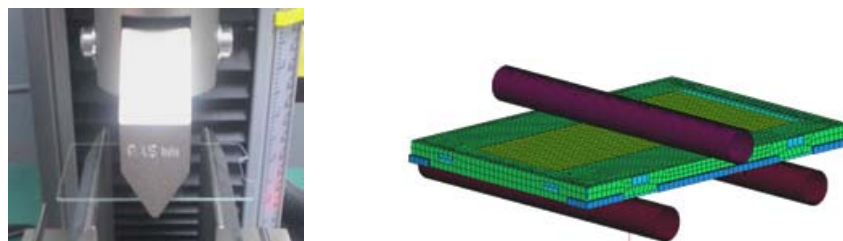
Fig. 10. 3-point bending test and simulation for LCD panel (component level)
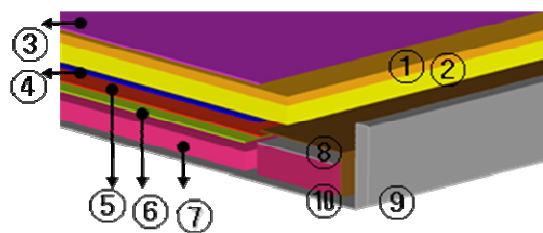
1. upper glass	2. lower glass	3. upper polarizer
4. lower polarizer	5. gap sheet #1	6. gap sheet #2
7. light guide panel	8. inner chassis	9. outer chassis
10. mold frame		

Fig. 11. Configuration of LCD module

(Step 2) Model validation execution planning: It includes (a) the model variable characterization planning, (b) the statistical calibration planning, and (c) the validity check planning.

(Step 2-a) *Model variable characterization planning*: Material properties, physical parameters, etc. defined as known model variables ($\mathbf{X}$) with randomness should be statistically characterized with multiple experimental data. Goodness-of-fit (GoF) hypothesis test such as the Kolmogorov-Smirnov goodness-of-fit (K-S GoF) hypothesis tests or chi-square GoF hypothesis test can be employed to determine the statistics of statistical variables [15]. Detail procedure will be explained in next subsection. For the cellular phone system, failure forces (loading conditions) of both 3-point bending test and dent test are decided as known model input variables.

(Step 2-b) *Statistical calibration planning*: The model calibration should be carefully executed as explained in Section 3.2.1. The statistical calibration planning using expert opinion and sensitivity studies is thus very important, since it determines the most significant but unknown model variables that affect uncertain responses of the computational model at any hierarchy. The success of statistical model calibration highly relies on the ability to identify a small number of unknown model variables ($\boldsymbol{\theta}$) that can be statistically calibrated with experimental data at each hierarchy. For the LCD module, sensitivity analysis uses a finite difference method to perturb the six unknown model variables in a computational model by 1% and identifies the variables that significantly affect the two primary failure mechanisms as shown in Fig. 12. The gap sheet thickness and tied scale factor turned out to be the most significant and were considered as the unknown model variables ($\boldsymbol{\theta}_{sb}$) in the

38

calibration process of the LCD module (subsystem). The other variables are defined as known variables and the values in references are used for the model calibration. As the LCD panel was decomposed from the module, this planning identified two unknown model variables (θ_c): the elastic moduli of the polarizer and the LCD panel. Between them, it is found that the elastic modulus of the LCD panel was far more significant. Therefore, the elastic modulus of the LCD panel was decided as the only unknown model input variable. In this planning, it is also required to decide a method for the UP analysis for statistical model calibration. The UP analysis develops the relation between random model variables and computational responses at any hierarchical level. Among many UP analysis techniques, this research mainly used the eigenvector dimension reduction (EDR) method, which is one of the approximate integration methods, because of its less computational effort. Details of the EDR method are explained in Section 3.3.2.
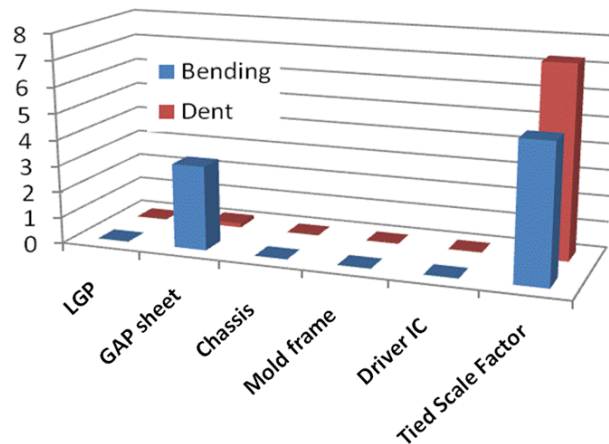
Fig. 12. Sensitivity analysis of LCD module

(Step 2-c) *Validity check planning*: Validity check will be planned with additional experiments because an insufficient amount of data and inaccurate basic assumptions could lead to false validation results after the statistical model calibration. This

39

validity check offers a chance to refine the computational model with a more realistic conceptual or mathematical model that better represents the physics of the system. It is recommended that the validity check be performed at any hierarchy after the statistical model calibration if the experimental resources are sufficient. Some available validity check metrics are introduced in Section 3.2.2.2, and the hypothesis test for validity check developed is explained in Section 3.4.

(Step 3) Virtual qualification planning: With a computational model after statistical calibration, the virtual qualification can be performed with two ways: (a) the absolute qualification and (b) the relatively qualification. The absolute qualification is performed if the PoI of a system has a strict margin, while the relative qualification compares the PoIs of several design alternatives to choose the best design among many candidates. By applying a technique of the reliability-based design optimization (RBDO), the optimal design can be also found with the computational model. Details are explained in Section 3.2.2.3.

3.2.2.2 Model Validation Execution

The model validation execution follows the model validation planning. The model validation execution is a bottom-up activity. The execution is composed of three primary steps: (Step 1) model variable characterization, (Step 2) statistical model calibration, and (Step 3) validity check.

(Step 1) Model variable characterization: Material properties, physical parameters and loading condition categorized as the known model variables in model validation planning should be statistically quantified with experimental data of multiple specimens. The sample specimens should be produced from the same manufacturing

40

line (or lot number). There are two types of random input variables as shown in Fig. 6: (a) random parameter variable, and (b) random field variable. While random parameter variable do not consider the spatial variability, random field variable is characterized as a function of spatial variables.

(Step 1-a) *Characterization of random parameter variable*: The K-S GoF hypothesis tests or chi-square GoF hypothesis test can be employed to determine the statistical parameters. Characterization of random parameter variable follows procedures below:

- Obtain optimum distribution parameters for candidate distribution types (e.g., normal, lognormal, weibull and gamma distributions) using one of the point estimation methods. The maximum likelihood estimation method is used in this research [15].

- Perform a quantitative hypothesis test for the candidate distributions. While the chi-square GoF test and K-S GoF test [15] were both considered, the K-S GoF test is recommended for model validation because it is known that the chi-square GoF test does not work well with a small data size. In the K-S GoF test, a hypothesized cumulative distribution function (CDF) is compared with its estimate, known as the empirical (or sample) cumulative distribution function. Four activities are required to perform the K-S GoF test:

 (1) Assume the data follow a specified distribution with corresponding parameters, obtained in Step 1.

 (2) Define a sample CDF for an ordered sample $y_{(1)} < y_{(2)} < y_{(3)} < \cdots < y_{(k)}$ as

$$S_k(z) = \begin{cases} 0 & -\infty < y < y_{(1)} \\ i/k & y_{(i)} \le y \le y_{(i+1)} \quad i = 1, \cdots, k-1 \\ 1 & y_{(k)} \le y \le \infty \end{cases} \tag{4}$$

where y_i is a component of the response vector $\mathbf{y}$; k is total number of data.

(3) Calculate a test statistic ($K\text{-}S$) to measure the maximum difference between $S_k(z)$ and a hypothesized CDF, $F(z)$, as

$$K - S = \max_i \left[\left| F(y_i) - S_k(y_i) \right|, \left| F(y_i) - S_k(y_{i-1}) \right| \right] \tag{5}$$

(4) Reject the hypothesis if

$$K - S > D_k(\alpha) \tag{6}$$

where α is an assigned significance level, and critical value for K-S GoF test, $D_k(\alpha)$, can be obtained from the Ref. [15].

• Select the best distribution based on p-value among the accepted distributions.

(Step 1-b) *Characterization of random field variable*: A random process modeling technique can be used for the characterization of random field variables. The technique includes the midpoint method [114], the spatial averaging method [115], the shape function method [116], and the proper orthogonal decomposition (POD) method [117]. The POD method has been improved to perform a random-field-based probabilistic design with few characterized random parameters [118,119]. Because statistical model calibration requires UP analysis repeatedly, a small number of random parameter is beneficial to reduce computational cost. The improved POD method is thus recommended to characterize random field variable for the statistical model validation. For the completeness of the thesis, the improved POD method is

briefly summarized although it is not demonstrated in the case studies. In the POD method, random field is characterized as

$$\delta(t,k) = \mu(t) + \sum_{i=1}^{\infty} v_i(k) \frac{\phi_i(t)}{\|\phi_i(t)\|} \tag{7}$$

where the random field, δ, is a function of the position, t. $\mu(t)$ and $\sum_{i=1}^{\infty} v_i(k) \frac{\phi_i(t)}{\|\phi_i(t)\|}$ indicate mean and variation parts, respectively. k indicates the number of snapshot (random field samples). ϕ is eigenvector that indicates the most significant signature of an ensemble of the random field variation and v is the coefficient of the corresponding eigenvector. The coefficients of important signatures, v, in Eq. (7) can be replaced by a small number of random parameters (V_i) as

$$\tilde{\delta}(x,t) = \mu(x) + \sum_{i=1}^{r} V_i \frac{\phi_i(x)}{\|\phi_i(x)\|} \tag{8}$$

(Step 2) Statistical model calibration: A statistical model calibration technique is essential to enhance the predictive capability of a computational model at any hierarchical level. For successful model calibration, the predictive models must be constructed at all hierarchical levels with the known and unknown model variables. Initially, the computational model will be built by modeling unknown model variables with a prior knowledge from experts or reference information. In the example of the cellular phone system, the initial statistics of the gap sheet thickness and tied scale factor are provided by manufacturing experts and product analysts, whereas the elastic modulus of the LCD panel is initially derived from the glass. Then, the constructed computational model develops the PDF of the response through UP analysis. Finally, the proposed statistical calibration technique in Section 3.3.1

43

improves the predictive capability of a computational model at any hierarchical level by compares the observed results with the predicted ones from a computational model. The improved model in a lower hierarchy is then fused into a model at a higher hierarchical level, and the validation execution continues for the model at the higher level. For the cellular phone system, validation begins at a component level (e.g. LCD panel model in Fig. 10) and the unknown model parameters (e.g. LCD panel modulus) at the component level become known at the higher hierarchical levels (e.g. LCD module in Fig. 9 and cellular phone system in Fig. 8). The predicted responses in the computational models can recursively be enhanced as

$$
\begin{aligned}
&\text{Component: } \hat{Y}_c(\mathbf{X}_c, \boldsymbol{\theta}_c, \zeta) = Y_c(\mathbf{X}_c, \boldsymbol{\theta}_c, \zeta) + e_c + \varepsilon_c \\
&\qquad \overset{\text{statistical calibration}}{\Rightarrow} \qquad \mathbf{X}_c^* = [\mathbf{X}_c; \boldsymbol{\theta}_c^{cal}] \\
&\text{Subsystem: } \hat{Y}_{sb}(\mathbf{X}_{sb}, \mathbf{X}_c^*, \boldsymbol{\theta}_{sb}, \zeta) = Y_{sb}(\mathbf{X}_{sb}, \mathbf{X}_c^*, \boldsymbol{\theta}_{sb}, \zeta) + e_{sb} + \varepsilon_c \\
&\qquad \overset{\text{statistical calibration}}{\Rightarrow} \qquad \mathbf{X}_{sb}^* = [\mathbf{X}_{sb}; \boldsymbol{\theta}_{sb}^{cal}] \\
&\text{System: } \qquad \hat{Y}_{sy}(\mathbf{X}_{sy}, \mathbf{X}_c^*, \mathbf{X}_{sb}^*, \boldsymbol{\theta}_{sy}, \zeta) = Y_{sy}(\mathbf{X}_{sy}, \mathbf{X}_c^*, \mathbf{X}_{sb}^*, \boldsymbol{\theta}_{sy}, \zeta) + e_{sy} + \varepsilon_c \\
&\qquad \overset{\text{statistical calibration}}{\Rightarrow} \qquad \mathbf{X}_{sy}^* = [\mathbf{X}_{sy}; \boldsymbol{\theta}_{sy}^{cal}]
\end{aligned}
\tag{9}
$$

After the model calibration, an unknown variable vector, $\boldsymbol{\theta}$, becomes a known variable vector, $\boldsymbol{\theta}^{cal}$. The augmented parameter vector $\mathbf{X}^*$ is introduced to simplify the notation as the computational models at all levels are aggregated into a system. $\mathbf{X}^*$ indicates a new known random variable vector that includes $\mathbf{X}$ and $\boldsymbol{\theta}^{cal}$ at a given hierarchical level. In this approach, it is acknowledge that it is hard to assure the predictive capability of improved model without the assumption that the uncertainty in observed results (Y) only comes from the uncertainty of unknown model parameters. For this reason, it is mandatory that the validation key principles addressed in Section 2.1 and the model validation planning addressed in Section

3.2.2.1 should be accompanied to set a model calibration problem to reduce unexpected observation errors (experimental error, ε) and prediction errors (computational error, e) during the hierarchical model validation activities.

(Step 3) Validity check: Validity check metrics such as graphical comparison, confidence interval approach [120] and u-pooling method [11] can be carefully chosen according to characteristics of the predicted and observed responses. For example, the confidence interval approach uses a type 1 error that is a conditional probability corresponding to the possibility that a null hypothesis (designated as H_0) is rejected when it is indeed true, $p(\text{reject } H_0 | H_0 \text{ is true})$. In other words, it is a probability that we reject a model when it is valid. Using a two-sided confidence interval, if all corresponding experimental results are found within the confidence intervals created, the model is not considered to be invalid with the specified significance level. The u-pooling method is explained in Section 3.4. In this dissertation, a new method named 'hypothesis test for validity check' is proposed and explained in Section. 3.4.

3.2.2.3 Virtual Qualification

Virtual qualification is a process for qualifying a product design through the use of valid computational model; thus, it will be executed only if a computational model is evaluated as valid using hypothesis test. The virtual qualification can be performed with the calibrated model in an absolute or relative manner. An absolute qualification can be conducted for a product design if its performance of interest (PoI) has a strict margin, as shown in Fig. 13(a). For example, the design 1 is qualified if its PoI is larger-the-better, whereas the design 2 is not. A relative qualification is preferred for

45

a product design if its PoI has no strict margin. Then, various product design alternatives can be compared with their PDFs of the PoI, as shown in Fig. 13(b). For instance, the design 1 is more highly qualified than the design 2 or 3. The virtual qualification can be performed quantitatively by constructing the design decision matrix, as shown in Fig. 13(c). This matrix can aid in rational decision-making on product designs. A value in the upper triangular part of the matrix indicates the probability that one design (i: column) is better than the other (j: row, $p(d_i > d_j)$). p indicates probability. d_i and d_j indicate i^{th} and j^{th} designs. The design decision matrix provides rich information for comparison of design alternatives and helps analysts make a rational decision in the product development process.

The benefits of the design decision matrix are: (a) it provides rich information for comparison of design alternatives and helps analysts make a rational decision in the system development process, and (b) it enables a quantitative decision making in determining better design alternative when a system involves multiple PoIs. Among the design alternatives, a design that has the highest weighted sum of probabilities over all the PoIs can be selected as the best design (d_{best}). For instance, as shown in Fig. 14, the sum of $p(d_A > d_B)$ over two PoIs is 0.8, while the sum of $p(d_A < d_B)$ is 1.2. Assuming that the weights are equally given, we can select the design B rather than design A because the former outperforms the latter in a statistical sense.

PDF

d_1: Design 1
d_2: Design 2
--- Margin

d_2 d_1

PoI of Product

(a) Absolute qualification

PDF

d_1: Design 1
d_2: Design 2
d_3: Design 3

d_3 d_2 d_1

PoI of Product

(b) Relative qualification
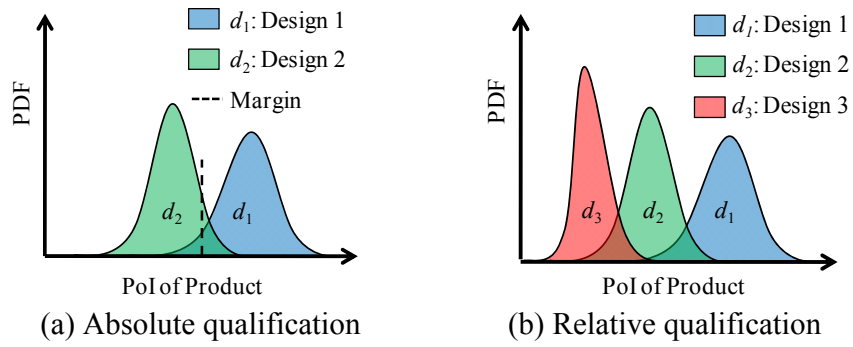
$p(d_i>d_j)$	d_1	d_2	d_3
d_1	0.500	0.85	0.99
d_2		0.500	0.79
d_3			0.500

(c) Design Decision Matrix (d_i indicates ith design)

Fig. 13. Virtual qualification methods

PDF of design A
PDF of design B

PoI 1

$p(d_A>d_B)=0.8\%$

$p(d_A<d_B)=0.2\%$

(a) Relative qualification for PoI 1

PDF of design A
PDF of design B

PoI 2

$p(d_A>d_B)=0\%$

$p(d_A<d_B)=1.0\%$

(b) Relative qualification of PoI 2
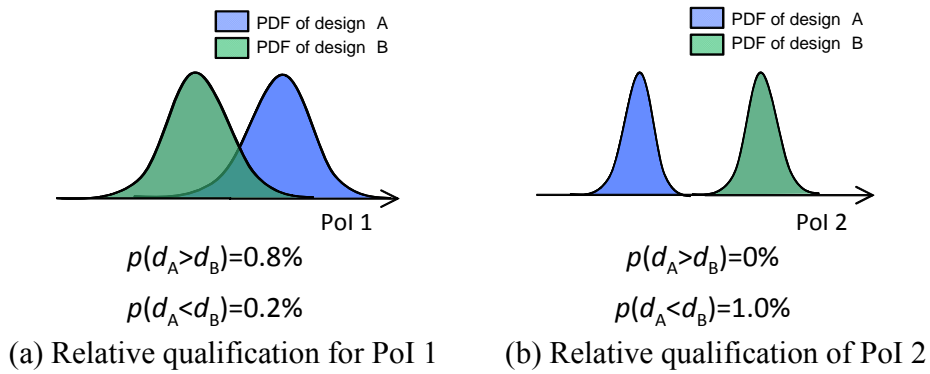
Fig. 14. Design decision making of a system with multiple PoIs

3.3 Statistical Model Calibration

3.3.1 Statistical Model Calibration Procedure

Although model calibration is a practical and appropriate method, the *ad hoc* adjustment of model input variables may degrade the predictive capability of the computational model. For example, Fig. 15 demonstrates the danger of model calibration with a single experimental result. In Fig. 15(a), it is assumed that the

blue-dashed curves represent the uncertain domain of experimental results and the red-solid curves do of the same for computational results. Since the domain information is normally unknown, the deterministic calibration to maximize the agreement between a deterministic computational result (plus mark) with experimental data (blue dot) may affect the predictive capability adversely, as shown in Fig. 15(b). This situation can be prevented as long as statistical model calibration is performed with multiple experimental data because it can easily recognize that the initial computational model is already "nearly valid". This explains why this research focuses on the statistical calibration activity in the model development process.
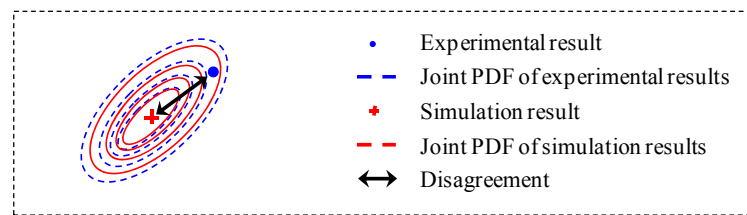
(a) Predicted and observed results before model calibration
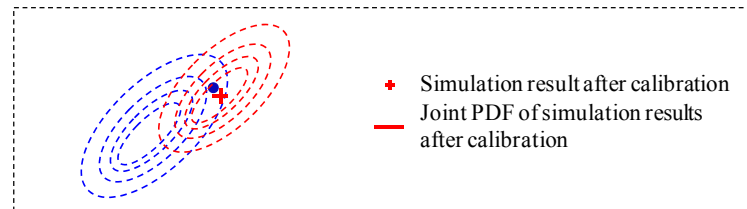
(b) Predicted and observed results after deterministic model calibration

Fig. 15. Importance of uncertainty in model calibration

The statistical model calibration is essential to enhance the predictive capability of a computational model in the proposed validation framework. The purpose of model calibration is to adjust a set of unknown model variables so that the agreement is maximized between the predicted and observed results. The relationship between the observed model, Y, and the predicted model, $\hat{Y}$, can be defined as

$$\hat{Y} = Y(\mathbf{X}, \boldsymbol{\theta}, \zeta) + e(\zeta) + \varepsilon \quad \mathbf{X} \in \Omega^l, \boldsymbol{\theta} \in \Omega^p, \zeta \in \Omega^q \tag{10}$$

where l, p and q are the number of the known, unknown and controllable variables. The statistical model calibration determines the statistics of unknown model variables ($\boldsymbol{\theta}$) that give a maximal agreement between the predicted and observed responses. The uncertainty of unknown model variable, $\boldsymbol{\theta} = \{\theta_1, \theta_2, \cdots, \theta_p\}$, can be represented by statistical parameters of a suitable distribution. For example, in case of a normal distribution, the augmented parameter ($\boldsymbol{\Theta}$) includes mean and standard deviation of $\boldsymbol{\theta}$ as $\{\mu_{\theta 1}, \sigma_{\theta 1}, \mu_{\theta 2}, \sigma_{\theta 2}, \ldots, \mu_{\theta p}, \sigma_{\theta p}\}$. Then, $\boldsymbol{\Theta}$ will be the calibration parameter vector in the statistical calibration. A distribution type, such as normal, lognormal and weibull, can be assumed or determined based on both historic data and expert opinions. Next, the statistical calibration determines the calibration parameter vector ($\boldsymbol{\Theta}$) that gives a maximal agreement between the predicted and observed responses. The statistical calibration can be formulated as

$$\text{maximize} \quad \mathrm{L}(\boldsymbol{\Theta} \mid \mathbf{y}) = \sum_{i=1}^{n} log_{10}[f(y_i \mid \boldsymbol{\Theta})] \tag{11}$$

where y_i is a component of the random response (e.g., failure displacement in cellular phone system) vector $\mathbf{y}$; n is the number of experimental data; L is likelihood function; f is the PDF of y for a given $\boldsymbol{\Theta}$. The likelihood function is used as the calibration metric to measure the degree of the agreement between the PDF of the predicted response and the experimental data. The EDR method can construct the PDF of predicted response (f) effectively for the statistical model calibration. An unconstrained optimization problem can be solved using a nonlinear optimizer, the "fmincon" function of MATLAB software. The choice of the calibration formulation and the calibration parameters is problem dependent. If the prior knowledge of model

49

error (e.g. linear form or nonlinear form) is known, it is beneficial to consider the model error in the calibration process, but in many cases it is hard to figure out the model error before model calibration. One potential weakness of the proposed calibration is that if many unknown parameters are involved in the calibration, the calibrated parameters could be going into absurd values. To mitigate this weakness, the model error term is ignored in the calibration process in this dissertation. Sensitivity analysis is another solution to leave out parameters that are insensitive to the model output prior to the calibration to. Figure 16 shows the concept of the likelihood function in the proposed calibration method. In the figure, x-axis denotes a controllable variable (e.g., operating condition), and y-axis denotes experimental data or predicted responses. The likelihood function between the experimental data and the response PDFs of Fig. 16(a) is larger than those of Figs. 16(b) or (c): the mean values of the response PDFs in Fig. 16(b) are deviated from those of experimental data, and the standard deviations of the PDF in Fig. 16(c) are larger than those of Fig. 16(a). Figure 17 summarizes the statistical model calibration procedure. Given our focus on prediction, the usefulness of the model calibration is apparent due to the improvement of statistical information of random variables by the analyses based on field data.

(a) High likelihood value   (b) Low likelihood value   (c) Low likelihood value
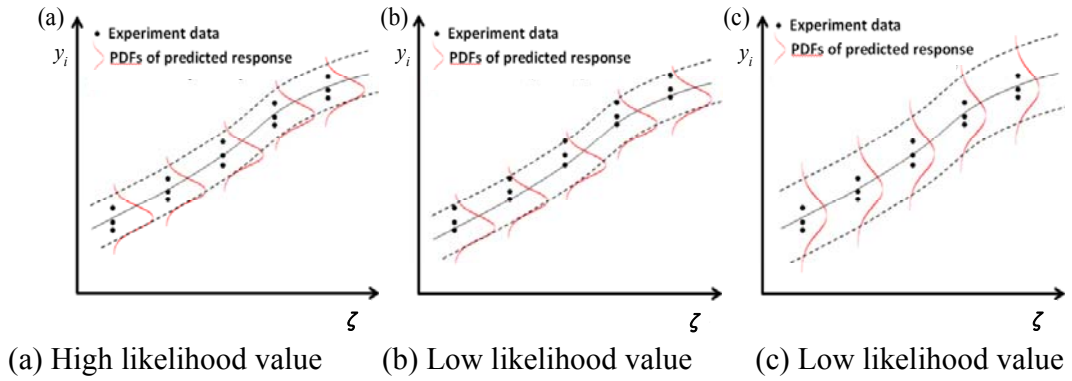
Fig. 16. The concept of likelihood function
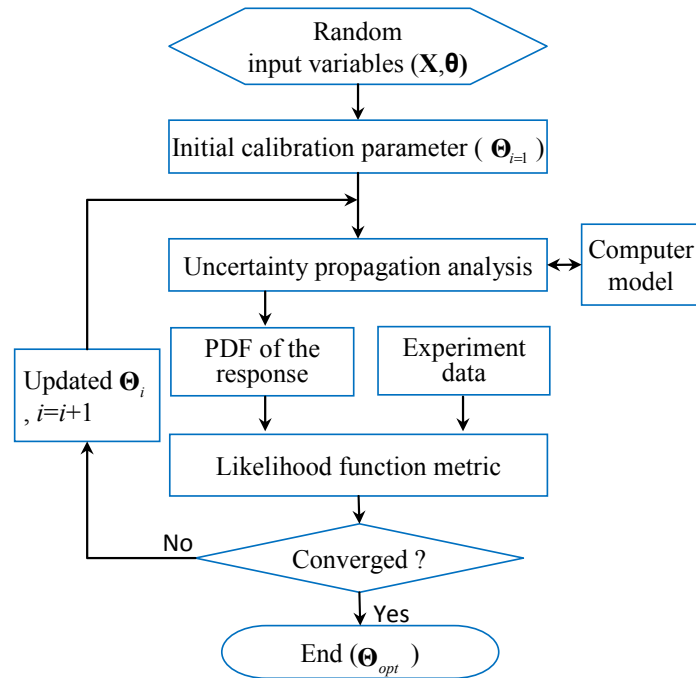
Fig. 17. Statistical model calibration procedure

3.3.2 Uncertainty Propagation Analysis

The proposed model calibration becomes difficult along with the increase of the dimensionality of the model input space, since the increased runs of the computation model are required.   Among many UP analysis approaches, the eigenvector dimension reduction (EDR) method [122] is mainly employed in the thesis because of

51

the less computational cost for UP analysis. The EDR method is an enhancement of the univariate dimension reduction method that calculates the statistical moments of a response. The statistical moments of the response, $\hat{Y}$, can be calculated as

$$\mathbf{E}\left\{\hat{Y}^m(\mathbf{Z})\right\} = \int_{-\infty}^{\infty} \int_{-\infty}^{\infty} \hat{Y}^m(\mathbf{z}) \cdot f_{\mathbf{Z}}(\mathbf{z}) \cdot d\mathbf{z}, \ m = 0,1,2,\cdots \tag{12}$$

where $\mathbf{Z}$ is an augmented variable vector ($\mathbf{Z} \equiv \mathbf{X} \oplus \boldsymbol{\theta}$). $\mathbf{E}\{\bullet\}$ indicates the expectation operator and $f_{\mathbf{Z}}(\mathbf{z})$ is the joint probability density function (PDF) of $\mathbf{Z}$. Multi-dimensional integration in Eq. (12) can be converted into multiple one-dimensional integrations using an additive decomposition. The additive decomposition, $\hat{Y}_a$, is defined as

$$\begin{aligned}
\hat{Y}(Z_1,...,Z_N) &\cong \hat{Y}_a(Z_1,...,Z_N) \\
&= \sum_{j=1}^{N} \hat{Y}(\mu_1,...,\mu_{j-1},Z_j,\mu_{j+1},...,\mu_N) - (N-1)\hat{Y}(\mu_1,...,\mu_N)
\end{aligned} \tag{13}$$

Although the additive decomposition ($\hat{Y}_a$) ignores all the interactive terms, the produced error is less than that of a second-order Taylor expansion method for probability analysis. Two reasons can explain this observation: (1) the additive decomposition ($\hat{Y}_a$) preserves the accuracy for all uni-variable terms; (2) after the expansion of the true response ($\hat{Y}$) using Taylor expansion at the mean value μ_i, the integration of the interactive variable terms in Eq. (13) becomes zero as long as one of the variables is odd-order, provided that all variables are independent and the integration domain is symmetric. The symmetry of the integration domain, namely the symmetric PDF of the variable, ensures that all odd-order central moments are zeros. For that reason, any asymmetric distribution must be transformed to a symmetric distribution. Therefore, the largest error incurred due to the additive

decomposition is at the fourth even-order term, producing a negligible error. In aid of the additive decomposition, the probability analysis of the response becomes much simpler. For reliability and quality assessment, the mth statistical moments for the response can be approximately obtained as

$$\mathbf{E}\left[\hat{Y}_a^m(Z))\right] = \mathbf{E}\left\{\left[\sum_{j=1}^{N}\hat{Y}\left(\mu_1,\cdots,Z_j,\cdots,\mu_N\right)-\left(N-1\right)\cdot Z\left(\mu_1,\cdots,\mu_N\right)\right]^m\right\} \quad (14)$$

Using a binomial formula, Eq. (14) can be evaluated by executing one-dimensional integration recursively. To enhance both accuracy and efficiency in probability analysis, three technical elements are considered: (1) the eigenvector sampling method to handle correlated and asymmetric random input variables, (2) the stepwise moving least squares method for one dimensional response approximation, and (3) a stabilized Pearson system for generating a PDF of a response. Thus, for N number of random variables, the EDR method only demands $2N+1$ or $4N+1$ eigenvector samples to obtain a PDF of a response.

3.4 Hypothesis Test for Validity Check

For validity check of a computational model, many experimental data from multiple samples (or physical products) are generally required; however, it is impractical to manufacture lots of prototypes due to expensive manufacturing cost. There are two challenges for validity check due to the lack of experimental data. First, the experiments for validity check are normally conducted with samples of different designs or under various operating conditions (or experimental settings) in a validation domain. When few sets of experimental data are collected for the corresponding prediction distributions, it is beneficial to integrate the evidence from

all the observations over the entire validation domain into a single measure of overall mismatch. Second challenge is that the small sample size of experiments will produce uncertainty in a validity check metric and make it difficult to assess whether the disagreement between the predicted and observed results is significant or not. The hypothesis test for validity check is thus developed to solve these two challenges while considering the effect of limited experimental data. In the hypothesis test, the null hypothesis (H_0) is defined as the claim about a calibrated model is valid. The null hypothesis can be rejected only if a validity check metric suggests that H_0 is false; otherwise not rejected. The rejected calibrated model should be further refined as shown in Fig. 4.

3.4.1 U-pooling Method

To solve the first challenge, the hypothesis test employed the u-pooling method for validity check [11]. The u-pooling method is beneficial since it allows integration of all experimental data from various experimental settings (e.g. environmental temperature, loading, etc.) into a single aggregate metric. In the u-pooling method, the cumulative density, u_i, should be first obtained by transforming every experimental datum (y_i) according to its corresponding predictive CDF (F_{yi}) of a calibrated model as

$$u_i = F_{yi}(y_i) \qquad (15)$$

where i is the number of experimental data. Under the assumption that the experimental data, y_i, truly come from the same mother distribution (i.e. the model is valid), the u_i values corresponding to all experimental data will follow a uniform distribution on [0,1]. This fact is called the probability integral transform theorem in

statistics [121]. In other words, the CDF of the uniform distribution (F_{uni}) indicates the line of perfect agreement between experimental data and predicted results of the calibrated model. Therefore, we can quantify a mismatch between dispersion of experimental data and distribution of predicted results by calculating an area (i.e. the area metric (U_m)) between the CDF of the uniform distribution (F_{uni}) and the empirical CDF of u_i values (F_u) as

$$\text{U}_m = area(F_u, F_{\text{uni}}) = \int_0^1 \left| F_u(u) - F_{\text{uni}}(u) \right| du \quad , \quad 0 < u < 1 \;,\; 0 \le \text{U}_m \le 0.5 \quad (16)$$

For example, there are three experimental data (y_i) and predicted PDFs (f_i) under different operating conditions (or experimental settings) as shown in Fig. 18(a). The u_i of each experimental datum is calculated and its empirical CDF is drawn in Fig. 18(b). The calculated area of shaded region in Fig. 18(b) indicates the U_m. The smaller the calculated the U_m, the closer is the predicted PDF to the distribution of experimental data. For example, if the model well represents the physical responses (i.e. the model is valid) the U_m will be zero when enough experimental data exists. Otherwise (i.e. the model is not valid), the U_m will be a positive value.

(a) Predicted and experimental results   (b) Area metric ($=U_m$)
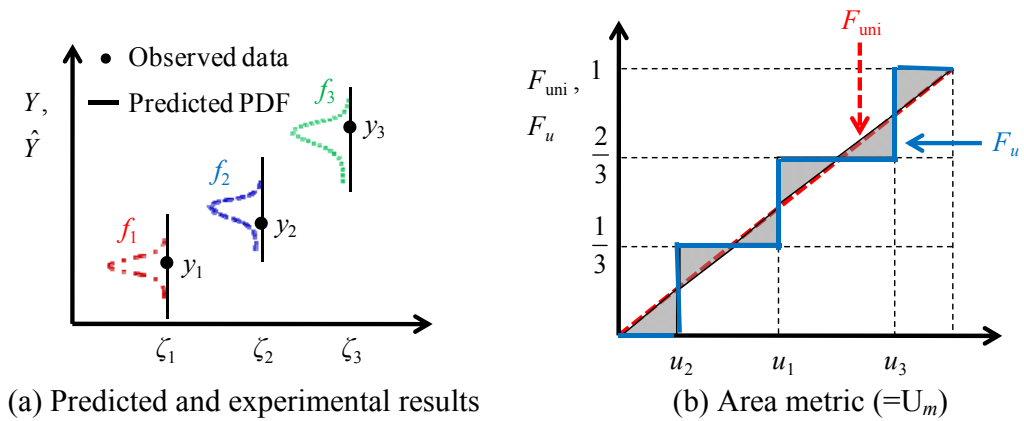
Fig. 18. Calculation of area metric

3.4.2 Epistemic uncertainty in the area metric

If experimental data are comprehensively collected for validity check, there is no sampling uncertainty in the U_m and it is definite the null hypothesis can be rejected unless the U_m is zero. While experimental data are limited in reality, the U_m has uncertainty although mother distributions of predicted and experimental results are identical (i.e. the model is valid). For example, the PDFs ($f_{u,i}$) in Fig. 19(a) shows uncertainty in the U_m when eighteen virtual experimental data (i=18) were used for validity check. The uncertainty in area metric is characterized using a virtual sampling technique with following three steps.

Step 1: It is assumed that mother distributions of predicted and experimental results are identical (i.e. the model well represents the physical responses or the model is valid).

Step 2: The i number of experimental data (i=18 in Fig. 19(a)) are virtually sampled from the mother distribution, and the u values and the corresponding U_m are calculated using Eq. (16).

Step 3: Step 2 is repeated several thousand times and the statistical distribution (i.e. PDF) of the U_m ($f_{u,i}$) is constructed with U_m values using pearson system [119]. It was check that the pearson system can appropriately represent the uncertainty in U_m. In Fig. 19(a), the PDFs ($f_{u,i}$) were constructed using ten thousand U_m values.

One vital characteristic of the $f_{u,i}$ is that it is unique irrespective of the shape of a mother distribution. To demonstrate this, three different mother distributions are used to characterize statistical models of U_m as shown in Fig. 19(b), where N and *Wbl*

indicate normal and weibull distributions, respectively. As shown in Fig. 19(a), the PDFs of area metric ($f_{u,18}$) are identical. It is because a set of u_i values always follows uniform distribution regardless of shape of mother distributions (f in Fig. 19(b)). Because of this characteristic, proposed hypothesis test can be applicable to any computational models with different statistical distribution of predicted responses. In addition, the $f_{u,i}$ converges to zero as the number of experimental data (i) is increased As shown in Fig. 20, as the number of experimental data is increased from 6 to 60, the uncertainty in the U_m is decreased and the area metric is converged to zero.

(a) PDFs of area metric ($f_{u,18}$)   (b) Three different mother distributions
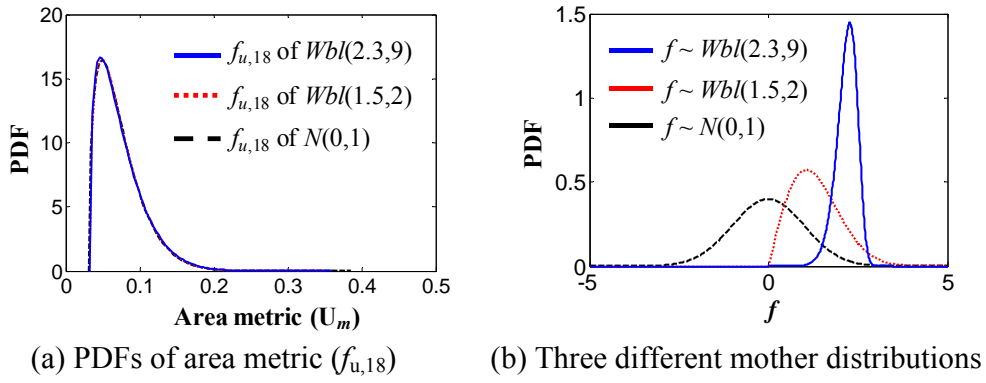
Fig. 19. PDFs of the U_m in case 18 experimental data are virtually sampled
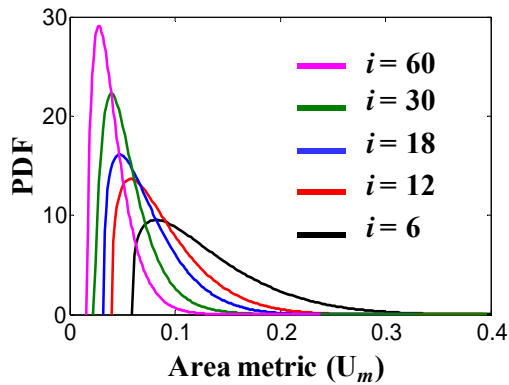
Fig. 20. PDFs of area metric: the effect of limited experimental data

3.4.3 Hypothesis test for validity check

The hypothesis test uses the PDF of area metric ($f_{u,i}$). Because the $f_{u,i}$ indicates plausible values of U_m in case mother distributions of predicted and experimental results are identical, upper-tailed test can be employed after deciding a rejection region as

$$U_m > D_i(\alpha) \qquad (17)$$

where $D_i(\alpha)$ indicates a critical value of area metric; α is a significance level. For example, $D_{18}(0.05)$ is 0.137 for the upper-tailed test as shown in Fig. 19(a). The null hypothesis will be rejected if and only if U_m falls is the rejection region. In the absence of such evidence, H_0 should not be rejected, since it is still quite plausible.

For the successful validity check, it is important to decide reasonable rejection region (or $D_i(\alpha)$). In this study, type 1 and type 2 errors are considered to determine the rejection region. A type 1 error is defined as a probability that we reject a calibrated model when it is valid. The type 1 error can be calculated as

$$\mathrm{Type\,1\,error} = \int_{D_i(\alpha)}^{\infty} f_{u,i}(x)dx \qquad (18)$$

The type 1 error is related with the cost of a product development. The type 2 error is differently defined as a probability that we do not reject a calibrated model when it is invalid. It is related with risk or confidence of predicted results. The type 2 error cannot be simply estimated with the $f_{u,i}$. It varies according to the Degree of Invalid (DoI) that is defined as a difference between distributions of predicted results (f^{compu}) and experimental results (f^{exp}). Two different metrics, joint area metric and cross entropy metric [11], were considered to quantify the DoI as

58

$$\text{Joint area metric} : d_J = \int_\Omega \min(f^{compu}, f^{exp}) \quad , \quad 0 < d_J < 1$$

$$\text{Cross entropy metric:} \ d_C = \int_\Omega f^{compu} \ln\left[\frac{f^{compu}}{f^{exp}}\right] \tag{19}$$

where d_J and d_C indicate the joint area metric and the cross entropy metric, respectively. Then, the DoI can be formulated as

$$\text{DoI}_{d_J} = (1 - d_J) \times 100 \qquad 0 < \text{DoI}_{d_J} < 100$$

$$or \ \ \text{DoI}_{d_C} = d_C \qquad\qquad 0 < \text{DoI}_{d_C} \tag{20}$$

The concept of DoI is described with five different PDFs in Fig. 21(a). It is assumed that the mother distribution of experimental results is the standard normal distribution (f^0). The PDF, f^{20}, shows the 20% DoI_{dJ} (d_J=0.8) by compared to the mother function (f^0) due to a prediction error. Superscript in the f^{20} designates 20% DoI_{dJ}. Similarly, the f^{40}, f^{60} and f^{80} have 40%, 60% and 80% DoI_{dJ}, respectively. Table 2 summarizes the DoI_{dJ} and DoI_{dC} of PDFs in Fig. 21(a).

Then, the PDFs of the area metric in case the mother function of predicted results is different with that of experimental results ($f_{u,i}^{DoI}$, i=18, see Fig. 21(b)) can be constructed by comparing five PDFs in Fig. 21(a) (as distributions of predicted results) with the sampled experimental data from f^0. For example, the $f_{u,18}^{20}$ was constructed with the mother distribution of predicted results, f^{20}, and experimental data sampled from f^0. To construct the distribution, $f_{u,18}^{20}$, step 2 and 3 in Section 3.4.2 were repeated ten thousand times. Similarly, the $f_{u,18}^{40}$, $f_{u,18}^{60}$ and $f_{u,18}^{80}$ were constructed with f^{40}, f^{60}, and f^{80} as the mother distributions of predicted results. We can check that the calculated area metric increases as the DoI increases (or as the

59

difference between predicted and experimental results increases). Finally, the type 2
error is defined using the $f_{u,i}^{40}$ as

$$\text{Type 2 error} = \int_0^{D_i(\alpha)} f_{u,i}^{\text{DoI}}(x)dx \qquad (21)$$

Table 3 shows the type 2 errors when $D_{18}(\alpha)$ is 0.1 as shown in Fig. 21(b). The type 2
error is decreased as the DoI is increased.

(a) Five PDFs (f^{DoI}) with different DoI   (b) PDFs of area metric ($f_{u,18}^{\text{DoI}}$)
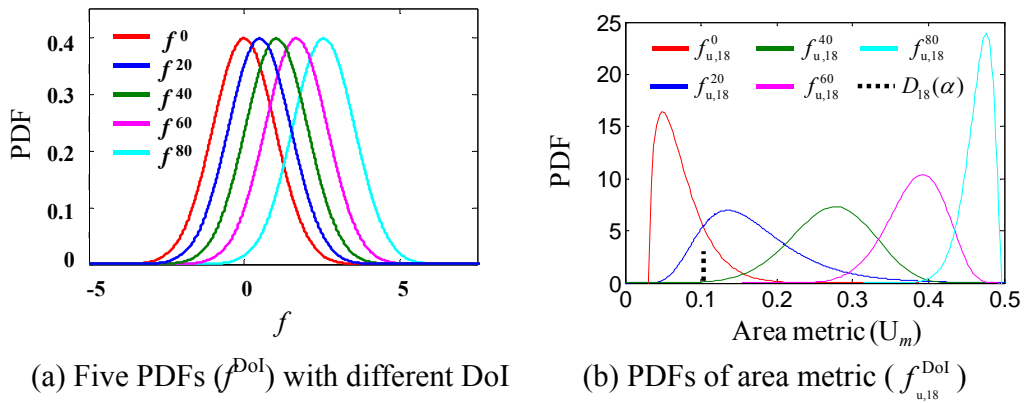
Fig. 21. Uncertainty in area metric due to DoI

Table 2 DoI of different predicted PDFs

PDF of predicted results	Mother function of experimental results	DoI$_{dJ}$	DoI$_{dC}$
f^0	f^0	0%	0
f^{20}	f^0	20%	0.185
f^{40}	f^0	40%	0.704
f^{60}	f^0	60%	2.044
f^{80}	f^0	80%	4.739

Table 3 The calculated type 2 error

Predictive PDF	Type 2 error
f^{20}	0.35
f^{40}	0
f^{60}	0
f^{80}	0

Based on the type 1 and type 2 errors, two approaches are devised to determine the
rational rejection region (or the critical value) for the validity check as:

(1) An approach based on a significance level: With an assigned significance level, α, this approach rejects the null hypothesis if and only if the U_m is less than the critical value, $D_i(\alpha)$. The significance level should be carefully decided based on the experts' knowledge. If the significance level is increased, the type 1 error increases while the type 2 error decreases.

(2) An approach based on the type 2 error: If engineered systems have high risk (e.g. products having catastrophic failure mode such as a li-ion battery system, a bridge, an airplane, etc.), the critical value ($D_i(\alpha)$) should be decided based on the type 2 error by following three steps. First, an acceptable maximum DoI should be determined. For example, the 40% DoI is selected as the acceptable maximum DoI as shown in Fig. 21(a). Next, $f_{u,i}^{\text{Max. DoI}}$ (Max. DoI =40%) is constructed (see $f_{u,18}^{40}$ in Fig. 21(b)). Then, the critical value ($D_i(\alpha)$) can be selected as the value that makes the type 2 error of the $f_{u,i}^{\text{Max. DoI}}$ zero (i.e. the $D_i(\alpha)$ that makes the type 2 error of the $f_{u,18}^{40}$ zero is 0.1). By defining rejection region as $U_m > 0.1$, we can reject invalid a computational model of which DoI is larger than 40%. The benefit of this approach is that we can reject all invalid computational models that have unacceptable large DoIs.

Chapter 4: Case Studies

For the feasibility demonstration of the proposed model validation framework, this chapter employs five case studies: (1) cellular phone, (2) tire tread block, (3) thermal challenge problem, (4) constrained-layer damping structure and (5) energy harvesting device.

4.1 Cellular Phone

4.1.1 Overview of Problem

Hand held electronic devices, such as cellular phones, may be subjected to many different mechanical loads during their lifetime. These mechanical loads include impact shock due to a drop, keypad pressing and phone twisting (and bending) when we sit down on a chair with a cellular phone in the pants pocket. Dent and 3-point bending tests or simulations have been normally used to examine mechanical failures of LCD panel and module in cellular phone systems. In this case study, two computational models are built using the proposed validation framework: (1) a computational model of a cellular phone system of LG Electronics (Section 4.1.2) and (2) a computational model of a TFT-LCD panel of Samsung Electronics (Section 4.1.3).

4.1.2 Model Validation of a Cellular Phone System

4.1.2.1 Model Validation Planning

The model validation planning of the cellular phone system is explained in Section 3.2.2.1. Before the model validation execution, it is assumed that code

verification for the used FE models was precisely exercised by the commercial FE analysis code, LS-DYNA. The calculation verification such as mesh convergence study went through before the model validation activities.

4.1.2.2 Model Validation Execution

This section is focused on the model validation execution in a hierarchical manner. The statistical model calibration is executed at two levels: LCD Panel (component level) and LCD Module (subsystem level). Finally the model validity check and virtual qualification are executed at the system level (cellular phone).

4.1.2.2(a) LCD Panel Validation (Component-Level)

Figure 9 displays the LCD module, which contains the LCD panel and other structural/electric components. The objectives of the LCD panel calibration are (1) to enhance the predictive capability of the LCD panel model through the statistical calibration and (2) to determine a failure criterion for an LCD panel. The validation planning identified a 3-point bending test for the LCD panel validation, and identifies the statistical property of the modulus of the panel elasticity (E) as the unknown model parameters. Figure 10 shows the 3-point bending test for the LCD panel. The cellular phone is facing upward. A load is applied at the center area and the two ends of the cellular phone are supported. As shown in Table 4, the test employed ten LCD panels. Both failure force and displacement data sets were used for the statistical model calibration. In the computational model, the failure forces were treated as the input, while the failure displacements were considered to be the response.

First, as explained in Section 3.2.2.2, the model variable characterization is performed to determine statistical model of the failure force (known model parameter

related with loading condition). The normal distribution (μ=7.578, σ=0.150) was found to be the most suitable for modeling the failure force of the LCD panel based on the K-S GoF, as shown in Table 5.

Table 4 LCD panel 3-point bending failure test results

Bending Test #	Displacement [mm]	Force [kgf]
1	1.604	7.597
2	1.627	7.405
3	1.529	7.516
4	1.809	7.105
5	1.489	7.550
6	1.586	7.594
7	1.484	7.883
8	1.547	7.769
9	1.388	7.469
10	1.499	7.572

Table 5 K-S GoF test for failure force in LCD panel

Distribution	K-S GoF Test	
	Result	p-value
Weibull	Accept	0.4661
Normal	**Accept**	**0.7296**

Second, the statistical calibration was conducted to determine the statistical properties of the elastic modulus (E) in the LCD panel. The calibration maximizes the likelihood function, the degree of the agreement between the observed and predicted failure displacement data. The calibration procedure is summarized as follows:

- Step 1: Set an initial calibration parameter vector (Θ), the statistics of the panel elasticity (E), and prepare the observed failure displacement test data.

- Step 2: Obtain the PDF of a failure displacement using the EDR method.

- Step 3: Evaluate the likelihood function.

- Step 4: Update the calibration parameter vector by maximizing the likelihood function.

- Step 5: Check whether the optimization process for the statistical calibration in Eq. (11) is converged.

- Step 6: If it is converged, stop the calibration procedure; otherwise go to Step 2.

The overall calibration procedure is summarized in Fig. 22(a). The calibration requires 205 simulations in total to calculate a likelihood value and its sensitivity. This computation was feasible with a parallel computing scheme. The PDF with the initial statistics of the panel elasticity was compared with the improved PDF having the calibrated statistics in Fig. 22(b). It is apparent that the likelihood value of the failure displacement is increased after the statistical calibration. The calibrated PDF of the failure displacement agrees well with the experimental data. As a result, the proposed validation determines the statistical property of the valid modulus of the panel elasticity, E ~ Lognormal(A, B). The parameters (A and B) are not disclosed since they are proprietary information of the sponsored company.

Third, the PDF of the panel failure stress is obtained using the updated computational model as displayed in Fig. 23. The obtained failure stress will be used for reliability prediction of the cellular phone system.
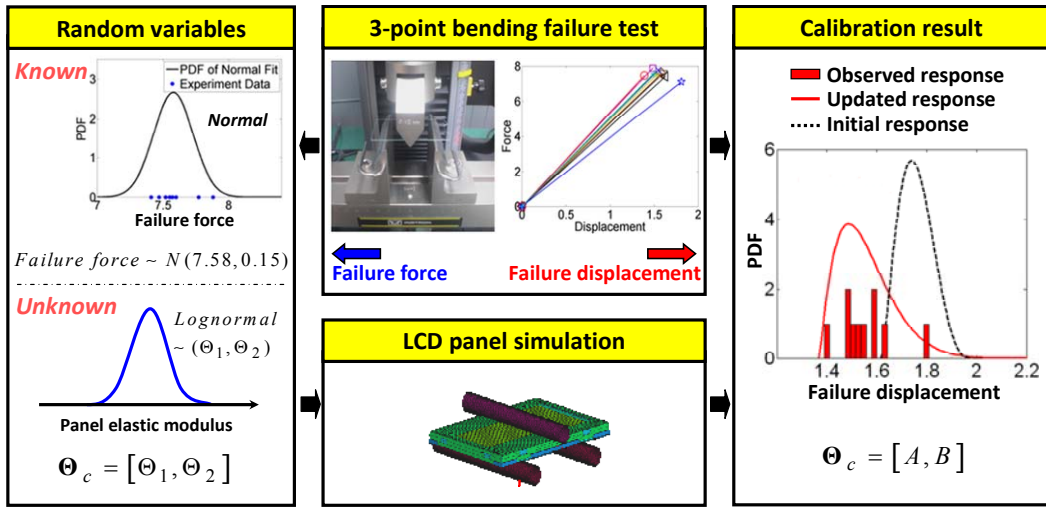
(a) Model calibration flow
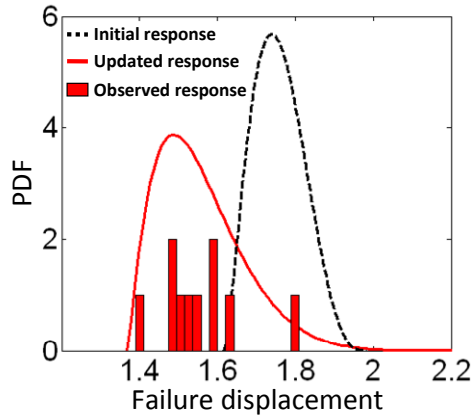
(b) Random output of failure displacement

Fig. 22. Statistical model calibration of LCD panel
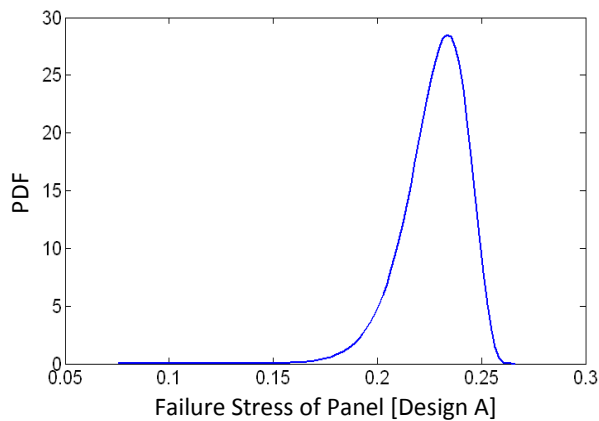
Fig. 23. Failure stress of a LCD panel (unit:GPa)

4.1.2.2(b) LCD Module Validation (Subsystem-Level)

The objectives of the LCD module validation are (1) to enhance the predictive capability of the LCD module and (2) to determine a failure criterion for a Driver IC mounted on the LCD module. The validation planning identified a dent failure test for the LCD module validation as shown in Fig. 9, and employed a sensitivity study to define the statistical properties of the unknown model variables (gap sheet thickness and tied scale factor between the layers 2 and 8). Table 6 shows the dent failure test results with ten LCD modules. Both failure force and displacement data sets were used for the model calibration. Similar to the LCD panel calibration, the failure force defined as the known parameter was modeled with a lognormal distribution (see Table 7).

Table 6 LCD module dent test results

Test number	Displacement [mm]	Force [kgf]
1	0.7459	2.123
2	0.9270	2.848
3	1.1337	3.250
4	0.7494	2.142
5	0.6379	1.814
6	0.9169	2.523
7	0.8379	2.508
8	0.8976	2.631
9	0.6308	1.861
10	0.7668	2.181

Table 7 Hypothesis test for failure force in LCD module

| Distribution | K-S GoF Test | |
	Result	*p*-Value
Weibull	Accept	0.8364
Normal	Accept	0.8602
Lognormal	**Accept**	**0.9348**
Gamma	Accept	0.8792

Next, the statistical calibration was executed to determine the statistical properties of the gap sheet thickness and tied scale factor in the LCD module. The overall calibration procedure is the same as that in Section 4.1.2.2(a). The calibration maximizes the likelihood function between the observed and predicted failure displacement data. The uncertainty propagation analysis employed two known random variables: Panel E ~ Lognormal(A, B) and Failure force ~ Lognormal(0.853, 0.187), where the parameters were two lognormal distribution parameters, respectively. The calibration requires 945 simulations in total. As a result, the proposed calibration of the LCD module determined the calibration parameters of the unknown model variables, gap sheet thickness ~ Normal(C, D) and tied scale factor ~ Normal(F, G). The parameters (C, D, F and G) are not disclosed since they are proprietary information of the sponsored company. Finally, the PDF of the Driver IC failure stress in the LCD module was also obtained using the calibrated LCD module model as displayed in Fig. 24.
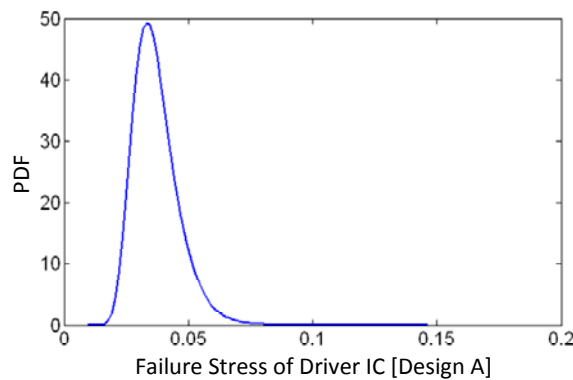
Fig. 24. Failure stress of a Driver IC (unit: GPa)

4.1.2.2(c) Cellular Phone Validation (System-Level)

The calibration models of the component and subsystem were included in the computational model of the system. A full-set dent simulation model was constructed

68

for the validity check. Figure 8 shows the dent simulation for a full set, and Table 8 lists the statistical properties of random variables in the full set model. The hierarchical model calibration process for the cellular phone model is advantageous for two reasons. First, this process provides the valid failure margins (or failure stresses) of the LCD panel and Driver IC from Sections 4.1.2.2(a) and 4.1.2.2(b). Second, the hierarchical model calibration built the calibrated model, whose predictive capability was maximized for the cellular phone system. The calibrated cellular phone system model and failure margins can be used for the validity check about reliability of system.

Table 8 Properties of random variables in the full set model

Random variables	Distribution type	Mean	Standard deviation
X1 (panel E)	Lognormal	A	B
X2 (Gap sheet T)	Normal	C	D
X3(Tied scale factor)	Normal	F	G

Uncertainty propagation analysis for the cellular phone system (design A) model assesses the PDFs of the stresses (dashed curves) in the LCD panel (lower and upper glasses) for a given dent loading as shown in Fig. 25. The PDFs of the stresses (dashed red curves) in Driver IC (three different designs) for a given dent loading are shown in Fig. 26. The failure stress PDFs (solid curve) in Figs. 26(a)-(c) were also obtained using the LCD module models with different designs. The PDFs were different because different materials were used for the different Driver IC designs. The three designs were identified by the cellular phone developers over a design domain. The designs are not disclosed since they are proprietary information of the sponsored company.

In the cellular phone system, the stress in LCD panel and Driver IC for a given dent loading could not be directly measured. Due to this limitation, the validity check could not be statistically executed using the hypothesis test for validity check in Section 3.4. The validity check was thus executed by comparing the predicted reliability with a tested survival rate. The integration of the constraint (= stress − failure margin ≤ 0) over a random stress domain gives the predicted reliabilities for the LCD panels and Driver ICs.
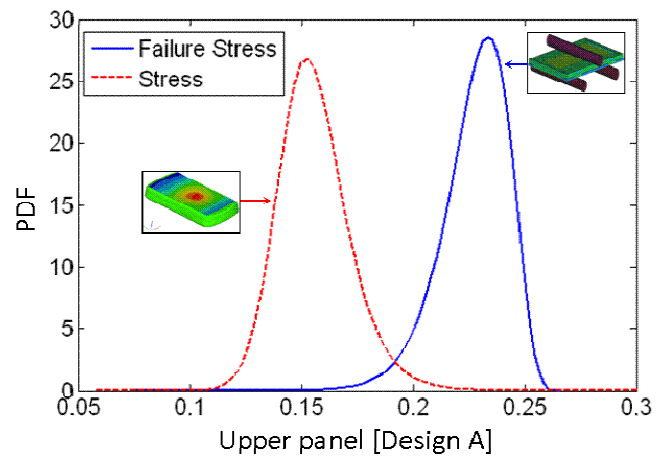
(a) Upper panel
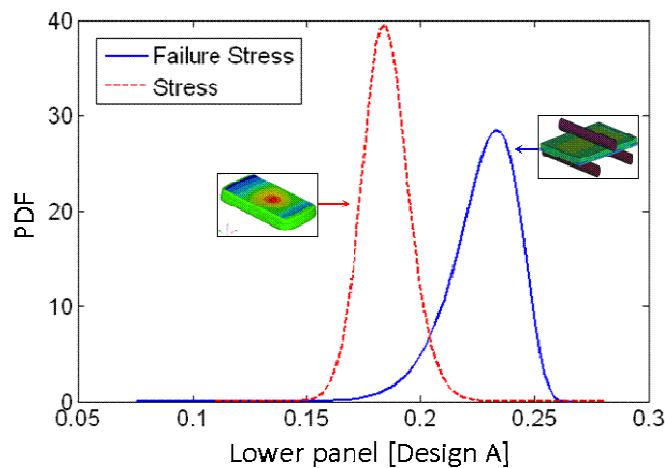
(b) Lower panel

Fig. 25. Predicted failure stress and marginal stress in glass panels

(a) Design A
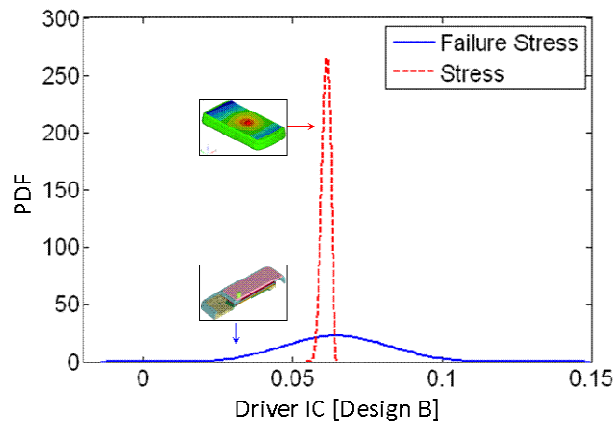
(b) Design B
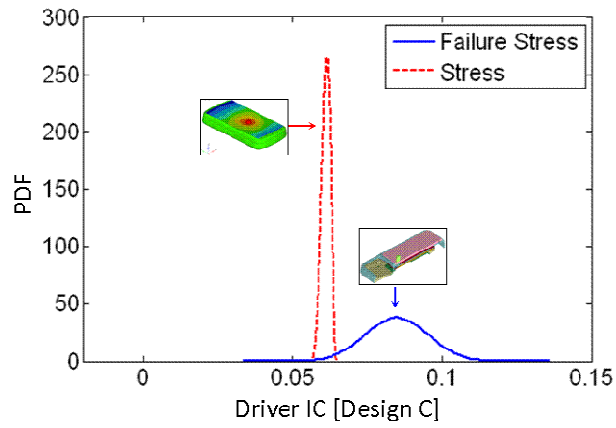
(c) Design C

Fig. 26. Predicted failure stress and marginal stress in Driver IC in the full set

Table 9 shows the reliabilities of the LCD panel and Driver IC, which are compared to the survival rates with five samples. For this comparison, five experimental data are grossly insufficient; however, the fabrication cost of five cellular phones amounted to about $60,000. In total, this validity check cost $180,000 for three designs. Due to this practical difficulty, it was not possible to increase the amount of test data.

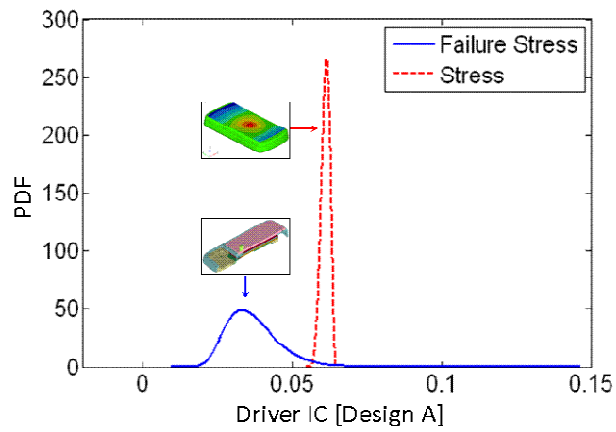Although it is difficult to extract statistical implication, the validity check results were very consistent for the three different designs. Therefore, we conclude that this study demonstrates the feasibility of the proposed hierarchical model calibration approach.

Table 9 Predicted reliability vs. tested survival rate

	Predicted Reliability	Tested Survival Rate
Upper Panel(Design A)	99.66%	5/5
Lower Panel(Design A)	97.56%	5/5
Driver IC(Design A)	1.81%	0/5
Driver IC(Design B)	57.56%	3/5
Driver IC(Design C)	99.47	5/5

4.1.2.3 Discussion

A hierarchical model validation was employed to the cellular phone system. In the validation planning phase, the system was decomposed in a systematic manner, based on ample understanding of the failure mechanisms, performance of interest of engineered system, available computation models and experimental resources. Specifically, this planning identifies vital computational models, modeling details, simulation tools, experimental tests, available resources for test samples at any hierarchical level. Then, the statistical model calibration was planned to determine the most significant but unknown model variables using expert opinion and a

72

sensitivity study. This planning helps define the calibration problems in all hierarchical levels. The validation execution took a bottom-up approach. The statistical model calibration was applied to improve the predictive capability of a computational model at any hierarchical level using the statistical calibration technique. This technique compares the observed test results with those predicted from the computational model in a statistical manner. This study used the likelihood function as the comparison metric, and employed the unconstrained optimization to maximize the likelihood function for determination of the unknown model variables. This hierarchical model validation was sequentially executed from the lowest hierarchical model to the highest with cellular phone computational models. It was observed that the proposed hierarchical model validation worked out very effectively for the cellular phone system to predict the system reliability. In this validation activity, the collaboration and shared expertise between researchers in industry/academia and simulation/experiment was another key to make the predictive model feasible.

4.1.3 Model Validation of a TFT-LCD Panel

4.1.3.1 Model Validation Planning

The proposed validation framework is employed to validate a computational model of a TFT-LCD panel (see Fig. 27(a)). This validation (1) enhances the predictive capability of the LCD panel model through the statistical model calibration and (2) evaluates the fidelity of the calibrated model with a hypothesis test for validity check. The overall validation procedure is similar with that in Section 4.1.2.2(a). The 3-point bending test employed thirty TFT-LCD panels. For the

experiments of top-x direction (i.e. the Driver IC is facing upward and jig is parallel to x axis), top-y direction (i.e. jig is parallel to y axis) and bottom-x direction (i.e. the Driver IC is facing downward) as shown in Fig. 27(b), three sets of ten TFT-LCD panels were prepared. While experimental data of top-x and top-y directions were used for statistical model calibration, those of bottom-x direction were used for validity check. The elastic moduli of glass panel (E_g) and polarizer in y direction (E_{p_y}) were selected as unknown model variables.

(a) Configuration of TFT-LCD panel   (b) Experimental settings
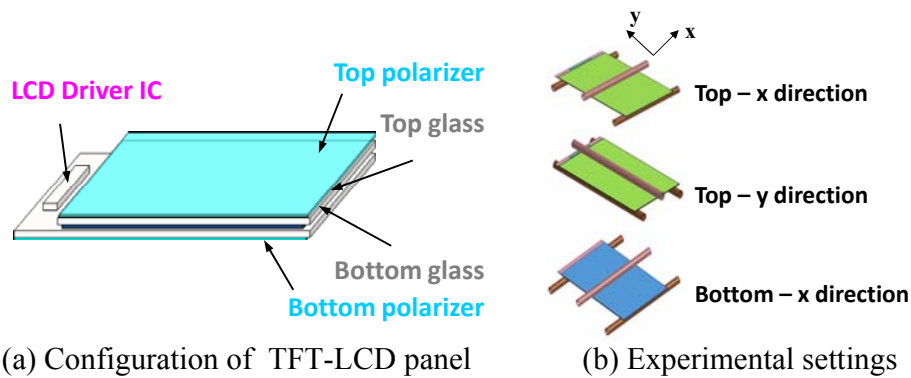
Fig. 27. The computational model of TFT-LCD panel

4.1.3.2 Model Validation Execution

4.1.3.2(a) Statistical Model Calibration

As shown in Figs. 28 and 29, the 3 point bending tests of top-x direction and top-y direction were performed with twenty TFT-LCD panels. In the computational model, the failure displacement was treated as the input, while the failure force was considered to be the response. First, the model variable characterization was performed to determine the statistical model of the failure displacement (known model variable related with loading condition). The lognormal distributions (μ=1.527, σ=0.09 for the test of top-x direction; μ=0.622, σ=0.232 for the test of top-y direction) were found to be the most suitable for modeling the failure displacement

74

of the TFT-LCD panel based on the K-S GoF test. Next, the statistical calibration was conducted to determine the statistical properties of the elastic moduli of glass panel (E_g) and polarizer (E_{p_y}). The statistical model calibration maximized the likelihood function, the degree of the agreement between the experimental results (test data of top-x direction and top-y direction) and PDFs of the predicted failure force. The overall calibration procedure is summarized in Figs. 28 and 29. The calibrated PDF of the failure force agrees well with the experimental data. It is apparent that the likelihood value of the failure force is increased after the statistical calibration. As a result, the proposed validation determines the statistical property of the valid elastic moduli of E_g ~ Lognormal(72.128, 2.858) and E_{p_y} ~ Lognormal(3.397, 1.294).
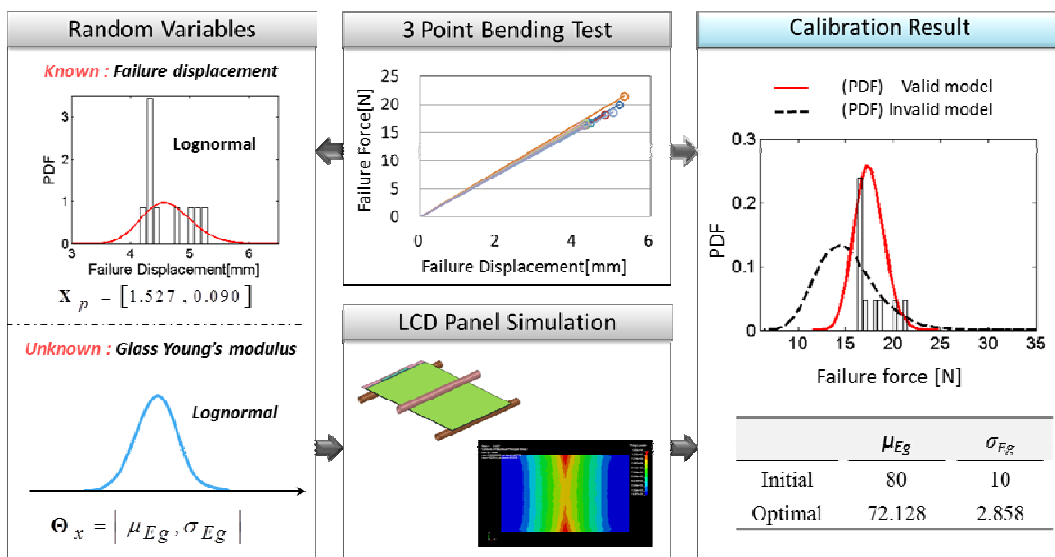
Fig. 28. Statistical model calibration of TFT-LCD panel: top-x direction
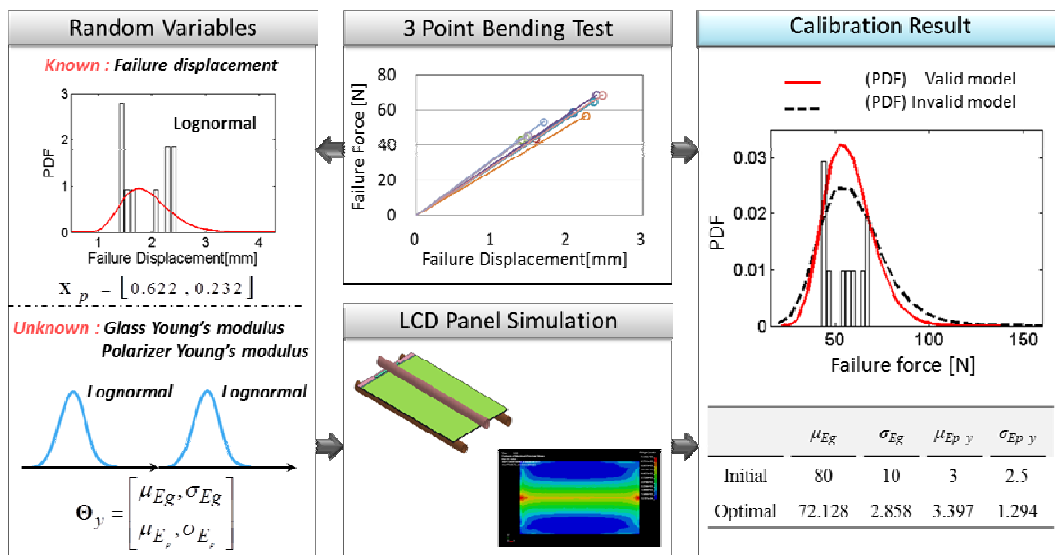
Fig. 29. Statistical model calibration of TFT-LCD panel: top-y direction

4.1.3.2(b) Hypothesis Test for Validity Check

For the hypothesis test, the PDF of the predicted failure force was compared with the data of bottom-x direction test as shown in Fig. 30. The model variable characterization was first performed and the lognormal distributions (μ=1.856, σ=0.112 for the test of bottom-x direction) was found to be the most suitable for modeling the failure displacement. With the statistical model of E_g, the PDF of failure force was predicted as shown in the right box of Fig. 31. Based on the graphical comparison, the predicted PDF showed good agreement with experimental data.

76
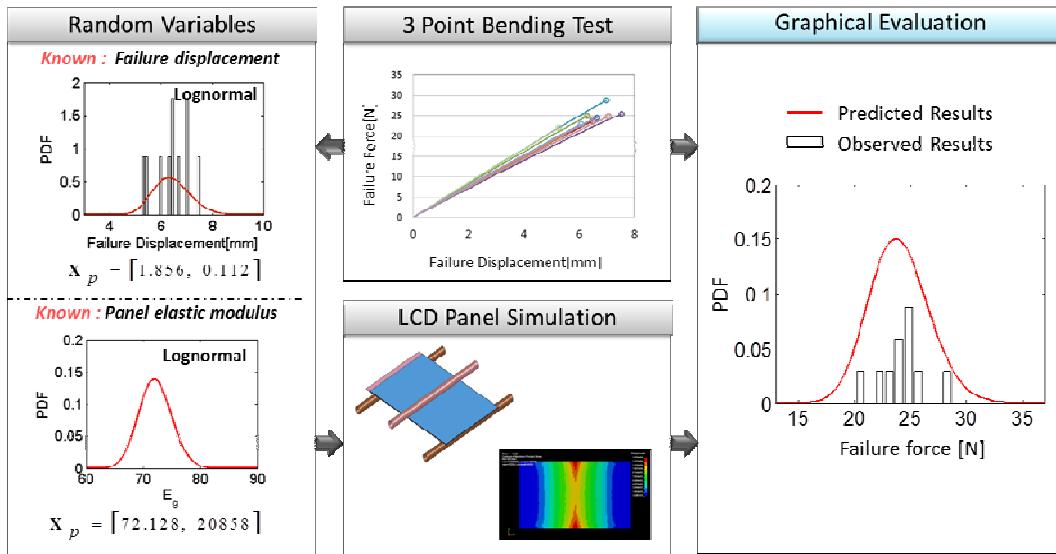
Fig. 30. Predicted PDF for validity check: bottom-x direction

An approach based on a significance level was employed. The area metric (U_m) between the predicted response and experimental data in Fig. 31(a) was 0.0732 as shown in Fig. 31(b). The critical value of the area metric at a significance level of 0.05 is $D_i(\alpha) = 0.1805$ in case ten experimental data are used for the validity check as depicted in Fig. 32. The null hypothesis would not be rejected since U_m (=0.0732) is far less than the $D_i(\alpha)$ (=0.1805). At this significance level, there is insufficient evidence to conclude that the calibrated model is invalid.

(a) Predicted and observed failure force   (b) Calculation of area metric
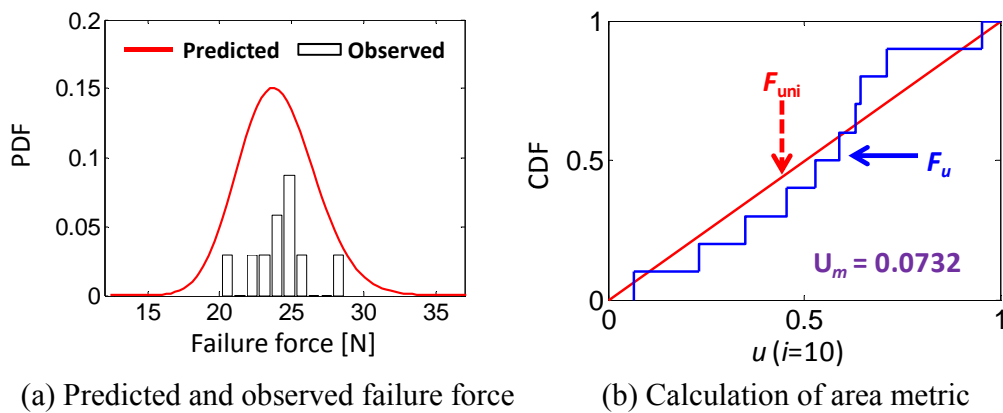
Fig. 31. Hypothesis test for validity check: bottom-x direction
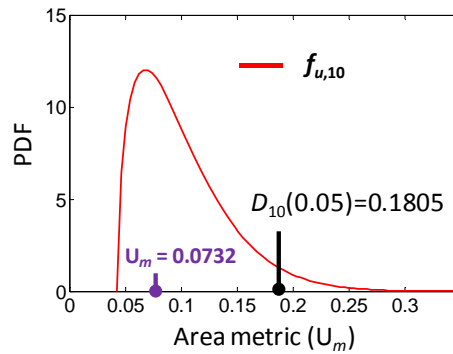
Fig. 32. PDF of area metric (i=10)

4.1.3.3 Discussion

A statistical model calibration was employed to the computational model of a TFT-LCD panel. The unknown model variables, elastic moduli of glass panel and polarizer were obtained by maximizing likelihood function. The validity of the calibrated model was evaluated with the hypothesis test for validity check. Using a significance level of 0.05, the calibrated model was assessed as valid. This case study shows that the proposed validation techniques can systematically construct a computational model of a TFT-LCD panel with high accuracy.

78

4.2 Tire Tread Block

The braking and cornering performances of a tire are highly related with a friction force between a tire and a road surface. The consideration of a single tread block, detached from a tire body, enables investigation of a friction behavior of a tire. Therefore, the tread block test (or block FE analysis) in Fig. 33 are widely used to measure (or predict) friction forces of tread blocks with different designs. In this case study, a computational model for block FE analysis was developed using the proposed statistical validation framework.

4.2.1 Overview of Problem

Figure 33 shows configuration of the block test and simulation. Top surface of a tread block specimen is fixed to a steel plate and bottom surface contacts a road surface as shown in Fig. 33(a). After applying a specific loading, the tread block specimen is pulled along x-direction in a constant velocity, and a friction force is measured.

(a) Tread block tester

(b) Tread block FE model (design A, size: 30×30×8mm)
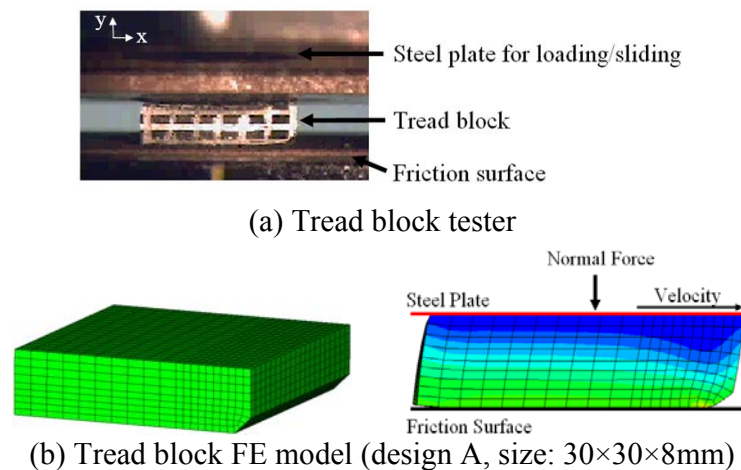
Fig. 33. Tread block tester and FE model

Commercial FE software, Abaqus, is used for the block FE analysis. As an activity of model verification [3], grid (mesh) density was adjusted properly to reduce discretization error in FE model. The most crucial aspect of the block analysis is the realistic description of a friction model. Generally, the friction model is a function of a contact pressure (φ) and a sliding velocity [123,124]. In the tread block tester, the sliding velocity is precisely controlled as 1cm/sec, thus this study employs a contact pressure-dependent model as

$$\mu_f = \mu_0 \times \left(\frac{\varphi}{\varphi_{ref}} \right)^{-\upsilon} \tag{22}$$

where μ_f is friction coefficient; φ_{ref} is reference contact pressure (= 1.0E5 Pa); υ is pressure exponential parameter; μ_0 is a friction coefficient when pressure is equal to φ_{ref}. The true values of two model parameters, υ and μ_0, vary according to the materials and the pair of surfaces in contact.

4.2.2 Model Validation Planning

Model validation planning follows three steps explained in Section 3.2.2.1. The performance of interest (PoI) of the block analysis is a friction force between a tread block and a road surface. In this case study, model decomposition is not necessary because the tread block is a simple system with one tier. The tread block model has three random input variables: elastic modulus of a rubber and two friction model parameters (μ_0, υ). While the elastic modulus is classified as known model variable, the friction model parameters (μ_0, υ) are grouped as a set of the unknown model variables. To characterize the elastic modulus of the rubber, tensile tests with twelve samples (size: 2.62×5×20mm) are prepared. For statistical calibration, twenty-four

solid block specimens (see Design A in Fig. 33(b)) are fabricated. Tests are executed under four different normal loading conditions (3, 5, 7 and 9 kg/cm^2) that are selected based on tire operating conditions. Figure 34 shows transient responses of measured friction forces with six tread blocks in case normal loading is 3 kg/cm^2. After one second from the starting of the test, the friction force is almost converged with little fluctuation. It is assumed that the fluctuation of friction force is mainly due to the wear of the rubber. In such reason, the friction forces measured at the time of two second are used for the model validation.
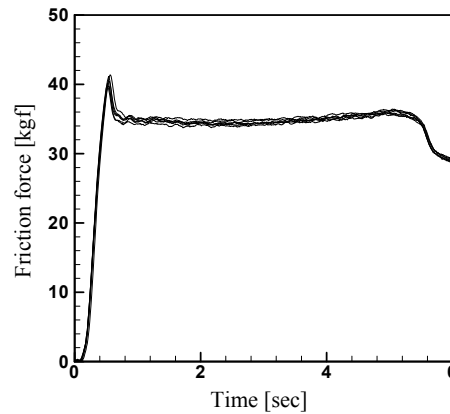
Fig. 34. Measured friction forces (normal loading=3kg/cm^2)

In this case study, the response surface models were constructed to reduce computational effort for FE analyses during statistical model calibration. After model calibration, hypothesis test for validity check and virtual qualification are carried out one by one.

4.2.3 Model Validation Execution

The model validation execution consists of three steps: (Step 1) model variable characterization, (Step 2) statistical model calibration, (Step 3) hypothesis test for validity check.

(Step 1) Model variable characterization: Tensile tests were conducted to characterize elastic modulus of rubber specimens as shown in Fig. 35. The ambient temperature and cross-head speed were set to 23°C and 500mm/min, respectively. The ten percent modulus of each sample was used as representative of elastic modulus, and the statistical model of the elastic modulus was constructed as shown in Fig. 36. The Weibull distribution (7.77, 22.07) is found as the most suitable distribution.
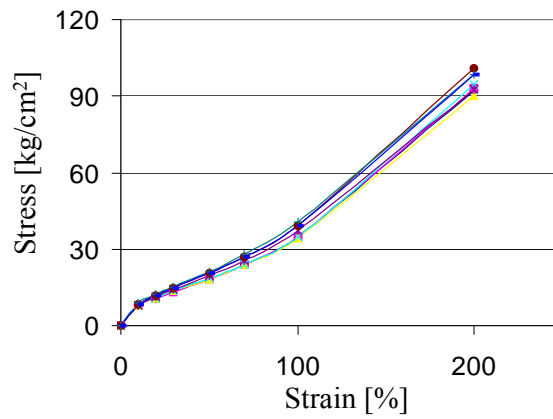
Fig. 35. Tensile test results of twelve rubber samples
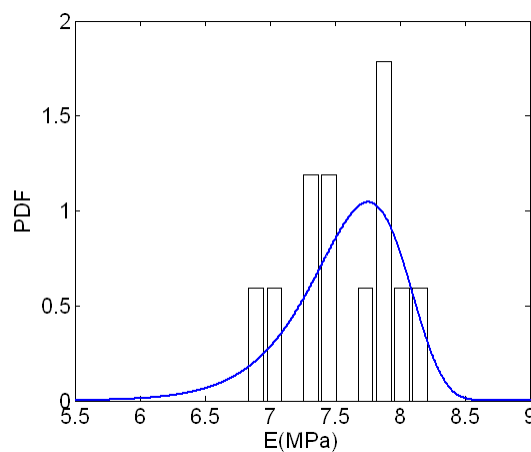
Fig. 36. Statistical distribution of elastic modulus

(Step 2) Statistical model calibration: Response surface models of three model variables (μ_0, υ and elastic modulus) were constructed with block FE analyses under 4 different operating conditions (3, 5, 7 and 9 kg/cm^2 normal loading). Figure 37 shows the response surface model of a 3kg/cm^2 normal loading condition. For a DOE table, four-level full factorial design was used. It is checked that all the response surface models well represents the results of FE analyses in the calibration domain. The statistical model calibration was employed by comparing experimental data with predicted results. The calibration parameter vector (Θ) includes mean and standard deviation of two unknown model variables (μ_0 and υ) since it is assumed that μ_0 and υ follows normal distribution. Table 10 summarizes calibration results. The predicted friction forces after statistical calibration show good agreement with experimental results as shown in Fig. 38.
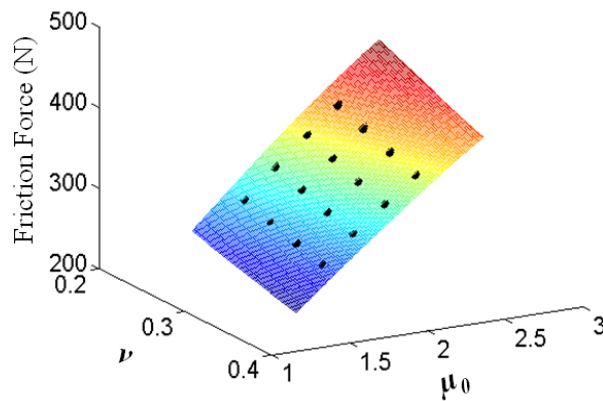
Fig. 37. Response surface model (normal loading = 3kg/cm^2)

Table 10 Updated calibration parameters of friction model

Random parameters	Normal Distribution	
	Mean	Standard deviation
μ_0	1.875	0.0246
υ	0.258	0.011

83
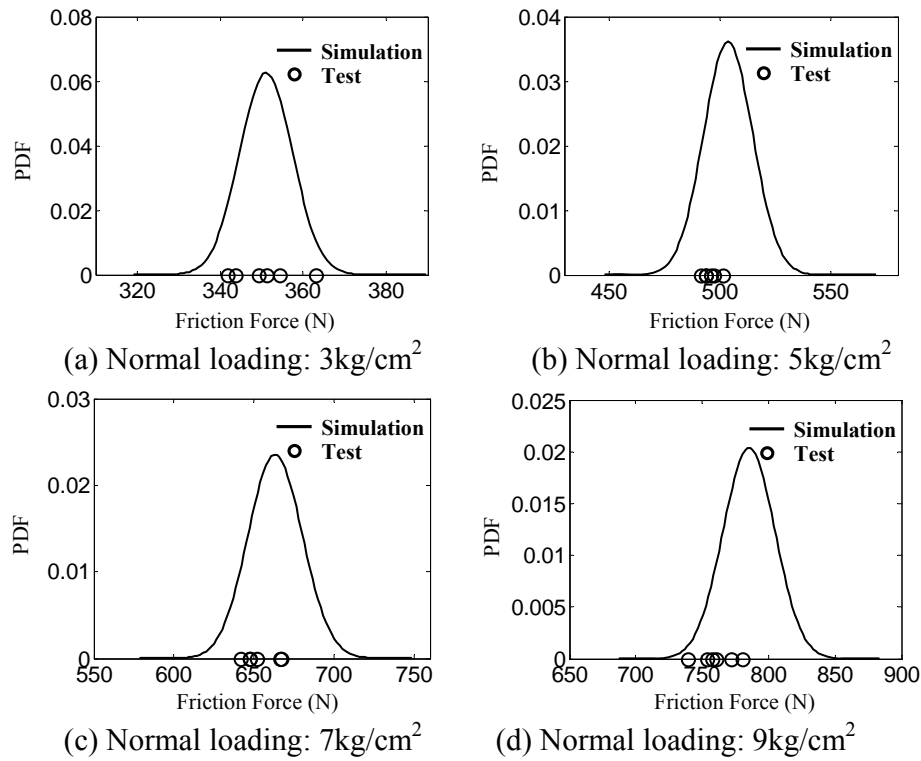
Fig. 38. Predicted and observed results after model calibration

(Step 3) Hypothesis test for validity check: An approach based on a type 2 error was employed. Twelve tread blocks of two alternative designs as depicted in Fig. 39 (six blocks for design B and six blocks for design C) were fabricated for the validity check experiments. The area metric (U_m) was 0.0525 that was calculated by comparing eighteen test data with corresponding predicted PDFs as shown in Fig. 40. Based on expert knowledge, the maximum allowable DoI was set to 40%. Then, the critical value, D_{18}, is 0.1 as shown in Fig. 21(b). Because U_m is less than the D_{18}, it is concluded that the calibrated model is valid, and the DoI between predicted and observed results is less than 40% with 100% confidence.

84
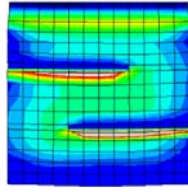
(a) Design B (longitudinal groove)   (b) Design C (vertical groove)
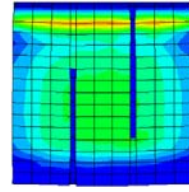
Fig. 39. Two design alternatives (contour: contact pressure)
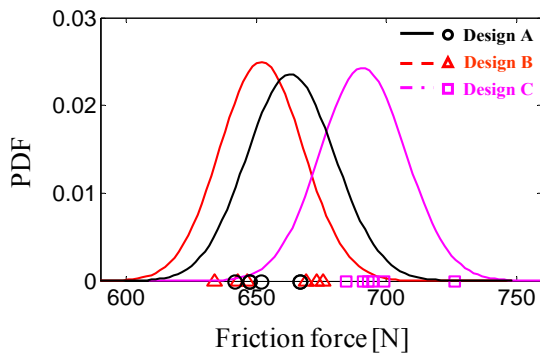
(a) Observed and predicted results   (b) Calculation of U$_m$
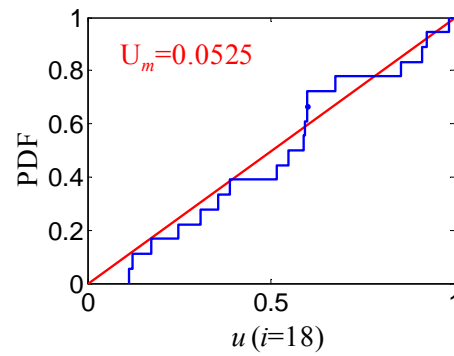
Fig. 40. Predicted and observed results (normal loading = 7kg/cm^2)

4.2.4 Virtual Qualification

Relative qualification is demonstrated with three PDFs of different designs in Fig. 40(a). Figure 41 shows the design decision matrix. A value in the upper triangular part of the matrix indicates the probability that one design is better than the other. For example, the probability that Design C is better than the Design B is 95.61%. Design C, which has groove along x-direction (see Fig. 39(b)), has the higher probability than the other designs. It is because of different contact pressure distributions that affect to the friction coefficient of the blocks in Eq. (22).

The statistical evidence in the design decision matrix can save time and cost of model development by reducing a confliction between predicted and experimental results, which is frequently occurred in traditional virtual testing activities. For

example, a deterministic computational model predicts design A is better than design B; however, the experimental results sometimes reveals that design B is better than design A. Without statistical evidence on predicted responses, it may be easy to conclude the computational model is invalid and reinvest to develop a new computational model although the model is valid in a statistical sense.

(%)	Design C	Design A	Design B
Design C >	50.00	88.01	95.61
Design A >		50.00	68.48
Design B >			50.00

Fig. 41. Example of design decision matrix (normal loading = 7kg/cm^2)

4.2.5 Discussion

The proposed model validation techniques were successfully applied to enhance predictive capability of the tread block FE model. Uncertainty in elastic modulus was first quantified using experimental data. Statistical models of unknown model variables (μ_0, v) were obtained by the statistical model calibration. The hypothesis test for validity check proved that the calibrated model is valid in a statistical sense. Relative qualification was demonstrated with the design decision matrix that provides statistical evidence for rational decision-making on new product designs. This case study shows that the validation framework is likely applicable to tire tread block problem to improve and assess the predictive capability of the block FE model.

4.3 Thermal Challenge Problem

In this case study, the statistical model validation was applied to the thermal challenge problem that was devised to compare various model validation approaches in the validation challenge workshop [16]. It is a heat conduction problem to predict a temperature in a body of a solid slab at a specific location and time.

4.3.1 Overview of Problem

Figure 42 shows the schematic of thermal challenge problem, i.e. a solid slab with thickness, *L*.
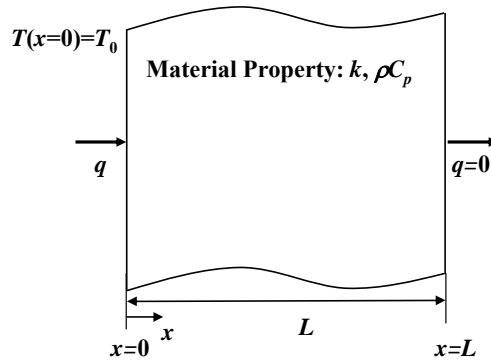
Fig. 42. Schematic of thermal challenge problem

The boundary conditions are heat flux, *q*, on the face with zero distance(*x*=0) from the surface to the point being measured and adiabatic on the *x=L* face. The problem has two thermal properties, thermal conductivity, *k*, and volumetric heat capacity, ρC_p. The computational model is based on one-dimensional, linear heat conduction in a slab. The temperature in the body at a specific location and time is calculated as

$$\hat{Y} = T(x,t) =$$

$$T_i + \left[\frac{qL}{k} \frac{(k/\rho C_p)t}{L^2} + \frac{1}{3} - \frac{x}{L} + \frac{1}{2}\left(\frac{x}{L}\right)^2 - \frac{2}{\pi^2} \sum_{n=1}^{6} \frac{1}{n^2} e^{-n^2\pi^2 \frac{(k/\rho C_p)t}{L^2}} \cos\left(n\pi \frac{x}{L}\right) \right] \quad (23)$$

87

where x is the distance from the surface to the point being measured; t is time; and T_0 (= 25°C) is the initial temperature of the device at t=0.

Three sets of experimental data are provided: (1) material characterization (MC) data, (2) ensemble validation (EN) data and (3) accreditation validation (AC) data. In the MC data, the thermal properties, k and ρC_p, are measured over the temperature range of the validation database and intended application as depicted in Fig. 43. It is note that k looks dependent on the temperature, but ρC_p has not tendency to temperature. In the ensemble validation experiment (EN data), four sets of experiments are conducted at different thicknesses and heat flux magnitudes with randomly selected four specimens (see Table 11). The experimental data are measured at discrete time spots with time interval 100sec within 0~1000sec. In the accreditation validation experiment (AC data), three sets of experiments at different thicknesses and heat flux magnitudes, which are different from the values investigated during the ensemble validation, are conducted with two specimens, respectively (see Table 11). The measured time interval is 50sec within 0~1000sec. All the test data are described in Ref. [125].

(a) Thermal conductivity, k (b) Volumetric heat capacity, ρC_p
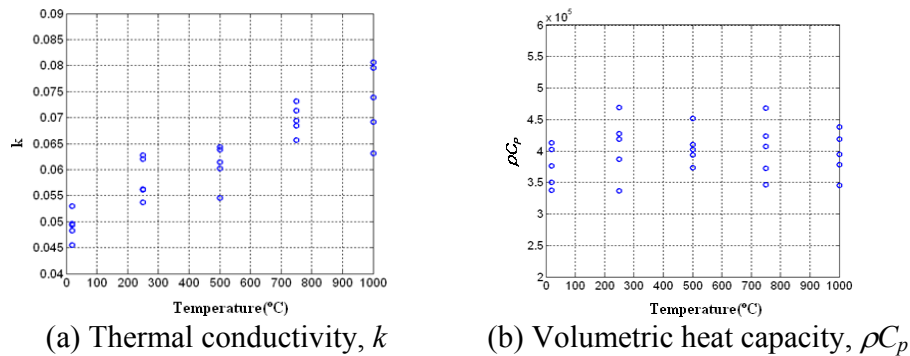
Fig. 43. Material characterization(MC) data

Table 11 Configuration of experiment sets

Data Set	Configuration Number	x(cm)	q(W/m^2) , L(cm)
EN	Configuration 1	$x=0$	$q=1000, L=1.27$
	Configuration 2		$q=1000, L=2.54$
	Configuration 3		$q=2000, L=1.27$
	Configuration 4		$q=2000, L=2.54$
AC	Configuration 5.1	$x=0$	
	Configuration 5.2	$x=L/2$	$q=3000, L=1.90$
	Configuration 5.3	$x=L$	

The failure probability of a system under the application condition is the PoI of the thermal challenge problem, and a predicted failure probability is defined as

$$p(T_s(t=t') > T_f) < p_f \qquad (24)$$

where p indicates a probability. T_s is measured temperature at a specific time, t', after exposure to a heat flux. T_f is a failure temperature (marginal temperature) and p_f is a marginal failure probability. Table 12 shows the application condition where the failure probability is predicted.

Table 12 The application condition for failure probability prediction

x(cm)	q(W/m^2)	L(cm)	T_f(ºC)	t'(sec)	p_f
0.0	3500	1.9	900	1000	0.01

4.3.2 Model Validation Planning

The PoI is the failure probability in Eq. (24). Similar with the tread block problem, this problem only has one tier, the system level. The computational model has two random variables, k and ρC_p, and two controllable variables, q and L. k and ρC_p are first characterized with the MC data. Three scenarios are considered to find out the best statistics for the variables. Next, the statistical model calibration is used to refine the characterized k and ρC_p with the EN data. Finally, validity check is

performed with the AC data, and virtual qualification is performed under the operating condition.

4.3.3 Model Validation Execution

The model validation execution consists of three primary parts: (Step1) the model variable characterization, (Step 2) the statistical model calibration, (Step 3) the hypothesis test for validity check.

(Step 1) Model variable characterization: For the characterization of random variable, k, two cases are were considered: (a) k is not dependent on temperature and follows normal distribution, and (b) k is dependent on temperature. For the case (a), the K-S GoF hypothesis test is was employed with all the MC data in Fig. 43(a). The initial statistics of k are listed in Table 13. For the case (b), k is was modeled with linear regression model on temperature as

$$k(T) = \xi_1 + \xi_2 \cdot T \qquad (25)$$

The regression coefficients are listed in Table 13. When it comes to volumetric heat capacity (ρC_p), the K-S GoF test is was employed with MC data in Fig. 43(b). Unlike the other journal papers in which ρC_p is assumed as the normal distribution [11,18-20,35], the lognormal distribution is also considered. The results of the K-S GoF test results and calculated statistics are listed in Table 14 and 15, respectively.

Table 13 Statistical model of the thermal conductivity

Distribution type	Characterized statistics		
Normal	μ_k 0.06284		σ_k 0.0099
Linear regression	ξ_1 0.0505	ξ_2 2.25E-5	$\hat{\sigma}$ 0.0047

Table 14 K-S GoF test of the volumetric heat capacity

Distribution type	p-Value
Normal	0.8768
Lognormal	0.9454

Table 15 Statistical model of the volumetric heat capacity

	ρCp	
Normal	$\mu_{\rho Cp}$ 393900	$\sigma_{\rho Cp}$ 36252
Lognormal	$\mu_{\rho Cp}$ 12.88	$\sigma_{\rho Cp}$ 0.0914

To evaluate the statistics of k and ρCp, three scenarios were considered as listed in Table 16. Predicted response (mean and 95% confidence intervals (CIs)) and the EN data of scenarios are plotted in Figs. 44, 45, and 46. It can be easily proved by Figs. that the PDF of scenario II and III show better agreement with EN data than scenario I. Likelihood and area metrics were calculated to quantitatively determine the best scenario. High likelihood and low area metrics mean better agreement with test data. The scenario III was evaluated as the best scenario (see Table 17).

Table 16 Three scenarios for random parameter characterization

	k	ρCp
Scenario I	Normal	Normal
Scenario II	Linear Regression	Normal
Scenario III	Linear Regression	Lognormal

Table 17 Metrics for scenario selection

	Likelihood Estimation	Area metric
Scenario I	-301.1	0.1812
Scenario II	-276.4	0.0508
Scenario III	-274.2	0.0393
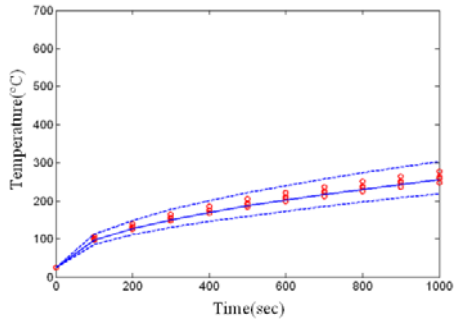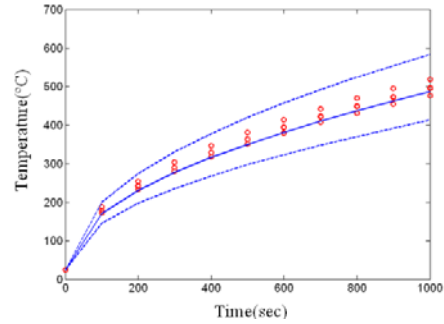
(a) Configuration 2   (b) Configuration 4

Fig. 44. Predicted temperature profile of scenario I and EN data
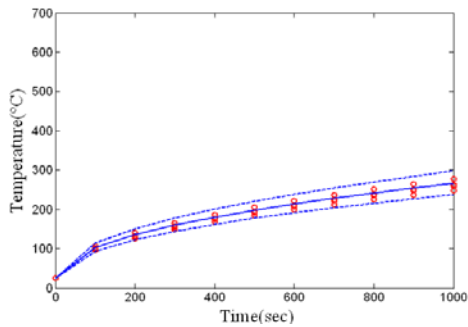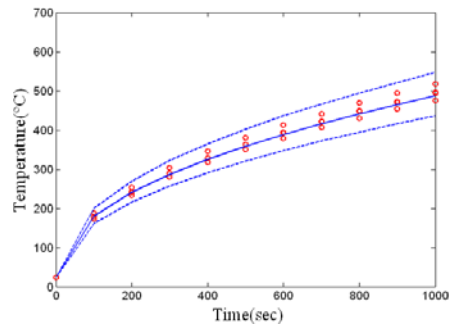
(a) Configuration 2   (b) Configuration 4

Fig. 45. Predicted temperature of scenario II and EN data
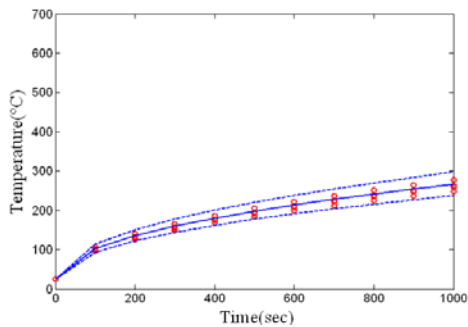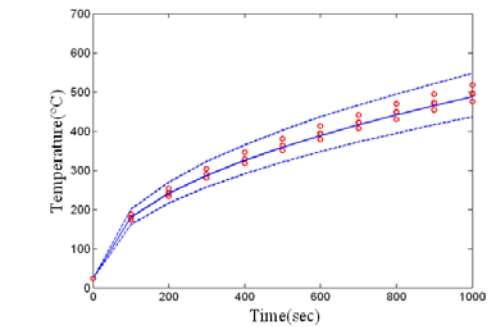
(a) Configuration 2   (b) Configuration 4

Fig. 46. Predicted temperature of scenario III and EN data

(Step 2) Statistical model calibration: The statistical model calibration was executed to refine the statistics of k and ρCp with the EN data. The calibration approach can be divided into two stages due to the temperature dependency of the k: (Stage 1) to find a converged temperature profile with respect to the dependency of

92

$k(T)$ on temperature, and (Stage 2) to find optimal statistics of k and ρCp by the statistical model calibration. Fig. 47 shows the calibration procedure.

• Stage 1: In a closed-loop situation where output temperature is not only the response of a computational model but also a factor changing the k (one of the model input variables), k should be iteratively updated according to the change of output temperature. Starting from the initial value of k, output temperature is first obtained. After that, k is recalculated based on the obtained output temperature. The resulting value of k conditional on current temperature is then used to calculate next output temperature. This process is repeated until the k and temperature distribution is converged to a specific value.
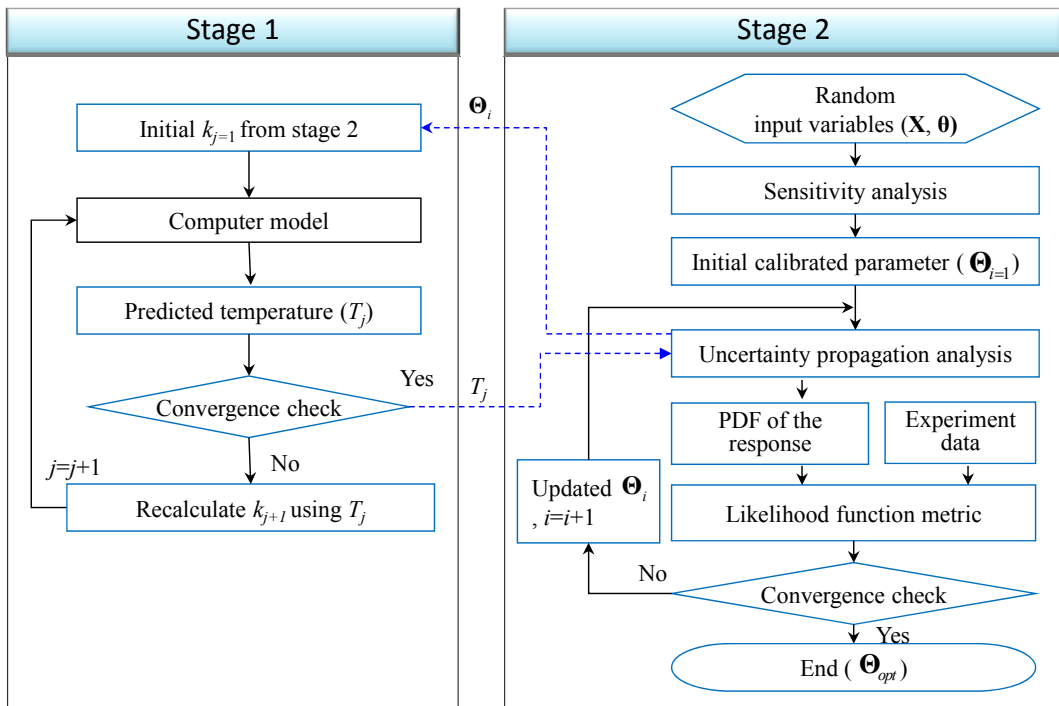
Fig. 47. Model calibration procedure of thermal challenge problem

• Stage 2: Statistical model calibration is conducted with the EN data (Configuration 1, 2, 3 and 4). The updated calibration parameters should be passed to the first

93

stage to find converged temperature profile for UP analysis. Table 18 and Fig. 48 show the optimal values of calibrated parameters and the predicted temperature profile after model calibration. After the model calibration, likelihood value is increased from -274.2 to -272.8 and area metric is decreased from 0.0393 to 0.0333.

Table 18 Model variables after statistical model calibration

	K			ρCp	
β_1	β_2	$\hat{\sigma}$	$\mu_{\rho Cp}$	$\sigma_{\rho Cp}$
0.05326	1.452E-5	0.002145	12.8569	0.08940

(a) Configuration 2   (b) Configuration 4
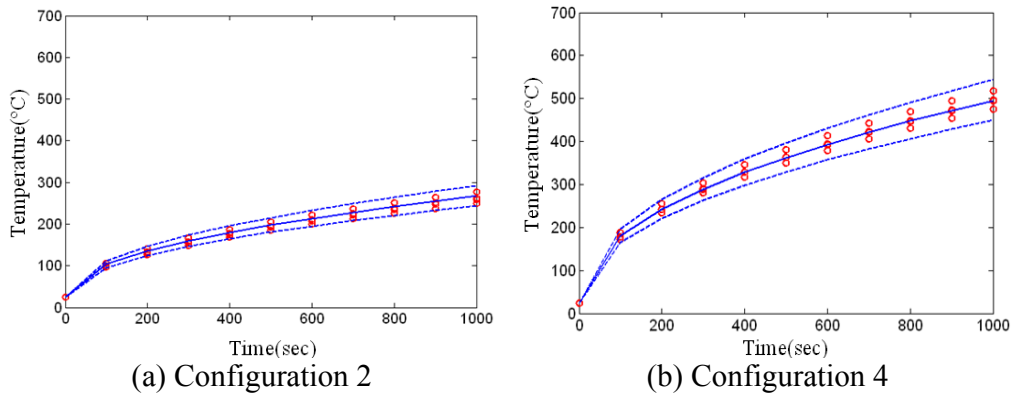
Fig. 48. Predicted temperature profile after model calibration and EN data

(Step 3) Hypothesis test for validity check: Figure 49 shows the predicted temperature of the calibrated model (mean and 95% CIs) and the AC data (Configuration 5.1-5.3). Validity check is performed with the six data at 1000 sec as shown in Fig. 50. The area metric is first calculated as shown in Fig. 51(a). With a 5% significance level, we cannot reject the hypothesis test since the area metric (0.191) is less than the critical value (0.2375); therefore, the calibrated model is evaluated as valid.

(a) Configuration 5.1   (b) Configuration 5.2

(c) Configuration 5.3
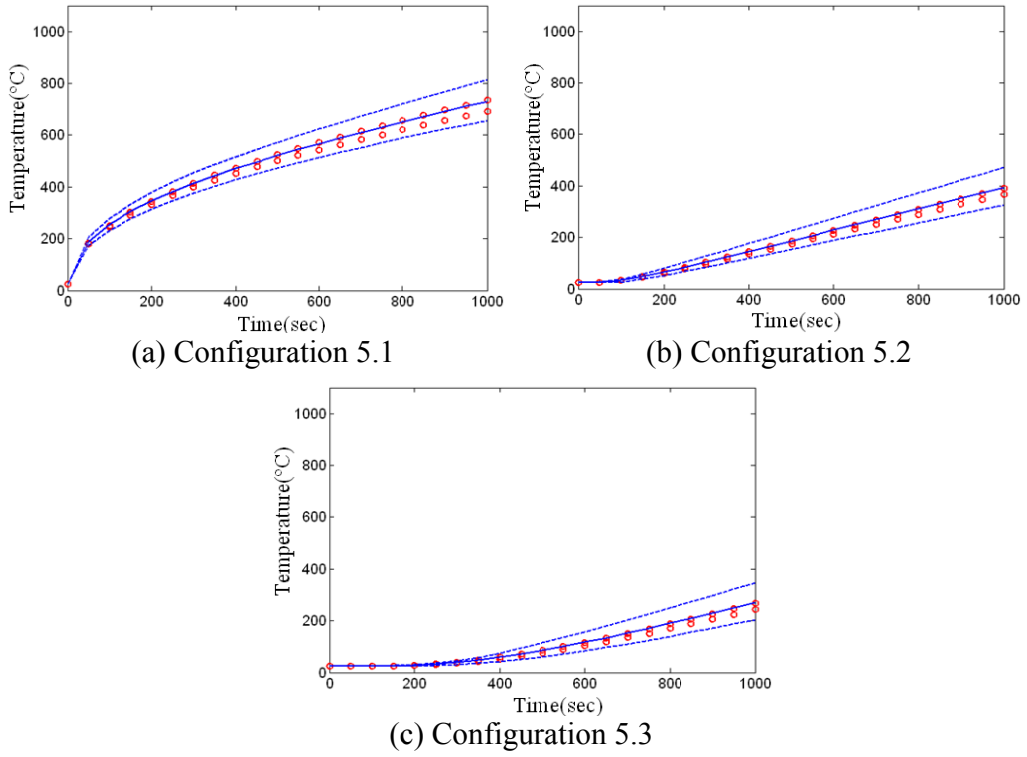
Fig. 49. Predicted temperature profile after model calibration and AC data

(a) Configuration 5.1   (b) Configuration 5.2

(c) Configuration 5.3
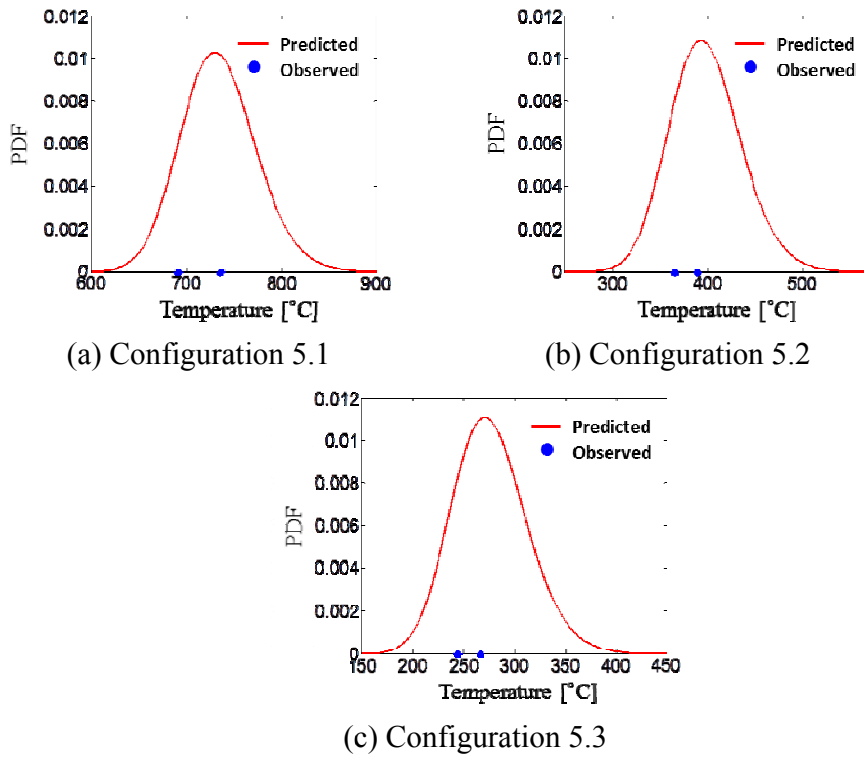
Fig. 50. Predicted PDF of temperature and AC data at 1000 sec

(a) Calculation of U_m (b) PDFs of area metric ($f_{u,6}$)
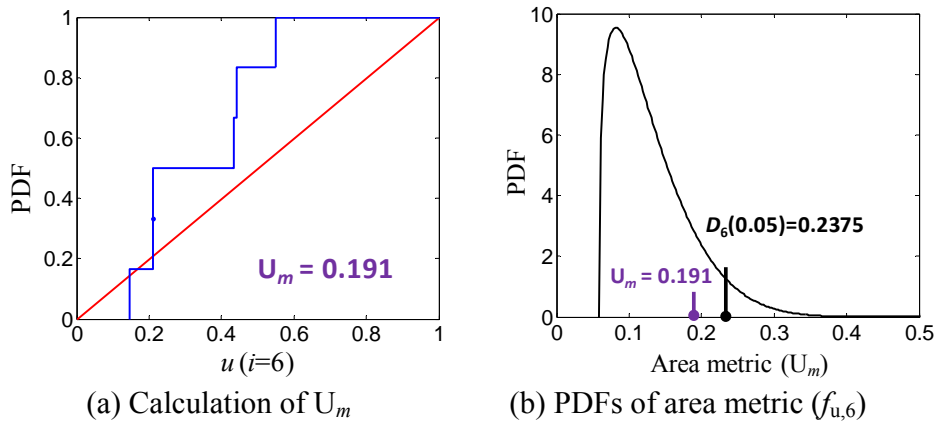
Fig. 51. Hypothesis test for validity check (i=6)

4.3.4 Virtual Qualification

As defined in model validation planning, the probability of failure under the application condition is the PoI of this problem. Since the computational model is evaluated as valid, absolute qualification is executed. Figure 52 Table 19 show the PDF of the predicted temperature and its statistical moments. The predicted probability of failure to the marginal temperature (T_f=900°C) is 0.1024, which is far larger than the marginal failure probability (p_f=0.01); thus the design is not applicable under the application condition. This result is consistent with those of other researches [16].
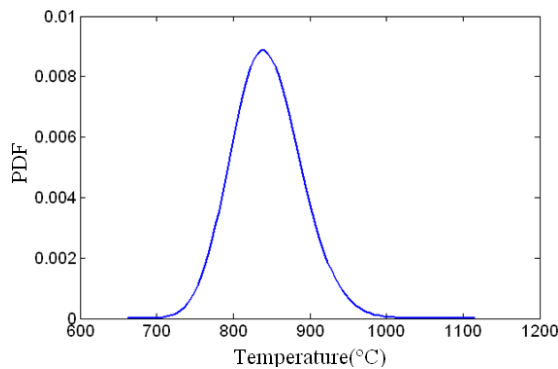
Fig. 52. Predicted PDF of temperature under the application condition

96

Table 19 Statistical moments of the predicted temperature PDF

Mean	Standard deviation	Skewness	Kurtosis
843.92	45.364	0.22967	3.10678

4.3.5 Discussion

This case study first showed that the variable characterization should be carefully performed to succeed the statistical model validation. The statistical model calibration was executed with two stages to take care of a closed-loop situation of this problem (i.e. an input of a computational model (k) is function of predicted output (temperature)). After the model calibration, the computational model is evaluated as valid using the hypothesis test for validity check. Finally, the failure probability was predicted, and it was concluded that the predicted probability was far larger than the marginal failure probability. This case study clearly provided a guideline of the statistical model validation for the heat conduction problem to improve and assess the predictive capability of the computational model.

4.4 Constrained-layer Damping Structure

4.4.1 Overview of Problem

The performance of surface damping treatments may vary once the surface is exposed to a wide range of temperatures because the performance of viscoelastic damping material is highly dependent on operational temperature. In addition, experimental data for dynamic responses of viscoelastic material are inherently random, which makes it difficult to design a robust damping layout. In this case study, the statistical model calibration is applied to the variability characterization of viscoelastic damping material to increase predictive capability of the computational model of the constrained-layer damping structure. First, the viscoelastic material property is decomposed into two sources: (i) a random complex modulus due to operational temperature variability, and (ii) experimental/model errors in the complex modulus. Next, the variability in the damping material property is obtained using the statistical calibration method by solving an unconstrained optimization problem with a likelihood function metric. Two computational models are developed to show the influence of the material variability on the acoustic performances in the structural-acoustic systems. It is shown that the variability of the damping material is propagated to that of the acoustic performances in the systems. In this study, a validity check activity of the computational models is not performed due to lack of experimental resources. As an activity of virtual qualification, the reliability-based design optimization (RBDO) is performed to obtain the robust and reliable damping layout designs of the two structural-acoustic systems amidst severe variability in operational temperature and the damping material.

This case study is organized as follows. In Section 4.4.2, a hybrid model for a structural-acoustic system analysis is briefly explained. Section 4.4.3 presents a variability characterization approach of a viscoelastic damping layer using statistical model calibration. In Section 4.4.4, reliability-based design optimization (RBDO) is carried out to determine an optimal robust design of two different constrained-layer damping layouts in structural-acoustic systems.

4.4.2 Structural-acoustic system analysis

A boundary-element analysis is employed to calculate an acoustic response of the structural-acoustic systems. As a viscoelastic constitutive model, the fractional derivative model is chosen to demonstrate variability characterization of the damping material property.

4.4.2.1 Boundary-element analysis of structural-acoustic systems

To compute an acoustic response of a structural-acoustic system, it is assumed that the structural-acoustic system is semicoupled; that is, the structural responses influence the acoustic responses but the acoustic responses do not affect the vibration of the structures. As a result, structural-acoustic problems can be solved sequentially. Finite element analysis for structural response and boundary element analysis for acoustic response are used in this study. The detailed procedures for these analyses can be found in Ref. [77]. The air density and the speed of sound are given as functions of temperature:

$$\rho = p_0 / (R \cdot T), \ c = 331.3 \cdot \sqrt{1 + T / (273.15)} \tag{26}$$

where ρ is the air density, c is the speed of sound, p_0 is sea-level standard atmospheric pressure, R is the specific gas constant, and T is temperature in Kelvin.

The constrained-layer damping beam in this study consists of three layers: a base beam, a viscoelastic damping layer, and a constraining layer. To compute a structural response of the constrained-layer damping beam, a 10-degree-of-freedom finite element is used. The eigenvalue problem of the constrained-layer damping beam problem is defined as:

$$\mathbf{K}\mathbf{u} = \lambda^c \mathbf{M}\mathbf{u}. \tag{27}$$

Here, $\mathbf{M}$ and $\mathbf{K}$ represent the global mass and stiffness matrices, respectively, and $\mathbf{u}$ is the complex eigenvector and λ^c is the complex eigenvalue. It should be noted that the stiffness matrix, $\mathbf{K}$, becomes a complex-valued and frequency-dependent matrix due to the viscoelastic damping layer. The natural frequency, ψ_k, and the modal loss factor, η_k, of the k-th mode are defined as:

$$\psi_k = \frac{\sqrt{\mathrm{Re}(\lambda_k^c)}}{2\pi}, \quad \eta_k = \frac{\mathrm{Im}(\lambda_k^c)}{\mathrm{Re}(\lambda_k^c)} \tag{28}$$

where $\mathrm{Re}(\bullet)$ and $\mathrm{Im}(\bullet)$ refer the real and the imaginary parts of the argument, respectively. To calculate the forced responses of the constrained-layer damping beam, the modal superposition method is used.

4.4.2.2 Fractional derivative model

Viscoelastic damping material is made of very long intertwined and cross-linked molecular chains, each containing thousands or even millions of atoms. The internal molecular interactions that occur during deformation in general and vibration in particular give rise to macroscopic properties such as stiffness and energy dissipation during cyclic deformation. The material properties of the viscoelastic material show highly frequency- and temperature-dependent characteristics. By introducing an accurate mathematical model for those dependencies, one can enhance the efficiency

100

of the finite element analysis in dynamic problems. The fractional derivative model is one of the most popular models in describing frequency-dependent characteristics of viscoelastic damping materials because of accuracy and simplicity of the model. In the fractional derivative model of order one, the constitutive equation is given as follows.

$$\tilde{\sigma}(t) + c_1 D^\beta \tilde{\sigma}(t) = a_0 \tilde{\varepsilon}(t) + a_1 D^\beta \tilde{\varepsilon}(t) \tag{29}$$

where ~ refers the Fourier transform; $0 < \beta < 1$; and D^β indicates the fractional derivative [87]. a_0, a_1, c_1, and β are the four variables of fractional derivative model. The Fourier transform gives a complex modulus expression as

$$\tilde{\sigma} = E * \tilde{\varepsilon} = (E' + iE'')\tilde{\varepsilon} = \frac{a_0 + a_1 [if_c]^\beta}{1 + c_1 [if_c]^\beta} \tilde{\varepsilon} \tag{30}$$

where f_c is frequency; E' and E'' are storage and loss moduli, respectively. Introducing the shift factor from the temperature-frequency equivalence hypothesis, the temperature-dependent characteristics of the complex modulus can be described as follows.

$$E* = (E' + iE'') = \frac{a_0 + a_1 [if_c \alpha(T)]^\beta}{1 + c_1 [if_c \alpha(T)]^\beta} \tag{31}$$

where $\alpha(T)$ is the shift factor and $f_c\alpha$ is called as reduced frequency. Knowing the shift factor at any given temperature (T) and a master curve at a reference temperature T_0, the complex modulus can be predicted from Eq. (31). The shift factor and temperature can be related by the Arrhenius equation as

$$\log[\alpha(T)] = d_1 (1/T - 1/T_0) \tag{32}$$

where d_1 is a material constant. It is known that the four-variable fractional derivative model sufficiently represents the real behavior of viscoelastic material over

a wide frequency range [126].   Finally, it is evident that the complex modulus expression of Eq. (31) can be applied to the shear modulus as well as Young's modulus.   Therefore, in this case study the complex Young's modulus and complex shear modulus will not be distinguished in symbols hereafter.

4.4.3 Statistical characterization of the viscoelastic damping material

The damping performance of a constrained-layer damping structure is related to the dynamic properties of the viscoelastic damping material. However, the dynamic properties of the damping material are highly sensitive to the environmental temperature and/or chemical composition of the material. In this section, a statistical approach to characterize the variability of the viscoelastic damping material using statistical model calibration is explained. In addition, the consequence of variability in the damping material on the variability of the dynamic response of the structural-acoustic systems is examined.

4.4.3.1 Variability decomposition of the viscoelastic damping material

The variability in the dynamic material properties of viscoelastic material primarily results from two sources: (1) operational temperature variation and (2) experimental/model errors associated with the viscoelastic damping material. To characterize the variability in the viscoelastic damping material properties, the complex modulus of the damping material can be expressed as

$$E^*(f_c, T) = E_1^*(T) + \varepsilon_E^*(f_c, T_0)$$

$$where \ E_1^*(T) = \frac{\mu_{a_0} + \mu_{a_1}[if_c\alpha(T)]^{\mu_\beta}}{1 + \mu_{c_1}[if_c\alpha(T)]^{\mu_\beta}},$$

$$\varepsilon_E^*(f_c, T_0) = \frac{a_0 + a_1[if_c\alpha(T_0)]^\beta}{1 + c_1[if_c\alpha(T_0)]^\beta} - \frac{\mu_{a_0} + \mu_{a_1}[if_c\alpha(T_0)]^{\mu_\beta}}{1 + \mu_{c_1}[if_c\alpha(T_0)]^{\mu_\beta}}$$

(33)

$E^*(f_c, T)$ indicates the uncertain complex modulus of the viscoelastic damping material, which is decomposed into two terms: the random complex modulus (E_1^*) and the error in the complex modulus (ε_E^*). E_1^* considers the operational temperature variability, whereas ε_E^* considers experimental/model errors at a given temperature (T_0). It is assumed that $\varepsilon_E^*(f_c)$ is the function of frequency only, and follows a Gaussian process. We need to determine the statistical information of two terms ($E_1^*(f_c, T)$ and $\varepsilon_E^*(f_c)$) to characterize the variability in $E^*(f_c, T)$. The variability of E_1^* and ε_E^* is characterized using the Arrhenius equation, the fractional derivative model and statistical calibration method in the next section.

4.4.3.2 Variability characterization using statistical model calibration

For the characterization of the random complex modulus, $E_1^*(f_c, T)$, an environmental temperature variation was first characterized with hourly temperature data measured for one year in Seoul as shown in Fig. 53. The variation in the temperature profile in Fig. 53 results in the variation in the Arrhenius shift factor ($\alpha(T)$) in Eq. (32). Sequentially, the variation in the Arrhenius shift factor propagates to the one in the complex modulus. It is thus definite that the storage shear modulus and the loss factor vary significantly due to the temperature variation, and the variation of the material properties can also affect the dynamic responses of structural-acoustic systems.
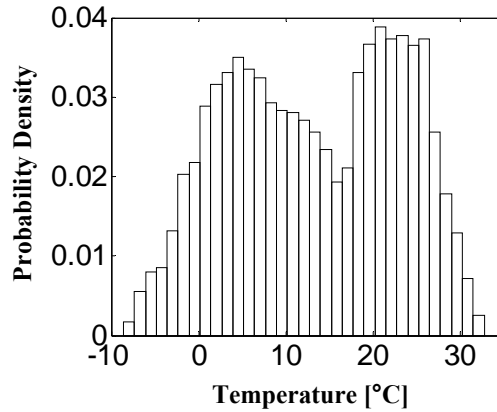
Fig. 53. Temperature histogram of Seoul in 2007

For the error in the complex modulus, ε_E^*, the statistical model calibration is employed to characterize the variability. The statistical calibration determines the unknown calibration parameter vector (**Θ)** of the four fractional derivative model variables (a_0, a_1, c_1, and β) while maximizing the agreement between the predictive response of the fractional derivative model and experimental data (storage shear modulus and loss factor data). The variability of the model variables (a_0, a_1, c_1, and β) can be represented by statistical parameters of a suitable distribution. For example, in case of the normal distribution, the **Θ** includes standard deviations of the model variables. Then, the statistical calibration method can determine the most suitable variability information of the complex modulus parameters for the best description of the experimental data (storage shear modulus and loss factor data).

4.4.3.3 Variability characterization of the ISD-110 damping material

In this section the variability characterization method is applied to a damping material, 3M ISD-110 which is a typical damping adhesive generally used in constrained-layer damping. Using the sandwich beam test data (storage shear modulus and loss factor data) in Ref. [87], the master curve at a reference temperature

104

(T_0) and the variables of the fractional derivative model are estimated. Figure 54 shows the uncertainty propagation map for variability characterization. Each side of the diagram in Fig. 54 displays the variability propagation for $E_1^*(f_c, T)$ and ε_E^*, respectively. First, for the characterization of $E_1^*(f_c, T)$, the uncertainty propagation using Monte Carlo simulation is employed using the temperature profile results in Fig. 53, Eqs. (31) and (32). The effect of the material constant (d_1) on the shift factor (α) is ignored during the Monte Carlo simulation, even though α is a function of both T (operational temperature) and d_1, due to its negligible effect on $\alpha(T)$. The estimated statistics of temperature and $\log(\alpha(T))$ are listed in Table 20..
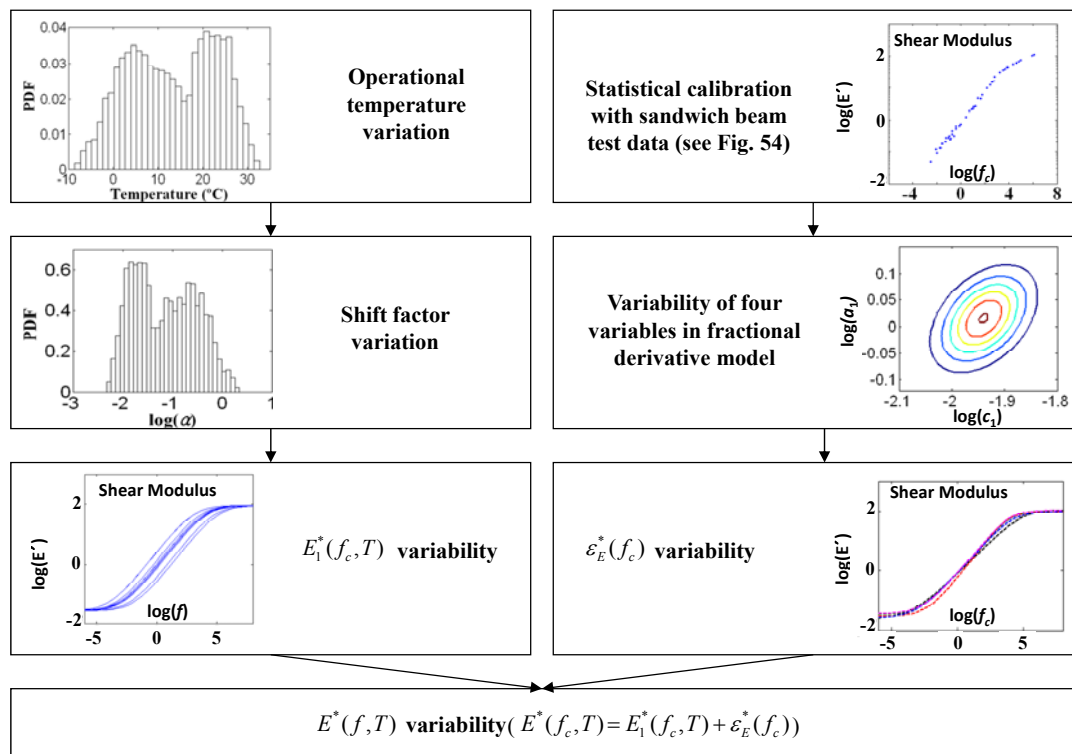
Fig. 54. Uncertainty propagation map for variability characterization

Table 20 Statistical model of random variables ($\gamma_{\log(a1),\log(c1)} = 0.4239$)

Random Variable	Mean	Standard Deviation	Distribution Type
Temperature(ºC)	13.28	9.79	Bimodal Data
$\log(\alpha(T))$	-1.14	0.63	Bimodal
$\log(a_0)$	$\log(0.0287)$	0.06897	Normal
$\log(a_1)$	$\log(1.0350)$	0.05360	Normal
$\log(c_1)$	$\log(0.0115)$	0.05360	Normal
β	0.5	0.05574	Normal

Next, for the variability of ε_E^*, the statistical calibration method is applied with the experimental data of ISD-110. Figure 55 shows the log-log plots of the experimental data (dots) at a reference temperature T_0 and the master curve (the solid line) of the complex modulus. The statistical properties of the model variables in the master curve are listed in Table 20. To define the calibration parameter vector, it is first assumed that logarithmic values of the three fractional derivative model variables ($\log(a_0)$, $\log(a_1)$, $\log(c_1)$) and β follow normal distribution. Because $\log(a_1/c_1)$ is equal to the asymptotic logarithmic value of the storage shear modulus, in the high frequency range (around 10^8 Hz in Fig. 55), $\log(a_1)$ is linearly proportional to $\log(c_1)$, say, $\log(a_1/c_1) = $ constant or $\log(a_1) = \log(c_1) + $ constant. Therefore, the principal directions of the anticipated joint PDF are [-1, 1] and [1, 1], which means that $\log(a_1)$ and $\log(c_1)$ have identical standard deviations and correlation coefficients [127]. Then, the calibration parameter vector, $\boldsymbol{\Theta}$, is decided as {$s_{\log(a0)}$, s_β, $s_{\log(a1),\log(c1)}$, $\gamma_{\log(a1),\log(c1)}$}, where s and γ indicate standard deviation and correlation coefficient, respectively. The experimental data shown in Figs. 55(a) and (b) are employed to calculate the likelihood function. Optimal values of the parameter vector, $\boldsymbol{\Theta}$, are obtained by statistical model calibration. The calibrated statistics of four parameters are listed in Table 20. When compared to the author's previous works in Ref. [127],

the standard deviation of β is significantly increased due to the consideration of the loss factor data in the variability characterization process. The increased standard deviation results in the wider 95% confidence interval (see Fig. 55) for the storage shear modulus and the loss factor than those in Ref. [127]. The characterized material parameters in Table 20 are used for RBDO of the constrained-layer damping layout in Section 4.4.4.

(a) Storage shear modulus　　　　(b) Loss factor
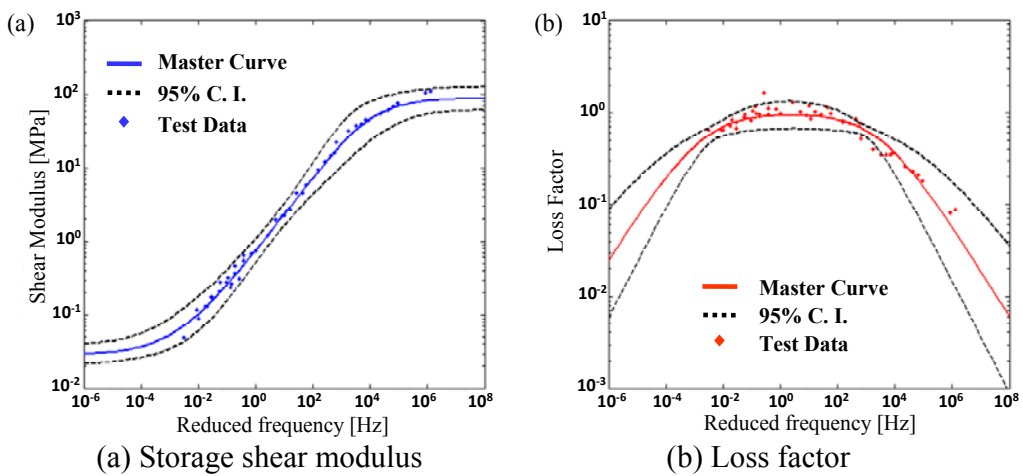
Fig. 55. Experimental data, master curve, 95% CI of ISD-110

4.4.3.4 Influence of material variability on structural-acoustic response

Two structural-acoustic systems are considered to show the influence of the material variability on the dynamic response in a structural-acoustic system as shown in Fig. 56. Figure 56(a) shows an interior rectangular cavity surrounded by three rigid walls and a constrained-layer-damping beam with simply supported boundary condition. A unit force, F, is imposed on the center of the aluminum beam. Figure 56(b) illustrates an air duct that consists of four flat panels under harmonic pressure loading. Four constrained-layer damping patches are bonded on the center of the panels to reduce the radiated sound power into infinite air space.

The four variables (a_0, a_1, c_1, β) in the fractional derivative model and operational temperature (or shift factor, α) are selected as the random variables as listed in Table 20. For the structure in Fig. 56(a), the sound pressure levels at a point A are calculated with one thousand random samples of the random variables generated by Monte Carlo simulation. For the structure in Fig. 56(b), the radiated powers are calculated with one thousand random samples. Figures 57(a) and (b) show the calculated variability bound (with 95% confidence interval) of the sound pressure level in a decibel scale over a specified frequency range.

(a) Rectangular cavity problem   (b) Air duct radiation problem
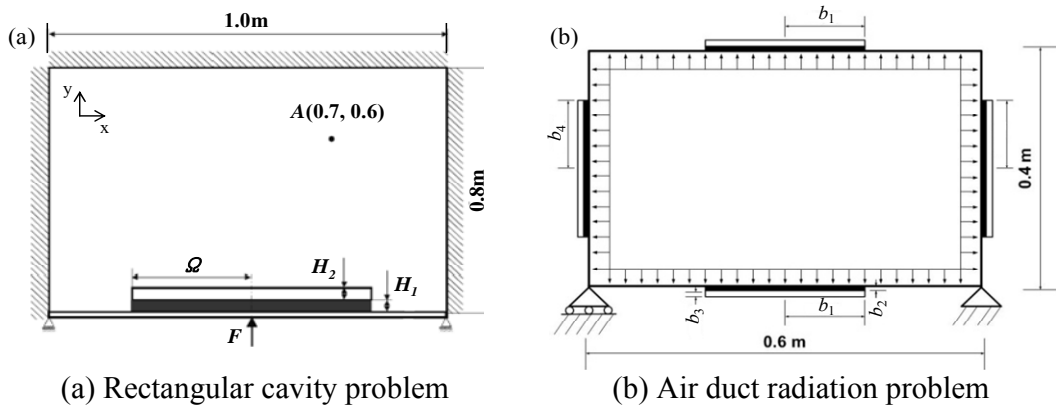
Fig. 56. Structural-acoustic systems with constrained-layer damping

(a) Rectangular cavity problem   (b) Air duct radiation problem
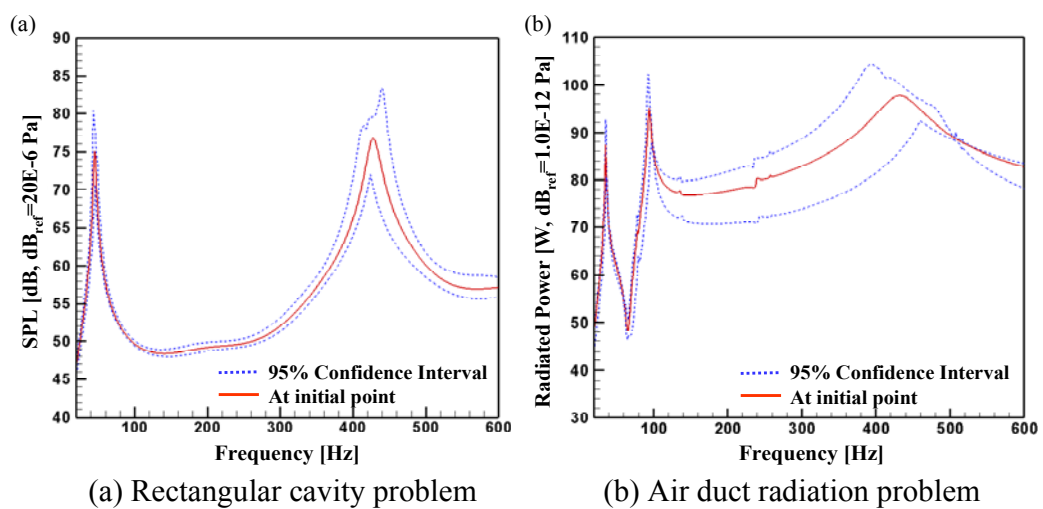
Fig. 57. Acoustic response variability in the structural-acoustic systems

108

The magnitude of the amplitude variation at the peak is beyond 10 dB. Because the variability of the viscoelastic damping material causes large variability on the acoustic responses of the structural-acoustic systems, it is important to consider the variability in the optimization of a damping layer design.

4.4.4 Reliability-based Design Optimization of structural-acoustic systems

The design objective of a constrained-layer damping treatment in structural-acoustic systems is to maximize the robustness of acoustic responses with the computational model while minimizing the amount of the damping layer and satisfying a reliability target on the acoustic response. Sections 4.4.4.1 and 4.4.4.2 deal with RBDO formulations and results of the structural-acoustic systems in Figs. 56(a) and (b), respectively.

4.4.4.1 RBDO of the rectangular cavity problem

A simple rectangular cavity problem surrounded by a simply supported aluminum beam with a constrained-layer damping in Fig. 56(a) is first considered. The ISD-110 damping material is used for the damping layer of the structure. The rectangular cavity problem has 3 design variables: the length of the constrained-layer (Ω), the thicknesses of the damping layer (H_1) and the constraining layer (H_2). The thickness of the base beam is 20 mm and remains constant during the optimization. The random variables for the damping material in Table 20 are used in the RBDO formulation. The manufacturing variability of the design variables is also considered. As listed in Table 21, their coefficients of variations are assumed to be 1%, 10%, and 5%, respectively. In addition, the variance of the location for sound pressure calculation (point A in Fig. 56(a)) is considered by treating the coordinates of the

location as random variables. In this study, it is assumed that the x and y coordinate of point A is distributed with the beta distribution as listed in Table 22, to reflect the uncertainty of the observation point.

Table 21 Design variables of the rectangular cavity problem

Design Variable	Initial Value	Lower Bound	Upper Bound	Coefficient of Variation	Distribution Type
Ω [m]	0.2	0.1	0.45	1%	Normal
H_1 [mm]	0.5	0.1	3	10%	Normal
H_2 [mm]	5	1	10	5%	Normal

Table 22 Variance of the location for sound pressure calculation

	Lower Bound	Upper Bound	Distribution Type
A_x	0.6	0.8	Beta(2, 2)
A_y	0.5	0.7	Beta(2, 2)

The RBDO problem can be formulated as:

Find $\mathbf{b}=\{\Omega, H_1,\ H_2\}$ such that

Minimize $\mu_\Phi + s_\Phi$ (34)

Subject to $p(G(\mathbf{b},\mathbf{X}) < 0) > R^t$, $\mathbf{b}_L \le \mathbf{b} \le \mathbf{b}_U$, $\mathbf{X}_L \le \mathbf{X} \le \mathbf{X}_U$

where $\mathbf{b}$ is the design variable vector; $\mathbf{X}$ is the random variable vector; Φ is the objective function; $p(\bullet)$ indicates probability; G is the constraint function; and R^t is the target reliability. The RBDO formulation minimizes the mean and standard deviation of the objective function for system robustness. The objective function is the weight performance in the damping structure as

$$\Phi(\mathbf{b}) = 2 \cdot \Omega \cdot \left(w_1 \cdot H_1 + w_2 \cdot H_2\right) \cdot \xi_t$$ (35)

where w_1 and w_2 are the densities of damping and constraining layers, respectively. ξ_1 is the width of the beam structure. Two performances are defined to represent the constraint function as

110

$$\Pi_1(\mathbf{b}, \mathbf{X}) = \int_{f_{c1}}^{f_{c2}} \left\langle 20 \log\left(\|\zeta^c\| / \zeta^c_{ref} \right) - \zeta^c_{dB0} \right\rangle df_c \quad , \quad \Pi_2(\mathbf{b}, \mathbf{X}) = \int_{f_1}^{f_2} \zeta^{c2} df_c \qquad (36)$$

where ζ^c is the sound pressure at point A; $\zeta^c_{ref} = 20.0 \times 10^{-6}$ Pa; ζ^c_{dB0} is a prescribed

level in the decibel scale; and $\langle \zeta^c \rangle = \zeta^c$ if $\zeta^c > 0$, $\langle \zeta^c \rangle = 0$ otherwise. The first

performance, $\Pi_1(\mathbf{b}, \mathbf{X})$, is a sound pressure level, which corresponds to the integration

of the sound pressure level beyond a target value (60dB in Fig. 57) within a specified

frequency range (e.g., up to 600Hz in Fig. 57). The second performance, $\Pi_2(\mathbf{b}, \mathbf{X})$, is

an overall acoustic damping performance that corresponds to the sum of sound power

within the frequency range. With these performances, the constraint functions can be

defined as

$$G_i = \Pi_i - \Pi_{i0} \cdot G^t \, (i = 1, 2) \quad \text{where} \quad G^t = 0.95 \qquad (37)$$

where Π_{i0} is the functional value of Π_i at initial design, and G^t refers to the target

constraint value. Two cases of the rectangular cavity design problem were conducted

for each constraint function: Case I with G_1 and Case II with G_2.

The RBDO problems defined in Eqs. (34) to (37) are solved for the rectangular

cavity (Fig. 56(a)) problem using the sequential quadratic programming algorithm in

MATLAB. Case I (or Case II) considers G_1 (or G_2) as the constraint function,

respectively. The frequency responses (Π_1, Π_2) and the design sensitivity information

are calculated using the discretized boundary element matrices and used for the

optimization. The constrained-layer damping beam in the rectangular cavity is

discretized with 20 elements: the 10-degree-of-freedom finite elements for the

constrained part, and the degenerated elements for the bare part. The acoustic cavity

is discretized with 80 quadratic boundary elements. The EDR method uses 41

analysis calls ($4 \times N + 1$, N is the number of random variables in Tables 20, 21 and 22)

for estimating the objective function and constraint in a probabilistic manner. The target reliability (R^t) is set to 3-sigma level (99.865%). For each case, deterministic design optimization (DDO) is first performed and the results are compared with the RBDO results. RBDO uses the statistical information of the random variables shown in Tables 20, 21 and 22. The optimization results of Case I and Case II are listed in Table 24.

Table 23 The optimization results of case I and case II

		Initial		DDO		RBDO	
		Case I	Case II	Case I	Case II	Case I	Case II
Design Variable	Ω [m]	0.20	0.20	0.1000	0.1163	0.1419	0.1430
	H1 [mm]	0.50	0.50	0.1838	0.2127	0.1781	0.1777
	H2 [mm]	5.00	5.00	7.0553	6.5335	9.7632	9.7611
Object Function		0.286	0.2856	0.1965	0.2121	0.4042	0.4072
Reliability	EDR	18.7	19.25	45.34	56.03	99.865	99.865
	MCS	-	-	-	-	99.8	99.8

When RBDO results are compared with the initial model, the weight performances (design objective) for Case I and II are sacrificed to improve the reliability of the acoustic performance (design requirement) to 3-sigma level by about 41.5% and 42.6%, respectively. In RBDO, the acoustic performances become reliable by reducing overall sound pressure level. As found in Table 23, the deterministic optimum designs turn out to be unreliable (45.34%, 56.03% reliability for Case I and II, respectively). The design becomes reliable by increasing the total amount of the damping material (the objective function). This underscores the strong need to consider the uncertainties in the design of constrained-layer damping layout.

Fig. 58 shows the PDFs of each constraint at the initial, deterministic, and reliability-based optimum design points. The acoustic performances (design requirement) are considerably improved to meet the reliability requirements. Figure

59 shows the sound pressure responses at the three different design points. As the design is improved from the initial to RBDO, it is clearly shown that the design requirement (damping performance) becomes reliable by increasing the damping performance. In Fig. 60, the PDF of G_1 from the EDR method is compared with the histogram from MC simulation with 1,000 random samples at the RBDO optimal design. Results show that the EDR method very accurately predicts the PDF and reliability in structural-acoustic systems.

(a) Case I　　　　　　　　(b) Case II
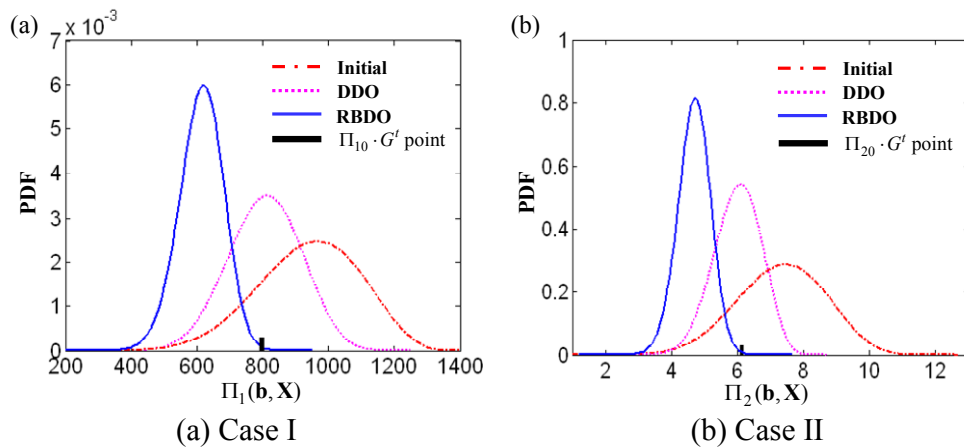
Fig. 58. PDFs of the constraint: initial, DDO and RBDO points

(a) Case I　　　　　　　　(b) Case II
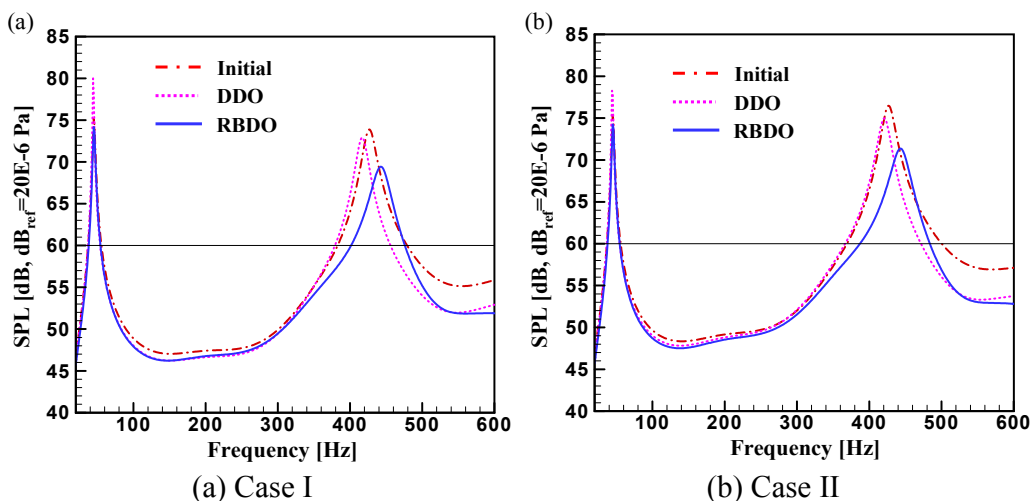
Fig. 59. Acoustic responses: initial, DDO and RBDO points

(a) Case I   (b) Case II
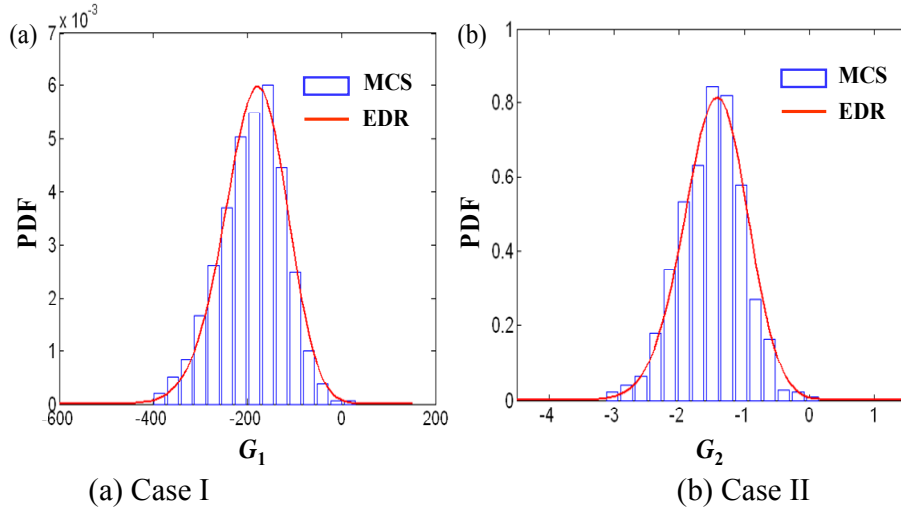
Fig. 60. MCS and EDR results

4.4.4.2 RBDO of the air duct radiation problem

The air duct radiation problem in Fig. 56(b) has four design variables as shown in Table 24: the length of the constraining layer in the top and bottom panels (b_1), the thicknesses of the damping layer (b_2), the thickness of the constraining layer (b_3), and the length of the constraining layer in the left and right panels (b_4). The thickness of the base beam is 2 mm and remains constant during the optimization. In this problem, the variability of ISD-110 damping material in Table 20 is only considered.

Table 24 Design variables of the air duct radiation problem

Design Variable	Initial Value	Lower Bound	Upper Bound
b_1 [m]	0.15	0.1	0.29
b_2 [mm]	1.5	0.1	3
b_3 [mm]	5	1	10
b_4 [m]	0.15	0.1	0.19

The RBDO problem is formulated as:

Find $\mathbf{b}=\{b_1, b_2, b_3, b_4\}$ such that
Minimize $\mu_\Phi + s_\Phi$ (38)
Subject to $p(G(\mathbf{b},\mathbf{X}) < 0) > R^t$, $\mathbf{b}_L \le \mathbf{b} \le \mathbf{b}_U$, $\mathbf{X}_L \le \mathbf{X} \le \mathbf{X}_U$

Here, the objective function is the weight of the damping structure as

114

$$\Phi(\mathbf{b}) = 4 \cdot (b_1 + b_4) \cdot (w_3 \cdot b_2 + w_4 \cdot b_3) \cdot \xi_2 \tag{39}$$

where w_3 and w_4 are the densities of damping and constraining layers, respectively. ξ_2 is the width of the beam structure. Two performance functions are defined to represent the constraint functions as

$$\Pi_3(\mathbf{b}, \mathbf{X}) = \int_{f_{c1}}^{f_{c2}} \left\langle 10 \log \left(\|r\| / r_{ref} \right) - r_{dB0} \right\rangle df_c$$

$$\Pi_4(\mathbf{b}, \mathbf{X}) = \int_{f_{c1}}^{f_{c2}} r \, df_c \qquad \left(r = \frac{1}{2} \int_\Gamma \text{Re}[\zeta \overline{v}_n] d\Gamma \right) \tag{40}$$

where r is radiated power from the structure into the air medium, v_n is outward-normal velocity of the structure to the boundary, and the overbar(-) represents complex conjugate of the argument. r_{ref} is 1.0×10^{-12} W, and r_{dB0} is a prescribed level in the decibel scale. The first function, $\Pi_3(\mathbf{b}, \mathbf{X})$, is a radiated sound power performance, which corresponds to the integration of the radiated sound power graph beyond a target value (80dB) within a specified frequency range (e.g., up to 600Hz in Fig. 57). The second function, $\Pi_4(\mathbf{b}, \mathbf{X})$, is the sum of radiate sound power performance within the frequency range. Then, the constraint functions can be defined as

$$G_i = \Pi_i - \Pi_{i0} \cdot G^t \, (i = 3, 4) \quad \text{where} \ \ G^t = 0.5 \tag{41}$$

where Π_{i0} is the functional value of Π_i at initial design, and G^t refers to the target constraint value. Two cases of the air duct radiation design problem were conducted for each constraint function: Case III with G_3 and Case IV with G_4.

DDO and RBDO are performed by considering the variability in the ISD-110 damping material. The target reliability of this RBDO problem (R^t) in Eq. (38) is also

set to 3-sigma level (99.865%). The optimization results of Case III and Case IV are listed in Table 25.

Table 25 The optimization results of case III and case IV

		Initial		DDO		RBDO	
		Case III	Case IV	Case III	Case IV	Case III	Case IV
Design Variable	b_1 [m]	0.15	0.15	0.1519	0.1379	0.29	0.2780
	b_2 [mm]	1.5	1.5	2.6009	2.8587	3.0	3.0
	b_3 [mm]	5	5	1.0	1.0	1.9390	1.0
	b_4 [m]	0.15	0.15	0.1	0.1	0.1	0.1
Object Function		1.6573	1.6573	0.4810	0.4758	1.1653	0.7601
Reliability	EDR	0.835	18.74	45.76	0.4179	99.865	99.865
	MCS	-	-	-	-	99.8	99.8

In the DDO results, b_3 and b_4 have converged at the low bounds. This result can be analyzed from the main effect plot in Fig. 61. This plot indicates the average response at each level of design variables. In this plot each design variable is set to have four levels. These plots show larger sensitivities of G_3 and G_4 with respect to b_1 and b_2 than those with respect to b_3 and b_4. Based on these plots, it is analyzed that b_3 and b_4 contribute to the minimization of the objective function rather than to the constraint satisfaction. Fig. 62 shows the PDFs of the constraint. As observed in the previous section, the RBDO results show the design with the reliability constraints satisfied: most of the PDF is located below $\Pi_{i0} \cdot G^t$ in Eq. (41) (the black bar in Fig. 62). Table 25 shows that the acoustic performance (design requirement) becomes reliable by increasing the total amount of the damping material. That is, the weight performances (design objective) are sacrificed to improve the reliability of the acoustic performance to 3-sigma level (0.48 to 1.17 for Case III, 0.48 to 0.76 for Case IV).

(a) The object function

(b) The constraint function G_3 (c) The constraint function G_4
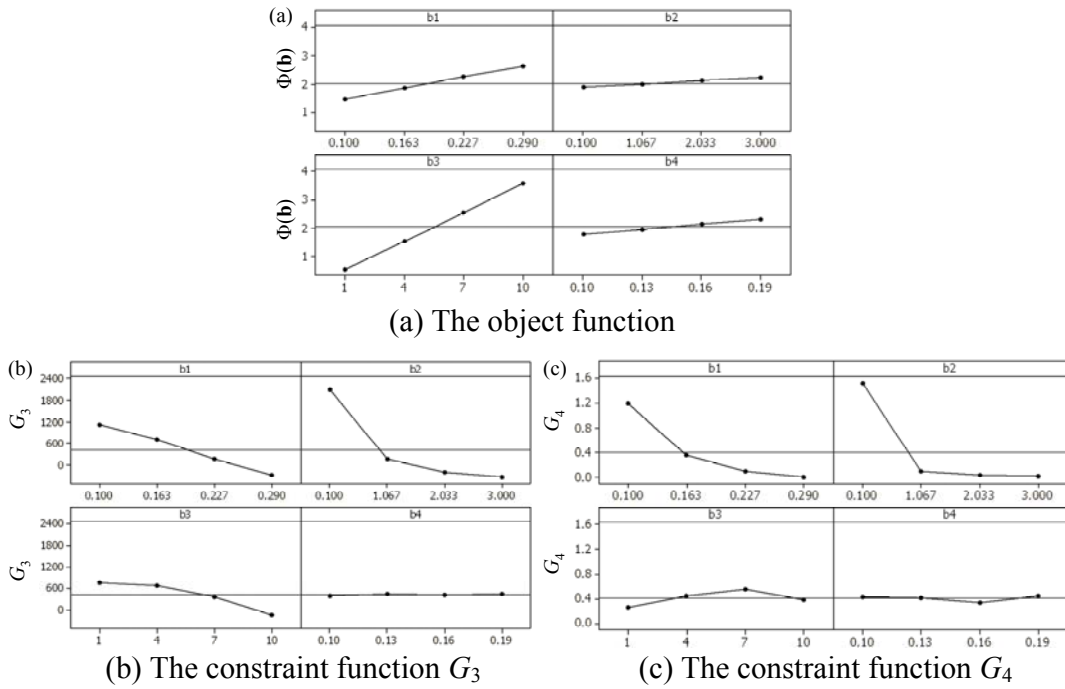
Fig. 61. Main effect plot

(a) Case III   (b) Case IV
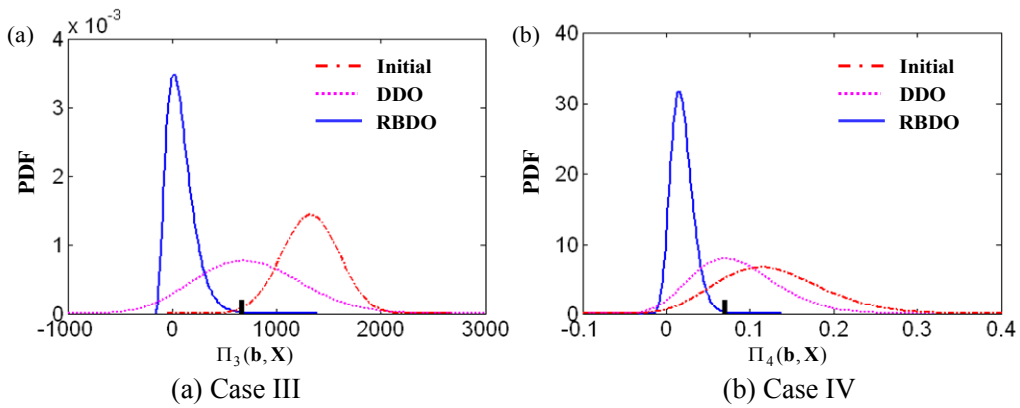
Fig. 62. PDFs of the constraint: initial, DDO and RBDO points

Figure 63 shows the acoustic responses at the initial, DDO, and RBDO design points. It is evident that the design requirement (radiated power) becomes reliable by increasing the amount of damping material. Figure 64 shows the mode shapes at the initial condition. Noting that the pressure loading in the air duct radiation problem is in-phase on the four panels, it can be seen that three modes (mode 2, mode 5 and

mode 10) are excited by the loading in Fig. 64. In addition, from the mode shapes we can understand why the contribution of the side panels is less dominant in the constraint functions than that of the top and bottom panels: the acoustic response especially around 430Hz (Mode 10) is reduced significantly where the relative vibration of the side panel is minimal.

(a) Case III   (b) Case IV
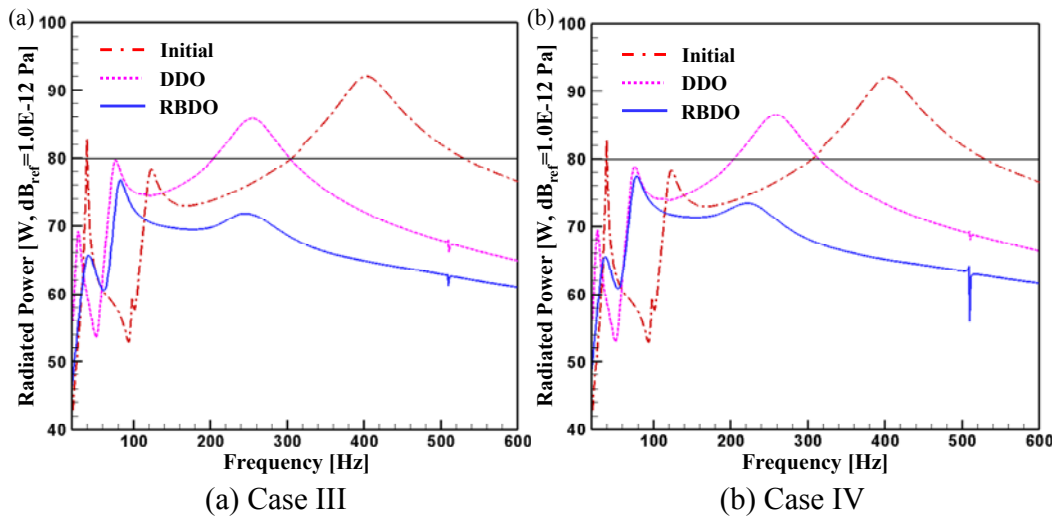
Fig. 63. Acoustic response: initial, DDO and RBDO points
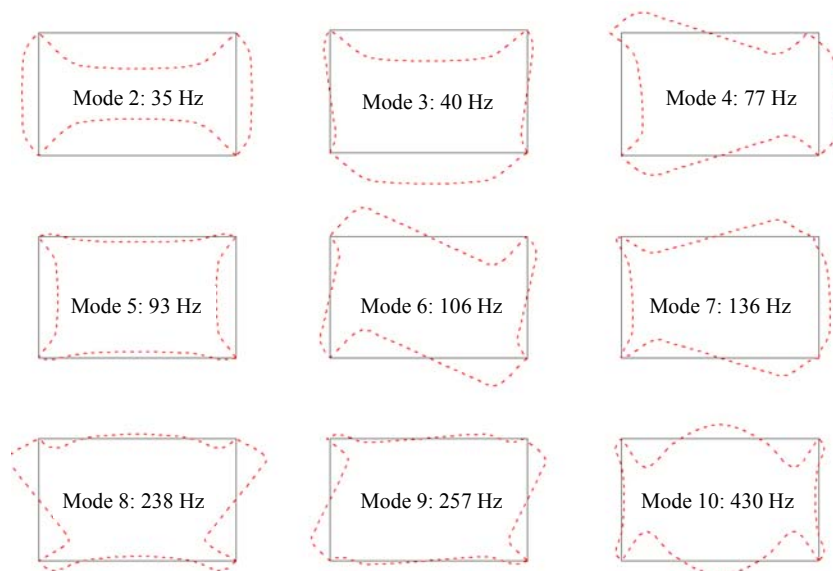
Fig. 64. Mode shapes of the air duct radiation problem

118

4.4.5 Conclusion

This case study mainly applied the statistical model calibration to build accurate computational models of the viscoelastic damping material and structural-acoustic systems. In the modeling of the viscoelastic damping material, two factors on the variability in the complex modulus were considered: operational temperature variation and experimental/model errors. The statistical calibration method characterized the variability of the complex modulus by maximizing the agreement with all available experimental data (storage shear modulus and loss factor data) using the likelihood function metric. The statistical calibration method can be easily expanded to other viscoelastic constitutive models for the variability characterization of the damping material property.

While the validity check is not considered due to lack of experimental resources, an RBDO of the structural-acoustic system was performed with the improved computational model as an activity of virtual qualification. Operational condition variability in addition to the material property variability was considered in the reliability-based robust designs of the constrained-layer damping layout. Two structural-acoustic systems were considered with acoustic performance requirements. It was demonstrated that the variability of the damping material is significantly propagated to that of the acoustic performances in two structural-acoustic systems. For the rectangular cavity problem, variability on manufacturing, the location for sound pressure calculation, the operational temperature, and the damping material were considered. The weights (design objective) were increased by about 40%, while the reliability of the acoustic performance (sound pressure and power) requirement

was improved to 99.865%. This formulation can be applicable for the damping layout design in a passenger vehicle to achieve robust and reliable cabin noise reduction. As an example of a sound radiation problem, an air duct problem with constraint on a radiated sound power was introduced and solved. This formulation can be applicable for general structure-borne noise problems in, for example, electronic appliances and automobiles. The numerical results show that RBDO yields more robust and reliable damping layout designs than the deterministic design optimization.

4.5 Energy Harvesting Device
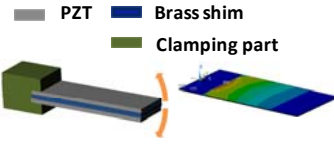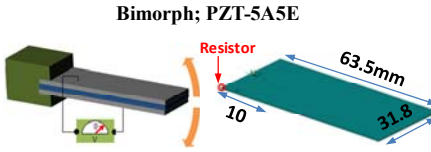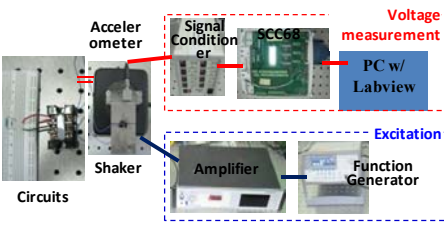
4.5.1 Overview of Problem

As mentioned in Section 2.5, most investigations on piezoelectric energy harvesting (EH) devices have focused on a cantilever-type energy harvester; however, it has some drawbacks as (1) the cantilever-type harvester requires an extra space for a bulky proof mass and additional clamping part, (2) the cantilever-type harvester must be protected from dirt, moisture, and other environmental harms; therefore, it is usually suggested that the cantilever-type harvester be kept inside a case, and (3) a great deal of vibration energy may be lost due to loosened clamping conditions after a long-time vibration. To solve the drawbacks of a cantilever-type harvester, Lee and Youn newly proposed the concept of a skin-type EH device (the EH skin) that generates electrical energy from the vibrating skin structure with an additional thin piezoelectric layer as one embodiment [128,129].

The proposed model validation framework facilitates to develop the valid computational model of a piezoelectric EH device. The EH skin was designed to generate a maximum electric power for wireless sensors. After a careful manufacture of the EH skin, a predicted electric voltage was compared with the experimental result for the validity check. It is also demonstrated that the EH skin can generate enough electric power for wireless temperature sensors and LEDs.

4.5.2 Model Validation Planning

In this case study, statistical model validation consists of two hierarchical levels: (i) top level: electrical response and (ii) bottom level: mechanical response, as summarized in Fig. 65.

Hierarchical level	Bottom (Mechanical response)	Top (Electrical response)
PoI	Natural Frequency	Voltage
Computer model	PZT, Brass shim, Clamping part	Bimorph; PZT-5A5E, Resistor, 63.5mm, 10, 31.8
Experimental resources	10 cantilever-type energy harvesters; Frequency sweep test	Accelerometer, Signal Conditioner, SCC68, Voltage measurement, PC w/ Labview, Circuits, Shaker, Amplifier, Function Generator, Excitation; Energy harvesting test
Unknown model variable	Elastic compliance (s_{11})	Piezoelectric strain coefficient (d_{31}) Permittivity (ε_{33})

Fig. 65. Statistical model validation framework for a EH device

The statistical model calibration was conducted with ten cantilever-type energy harvesters from Piezo System Inc. [130]. The specimen is composed of 9 layers in total as shown in Fig. 66: two PZT patches (with PZT-5A and two nickel electrode layers), a center brass shim and two conductive adhesive layers. The nickel electrodes and adhesive are ignored in the FE model because of their ignorable thickness in the simulation and an assumption of a perfect bonding condition. The computational model was developed with Ansys software as shown in Fig. 67. The PZT plates were modeled using a SOLID5 element with four coupled-field degrees of freedom (three translational and one electric potential degrees of freedom), and the

122

center shim by SOLID45 element with three translation degrees of freedom. The specimen harvests energy using '31' mode; when it extends or compresses in *x*-direction (due to a bending in *y*-direction) and, as a result, voltage drop is generated in *z*-direction (see Fig. 67 for axes). The specimen with series operation is modeled by facing two polarization axes (along *z*-direction). The two electrode surfaces facing the center shim are grounded. The voltage degrees of freedom at the finite element nodes on both top and bottom surfaces are coupled to simulate the electrodes. These two electrodes are connected with a resistor.
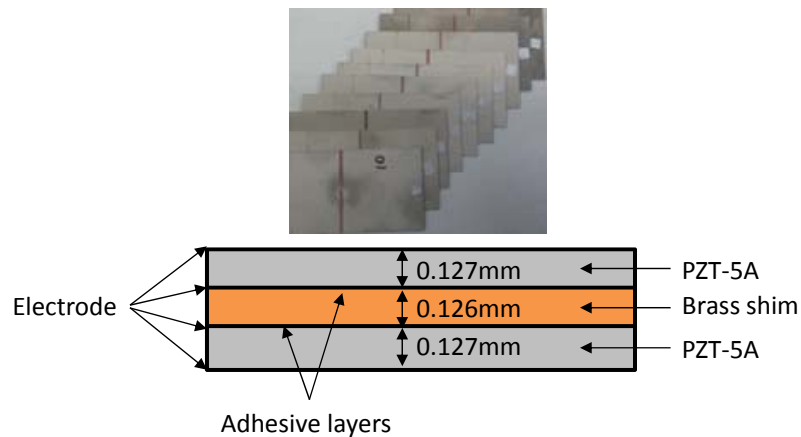
Fig. 66. Ten cantilever-type energy harvesters and its cross section
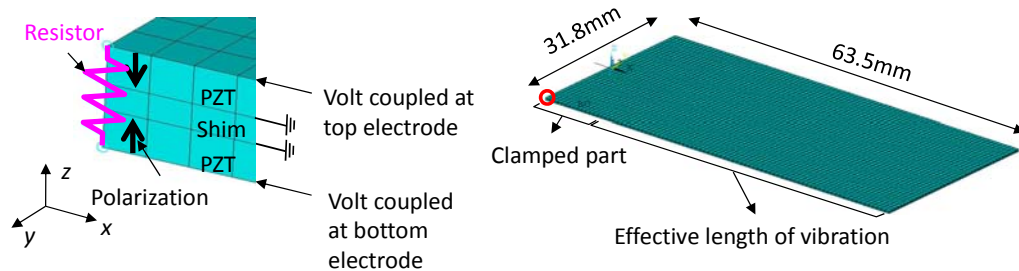
Fig. 67. FE model of a cantilever-type energy harvester

The cantilever-type energy harvester has two primary physical responses related with the harvestable power: natural frequency of a cantilever beam (f_r) and voltage

123

spectrum at a specific excitation and resistance. To make the statistical model calibration affordable, the EH model was decomposed into top and bottom levels. This decomposition was designed to isolate the responses of the EH device and identify unknown model variables along the hierarchy. Energy harvesting tests were conducted to measure the electric responses as shown in Fig. 65. Subsequently, sweep tests were designed to measure the natural frequency of the cantilever-type energy harvester. A mechanical damping ratio (ς) is measured through frequency sweep tests and calculated as half power bandwidth method as

$$\varsigma = \frac{\Delta f_r}{2 \times f_r} \tag{42}$$

where f_r is natural frequency, and Δf_r indicates half-power bandwidth. In this study, damping ratio was measured with 10 energy harvesters and the average value was 1.73%.

Model calibration must be carefully conducted using expert opinion and a sensitivity study, which determine the most significant but unknown model variables affecting the uncertain responses of the computational model at any hierarchy. The constitute equations of linear piezoelectricity is

$$S_z = s^E T_z + dE_z$$
$$D_z = dT_z + \varepsilon^T E_z$$

$$s^E = \begin{bmatrix} s_{11} & s_{12} & s_{13} & 0 & 0 & 0 \\ & s_{11} & s_{13} & 0 & 0 & 0 \\ & & s_{33} & 0 & 0 & 0 \\ & & & s_{44} & 0 & 0 \\ & sym & & & s_{44} & 0 \\ & & & & & s_{66} \end{bmatrix}, d = \begin{bmatrix} 0 & 0 & d_{31} \\ 0 & 0 & d_{31} \\ 0 & 0 & d_{33} \\ 0 & d_{15} & 0 \\ d_{15} & 0 & 0 \\ 0 & 0 & 0 \end{bmatrix}, \varepsilon^T = \begin{bmatrix} \varepsilon_{11} & 0 & 0 \\ & \varepsilon_{11} & 0 \\ sym & & \varepsilon_{33} \end{bmatrix} \tag{43}$$

where S_z, T_z, E_z, and D_z represents strain, stress, electric field and electric displacement tensors, respectively. s^E, d and ε^T are strain compliance matrix, piezoelectric matrix and permittivity matrix, respectively. Among many, three model variables, s_{11}, d_{31}, and ε_{33}, which are sensitive to the responses of a cantilever-type energy harvester, were decided as unknown model variables. According to the analytical equations of a bimorph energy harvester in Ref. [131], the natural frequency is related with compliance of PZT and brass, geometry information and mass of the bimorph. The voltage is a function of piezoelectric coupling coefficient ($k_{31}= d_{31}/(s_{11}\cdot\varepsilon_{33})$), excitation, capacitance of PZT, geometry information of bimorph and resistance. Thus, the compliance (s_{11}) was considered as an unknown model variable ($\boldsymbol{\theta}_{bot}$) in the bottom level, whereas the piezoelectric strain coefficient (d_{31}) and the permittivity (ε_{33})) were selected as unknown model variables ($\boldsymbol{\theta}_{top}$) in the top level.

4.5.3 Model Validation Execution

4.5.3.1 Bottom level calibration: mechanical response

The statistical calibration in the bottom level consists of two steps: (step 1) to characterize the statistical model of a known random variable related with manufacturing tolerance, PZT thickness, and (step 2) to obtain the statistical distribution of an unknown random variable (s_{11}) using the statistical model calibration.

(Step 1) The thickness of PZT is back-calculated using the weights of 10 cantilever-type energy harvesters measured. It is assumed that the densities of brass shim and PZT are constant, and the weights among harvesters are different mainly

due to the manufacturing tolerance of a PZT thickness. The weibull distribution (T_{PZT} ~ Weibull(0.1272,60.42)) was found to be most suitable for modeling the thickness of PZT based on the K-S GoF test, as shown in Table 26.

Table 26 K-S GoF test results

Distribution	K-S GoF Test	
	Result	p-value
Weibull	**Accept**	**0.2695**
Normal	Accept	0.1506
Lognormal	Accept	0.1462
Gamma	Accept	0.1320

The characterized statistical model of PZT thickness is shown in the left box of Fig. 68(a).

(Step 2): The statistical model calibration was conducted to determine the statistical distribution of the s_{11}. Figure 68(a) shows the 4-staged calibration procedure.

- Stage 1: The observed data of the natural frequency must be provided with an initial setting of the calibration parameter vector (Θ), which includes the statistics of the compliance (lognormal~(μ_{s11}, σ_{s11})) and the elastic modulus of brass (E_{brass}), (i.e., Θ={ μ_{s11}, σ_{s11}, E_{brass}}).

- Stage 2: The UP analysis approximates the PDF of the natural frequency.

- Stage 3: The likelihood function is calculated in the optimization process for the statistical model calibration.

- Stage 4: If the process is converged, stop the calibration procedure; otherwise update the calibration parameter vector and go to Step 2 to maximize the likelihood function.

Table 27 shows the ten data of the first natural frequency measured using the frequency sweep test.

Table 27 Frequency sweep test results.

Test #	Natural frequency	Test #	Natural frequency
1	68.0	6	70.5
2	71.2	7	70.5
3	70.0	8	69.0
4	71.0	9	70.0
5	68.0	10	70.5
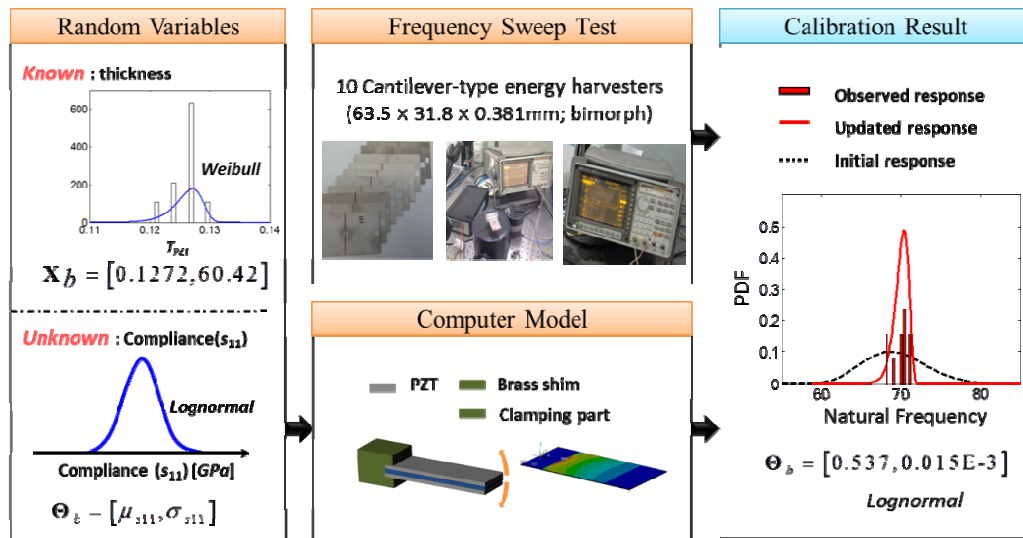
(a) Model calibration flow
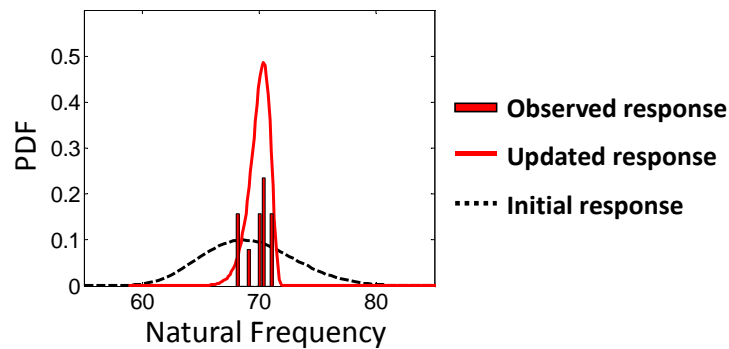
(b) Predicted and observed natural frequency

Fig. 68. Statistical model calibration (bottom level-mechanical response)

Figure 68(b) shows the predicted PDFs of natural frequency before and after statistical model calibration. It is apparent that the likelihood function is increased

after the model calibration and the predicted PDF after the calibration agrees well with the experimental data. As a result, the statistical calibration determines the statistical property of the compliance, s_{11}~ Lognormal(0.537, 0.015E-3).

4.5.3.2 Top level calibration: electrical response

The objective of the top level calibration is to obtain the statistical models of d_{31} and ε_{33}. The overall calibration procedure is same with that in Section 4.5.3.1 as shown in Fig. 69. The calibration maximizes the likelihood function between the observed and predicted voltage. Table 28 shows the measured voltage with a 30kΩ resistor. The UP analysis employed two known random variables: (1) the thickness of PZT ~ Weibull(0.1272,60.42), and (2) the compliance (s_{11}) ~ Lognormal(0.537, 0.015E-3).   As a result, the statistical calibration determined the calibration parameters of two unknown model variables, (1) d_{31} ~ Lognormal(0.730, 0.168) and (2) ε_{33} ~ Lognormal(6.892, 0.035).
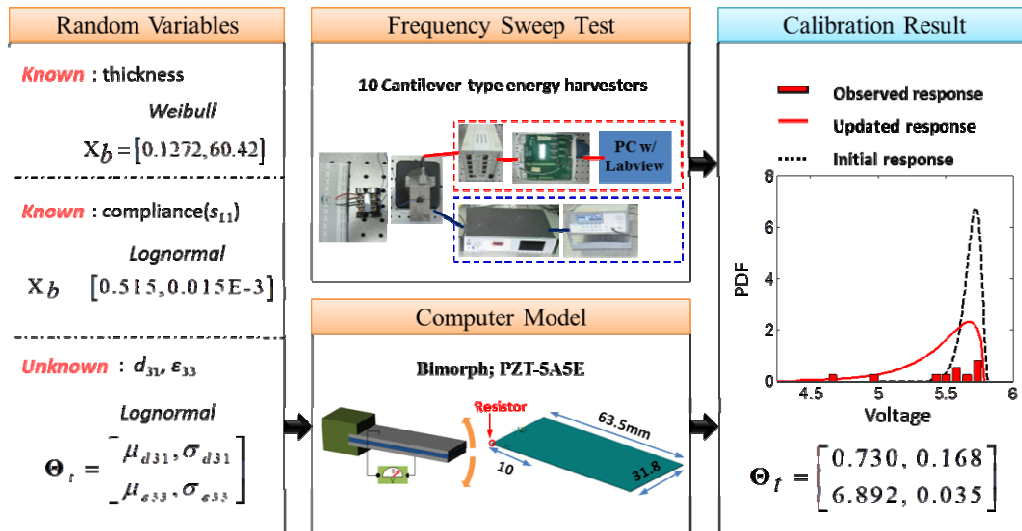
Fig. 69. Statistical model calibration (top level-electrical response)

Table 29 summarizes the model input variables after the model calibration. The deterministic values in strain compliance matrix, permittivity matrix and piezoelectric matrixes are taken from the Ref. [133] and summarized in Table 30.

Table 28 Measured voltages of the energy harvesters.

Test Number	1	2	3	4	5
Voltage at 30kΩ	5.01	4.63	5.63	5.77	5.72
Test Number	6	7	8	9	10
Voltage at 30kΩ	5.44	5.6	5.70	5.60	5.51

Table 29 Summary of model input variables

Classification		Variable	Value	Sources of value
Known	Deterministic	Length	63.5mm	Measurement
		Width	31.8mm	Measurement
		ρ_{brass}	7858 kg·m^3	Back-calculated using measured weight
		ρ_{PZT}	7800kg·m^3	Catalog
	Random	T_{PZT}	Weibull(0.1272,60.42)	Back-calculated using measured weight
Unknown	Deterministic	E_{brass}	126.6GPa	Calibration(Bottom)
	Random	s_{11}	Lognormal(0.537, 0.015E-3)	Calibration (Bottom)
		d_{31}	Lognormal(0.730,0.168)	Calibration (Top)
		ε_{33}	Lognormal(6.892,0.035)	Calibration (Top)

Table 30 Material properties of PZT-5A

PZT-5A	Components of compliance matrix	s_{11}	in Table 4
		s_{12}	-5.74E-12 m^2/N
		s_{13}	-7.22E-12 m^2/N
		s_{33}	1.88E-11 m^2/N
		s_{44}	4.75E-11 m^2/N
		s_{66}	4.43E-11 m^2/N
	Piezoelectric coupling coefficient	d_{31}	in Table 4
		d_{33}	3.74E-10 C/N
		d_{15}	5.84E-10 C/N
	Relative permittivity at constant strain	ε_{11}	916
		ε_{33}	in Table 4

4.5.4 Development of the Energy Harvesting Skin

4.5.4.1 Design of the EH skin

The EH skin consists of two thin plates to harvest electric power: (1) vibrating shell structure (base structure), and (2) thin piezoelectric patches that are directly attached onto a base structure. First, a base structure (steel plate) was designed and manufactured to have the first natural frequency of 50Hz under fixed boundary condition. Figure 70(a) shows the prototype of the base structure with a size of 483 x 431 x 1mm.

Next, the piezoelectric layer was designed to avoid cancellation effect [128,129] to maximize harvestable power. Figure 71 shows an example of the cancellation effect from the second vibration mode of a cantilever beam. Voltage cancellation occurred where the dynamic strain distribution changes sign in the direction of beam length. This effect can be minimized by eliminating material where the amount of in-plane strain is small due to strain change. Figure 70(b) and (c) shows the first and second mode shapes of the base structure. Figure 72 shows the corresponding inflection lines and the final design of piezoelectric layer for the EH skin.

(a) Size of base structure   (b) 1st mode shape (50Hz)   (c) 2nd mode (94Hz)
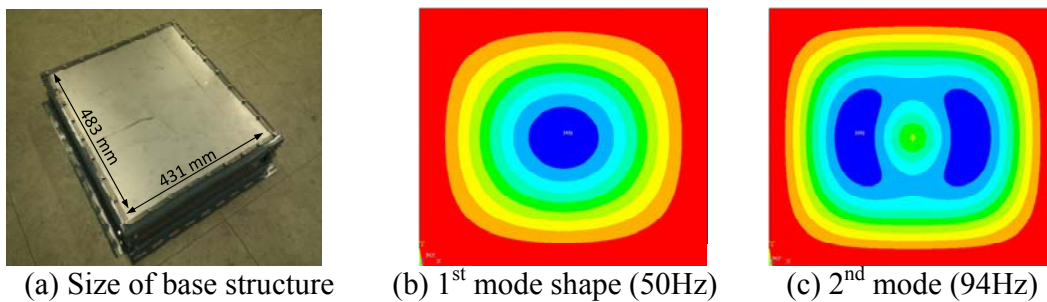
Fig. 70. Base structure of the EH skin
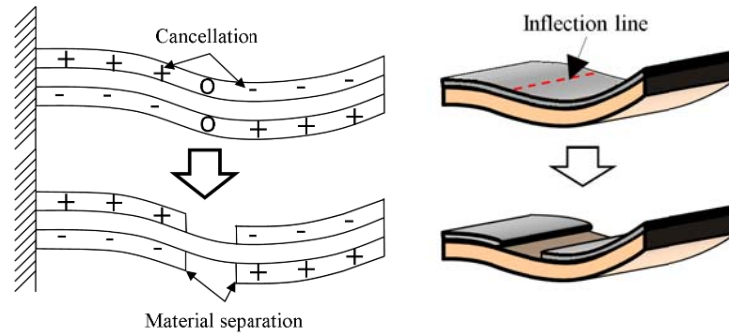
Fig. 71. Power cancellation effect of a cantilever-type energy harvester

(a) 1st mode   (b) 2nd mode   (c) Final inflection lines
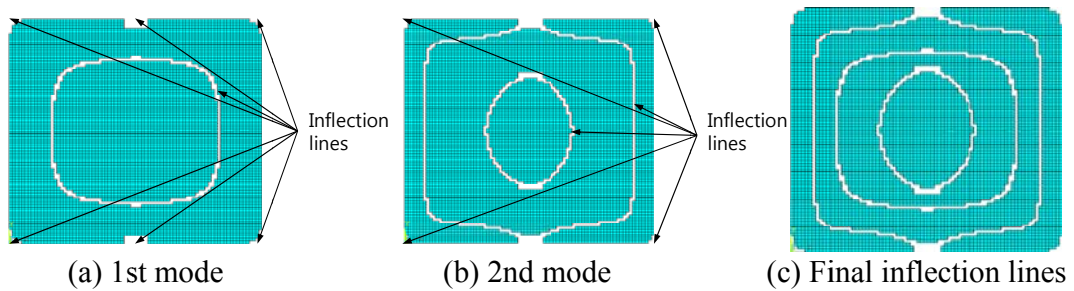
Fig. 72. Inflection lines of the EH skin

Last, the power of each PZT segment was predicted with 4.5kΩ resistor as shown in Fig. 73. The sinusoidal vibration with a frequency of 50Hz and 1g acceleration was applied. Damping ratio of the base structure was measured using the frequency sweep test and the average value (=2.7%) was used. The predicted power was between 0.01mW and 0.2mW as shown in Fig. 73. The amount of power is enough to operate low power wireless sensors [134]. With the statistical computational model, the EH skin can be designed to harvest robust and reliable power for the real-time and self-powered wireless sensor network.
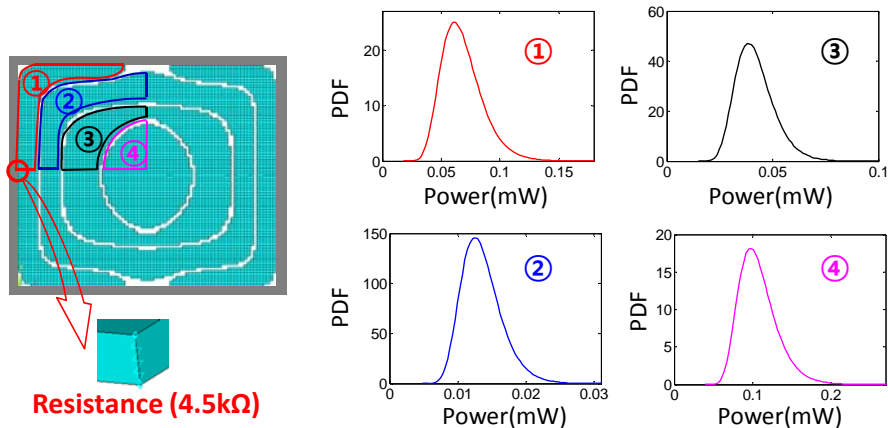
Fig. 73. Predicted power of PZT segments

4.5.4.2 Manufacturing of the EH skin

The EH skin designed in Section 4.5.4.1 was manufactured to evaluate the performance and check the validity of the computational model by experiments. The manufacturing process was composed of five steps: (1) assigning PZT patches, (2) cutting, (3) bonding, (4) curing and (5) checking short circuitry as shown in Fig. 74. First the PZT patches are assigned on the base structure for cutting. Eleven PZT patches are needed for one-quarter of the base structures. Thus total 44 PZT patches from Piezo System Inc. (PZT-5A with two nickel electrode layers; size of 50 x 50mm) to prototype the EH skin. Next, the PZT patches were cut by Universal Laser M300 from Universal Laser System Inc. For the machining process in Fig. 74 (a) and (b), a special care must be made to cut the PZT plates because piezoelectric material is very brittle. The power and speed of laser were set to prevent brittle fracture of PZT patches. In the bonding process, a conductive epoxy was used to glue the machined PZT segments on the base structure. Epoxy adhesive was applied to the PZT segments in a thin layer by spreading with a knife blade. The PZT segments are attached on the base structure, and cured for 15 minutes (70°C) in a hot chamber.

132

The process was repeatedly done for all area of the base structure. Lastly, the short circuitry was checked between the top and bottom electrode because the "paste" state epoxy may be squeezed out and reached at top electrode.

(a) Assigning PZT patches on base structure (b) Laser cutting of PZT patches

(c) Bonding   (d) Curing   (e) Checking short circuitry
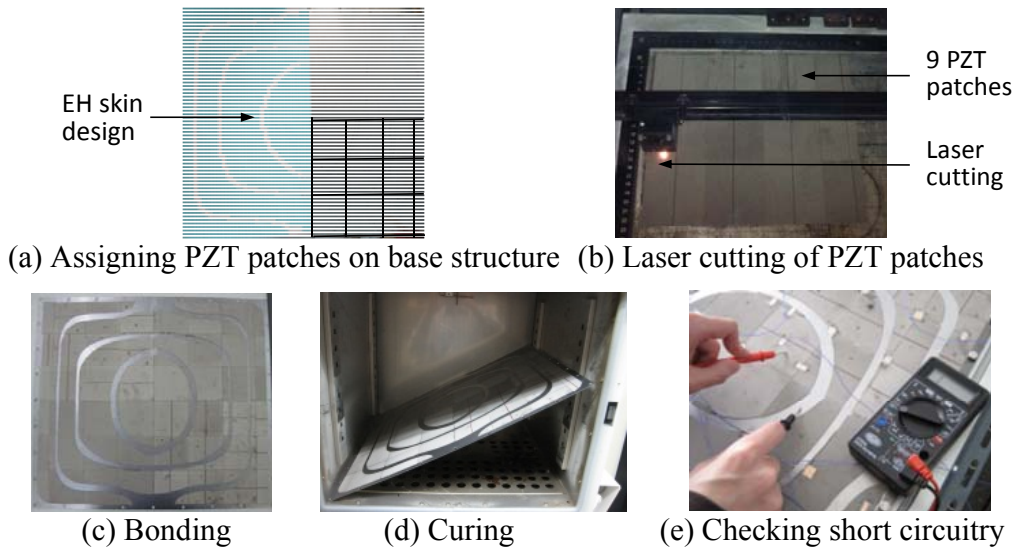
Fig. 74. Manufacturing process of the EH Skin

4.5.4.3 Power verification of the EH skin

The voltage of the each segment was measured to check the validity of the computational model. Figure 75 shows testbed to measure the voltage.
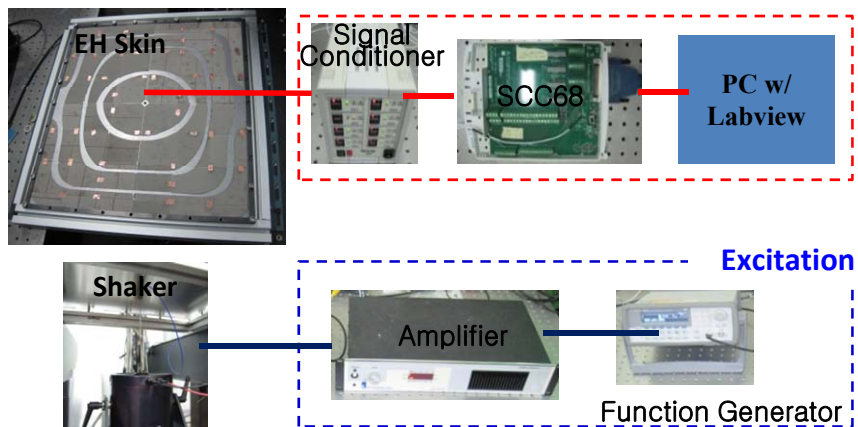
Fig. 75. Testbed for the EH skin verification

The EH skin has 16 PZT segments as shown in Fig. 76(a). The PZT patches in one segment were connected parallel so that they electrically behaved as one big patch. That is, top electrodes of the PZT patches were connected together with conductive tapes to share the same voltage in one segment, and the wire connected to the base structure was electrically connected to bottom electrode of each segment. Group A includes segments 1, 5, 9 and 13 that experience same vibration excitation. Similarly, Group B, C, and D include four segments as shown in Fig. 76(a).
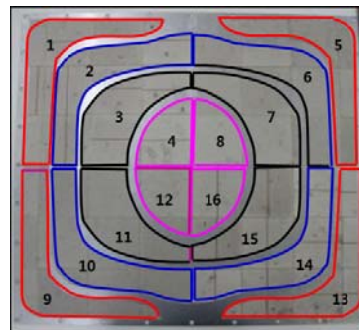
(a) PZT segments of the EH skin
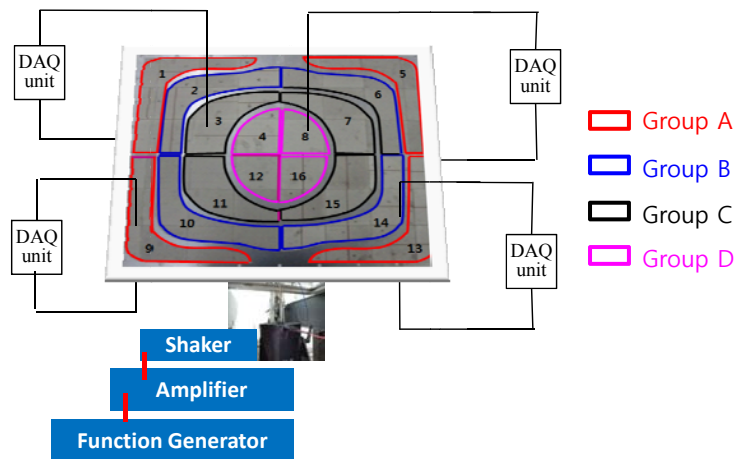
(b) Experimental setting for voltage measurement

Fig. 76. Testbed for voltage measurement

NI USB-6009 portable DAQ device (see Fig. 76(b)) were installed to measure the open circuit voltage of each segment. Table 31 shows the measured voltages when sinusoidal vibration – 50 Hz at 1g acceleration – is applied. To prevent short

134

circuitry, a nice method to bond the PZT segments on the base structure should be devised in the future. The measured voltages are graphically compared with predicted PDFs as shown in Fig. 77(a). Among 16 PZT segments, only eight segments can generate voltages that are within 99% confidence intervals of the corresponding predicted PDFs (see Fig. 76(b)). The voltages of the other segments are lower than the predicted voltages.

Table 31 Summary of measured and predicted voltage

# of segment	Measured (V)	Predicted (mean; V)	# of segment	Measured (V)	Predicted (mean; V)
1	0.535	1.050	9	0.443	1.050
2	0.337	0.462	10	0.585	0.462
3	0.000	0.870	11	0.352	0.870
4	2.343	2.087	12	0.036	2.087
5	0.395	1.050	13	0.723	1.050
6	0.095	0.462	14	0.365	0.462
7	1.001	0.870	15	0.875	0.870
8	1.765	2.087	16	0.425	2.087

(a) All measured data   (b) Valid data only
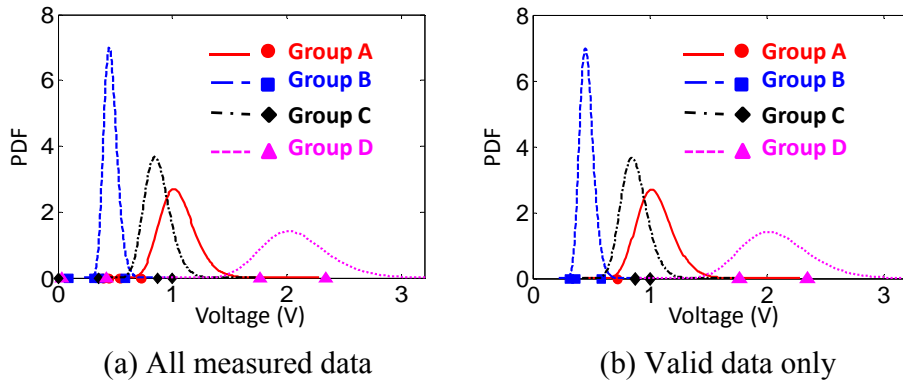
Fig. 77. Graphical comparison of measured and predicted voltage

Hypothesis test based on a significance level was employed. The area metric (U_m) between the predicted response and experimental data in Fig. 77(a) was 0.2896 as shown in Fig. 78(a). The critical value of area metric at a significance level of 0.05, $D_{16}(0.05)$, was 0.1451 in case sixteen experimental data were employed for the

validity check. The null hypothesis would be rejected since U_m (=0.2896) is far larger than the $D_i(\alpha)$ (=0.1451).

(a) Calculation of area metric   (b) PDF of area metric (i=16)
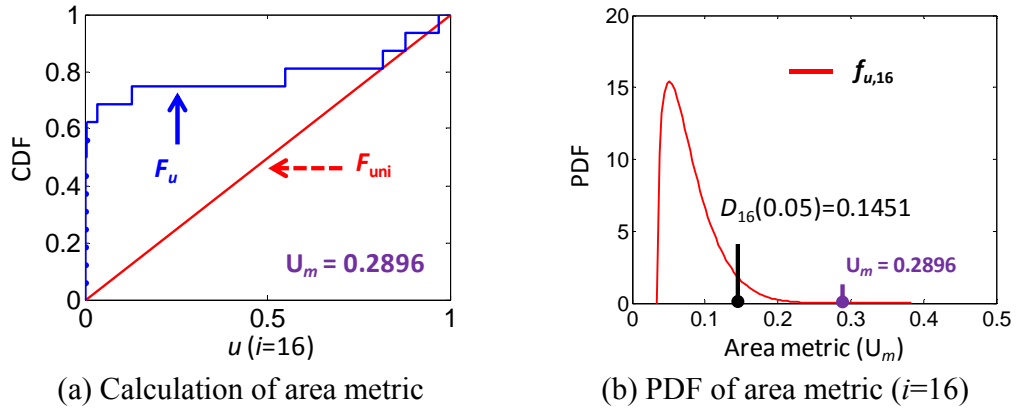
Fig. 78. Hypothesis test for validity check

The discrepancy between the predicted and measured voltages can primarily be attributed to some of the following factors:

- Imperfect bonding condition of PZT patches: The simulation assumes perfect bonding of PZT patches. However, perfect bonding is never possible in a real-world setting; in addition, the quality of bonding is highly dependent on the skill of workers. Thus, it is necessary to develop an advanced technique to tightly bond the PZT patches and minimize the manufacturing uncertainty.

- Possible partial damage or degradation in PZT patches due to high temperature during laser cutting and curing.

Although the null hypothesis is rejected, the main reasons of the mismatch were the manufacturing error and the unexpected uncertainty due to material damage and/or degradation. This founding reveals that the uncertainty in the experimental data should be carefully considered in the model validation process. This will be the future work of this research.

4.5.4.4 Demonstration of the EH skin: real time wireless sensor monitoring

The EH skin was demonstrated to produce electric energy from vibration energy (frequency=50Hz, acceleration=1g).   This study employs LEDs and wireless temperature sensor nodes [134]. Figure 79 shows a schematic view of the connection among the EH skin, the EH circuit and the wireless sensor nodes (or LEDs). To show how EH skin can be used for structural health monitoring first, we built four electric circuits with capacitor, rectifier and LED. The circuits were attached on the base structure, and were connected with each segment of PZT nearby. As shown in Fig. 80, the LEDs are on when the base structure is vibrating. Next, the wireless sensor node with analog temperature sensor, wireless sender and wireless receiver, and the monitoring system (USB connection for the receiver to a PC) was used for demonstration. The temperature sensor node requires 5.3V for initiating and 2.7V for data transmitting.   It requires about 15μW for continuous temperature monitoring [133]. We connected the temperature sensor with one PZT segment and confirmed that the segment can harvest enough power to operate the temperature sensor node.
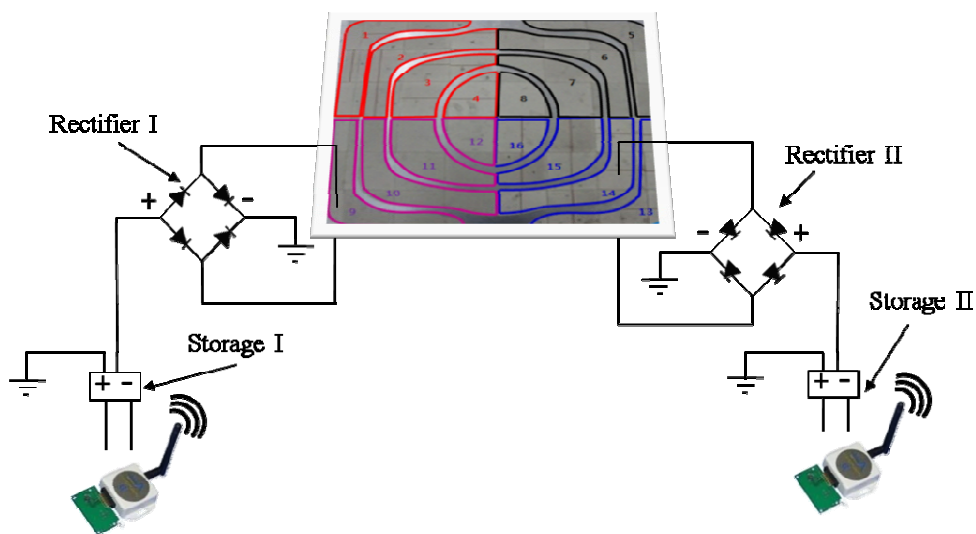
Fig. 79. Configuration of electric circuits for the EH skin demonstration

| (a) Operation of LEDs | (b) Operation of wireless sensor nodes |
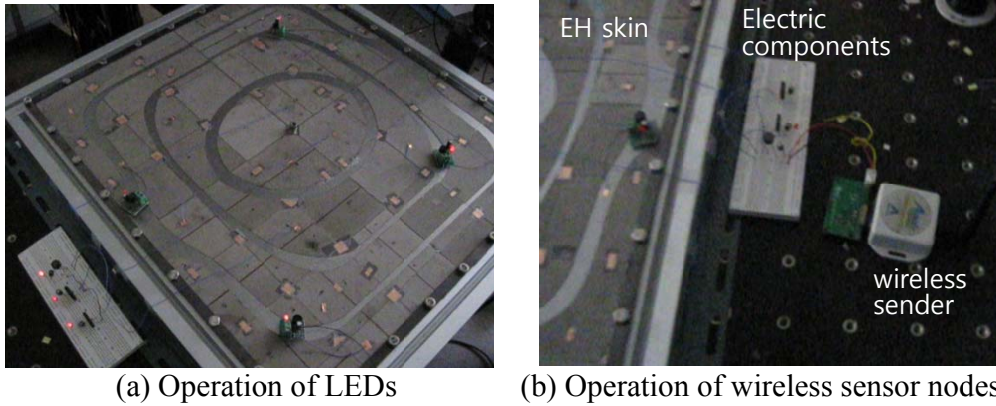
Fig. 80. Demonstration of the EH skin with LEDs and a wireless sensor node

4.5.6 Discussion

This case study built the computational model using the statistical model validation to design a robust and reliable EH device. The validation framework consists of two hierarchical levels: (i) top level: electrical response and (ii) bottom level: mechanical response. Statistical model calibration was employed with predicted and observed results at each hierarchy. The statistics of unknown model variables, s_{11}, d_{31}, and ε_{33}, were found and applied to the computational model of the EH skin. The EH skin was designed and manufactured to maximize harvestable power while considering the voltage cancellation effect. It is found that the PZT patch can be precisely cut using the laser cutting device with an appropriate speed and power level of the device. The voltage of each PZT segment was measured for the validity check of the computational model. Some voltage levels were lower than predicted results due to the imperfect bonding condition of the PZT patches. To verify the reason of voltage drop, measuring the dynamic strain and comparing with the predicted results can be considered as a future study. Despite this voltage drop, a

138

significant power level has been achieved. This case study illustrates the greater capabilities of the EH skin from three primary perspectives as:

(1) A framework of building the statistical model of the EH skin to design robust and reliability EH skin while considering variability in materials.

(2) Sustainable and relatively high power generation to operate low-power electronics, such as wireless sensors used for health monitoring of engineered systems in plant, airplane, or ground transportation [134] and/or building automation.

(3) Compact design to require no need of fixture and proof-mass.

Chapter 5: Contributions and Future Works

5.1 Principle Contributions and Significances

This dissertation presented a hierarchical framework for statistical model validation and conducted a feasibility study of the framework with various industrial problems. The contributions made through this study can be summarized as:

(1) With the help of commercial FE software and high computational power, simulation engineers can easily develop sophisticated computational models and carry out virtual testing for an efficient system development. However, the predictive capability of a computational model has been a grand challenge for use in the product development process since there is no generic validation framework in a statistical sense. This dissertation research thus aims at developing a generic model validation framework so that it offers a standard guideline to simulation engineers (or validation engineers) for improving the predictive capability of computational models. It is shown that the proposed hierarchical model validation framework plays a great role in doing so. Model validation planning allows analysts to systematically decompose a computational model while identifying the PoIs, required experiments and model input variables. This strategic planning facilitates the execution of the model validation successfully for an engineered system with a large number of unknown model input variables. Various statistical techniques have been integrated into the model validation execution at every decomposed level so as to improve and assess the predictive capability of computational models of engineered products. The increased confidence in the computational model and reduction of conflict between predicted

and experimental results can significantly save on the cost and time of developing new computational models of engineered systems.

(2) A good agreement between the computational and experimental results could mislead design engineers unless the agreement is made in a statistical sense. This dissertation developed a statistical model calibration technique to improve the predictive capability of computational models under various sources and types of variability and/or uncertainty.

(3) In the model validation process, it is unrealistic to manufacture many prototypes for the validation experiments due to expensive manufacturing cost. In this dissertation, a validity check engine named the hypothesis test for validity check is developed to overcome this challenge of limited experimental data. The hypothesis test for the validity check can give a clear guideline to accept (or reject) computational models while considering uncertainty in the validity check metric, and help utilize limited experimental data measured at different operating conditions for the validity check. In addition, statistical fidelity evaluation can increase a confidence level about a computational model and significantly save the cost and time in developing new computational models.

(4) Virtual qualification will be a great addition to the existing system development capability. This enhanced capability such as absolute qualification, relative qualification and reliability-based design optimization enables design engineers to explore various design alternatives in an efficient manner. It can also promote the knowledge base of system design engineers and analysts along with plenty of simulation model database.

(5) The feasibility of the framework has been successfully demonstrated with five engineering problems having different computational models, experimental resources, analysis types, and PoIs. The model validation activity has been executed by fully or partially implementing the proposed statistical techniques. Although this feasibility study is somewhat limited, it shows that the framework is likely applicable to diverse classes of engineering problems with uncertainties in computational models and experimental data.

5.2 Recommended Future Researches

Although the proposed research solutions in this dissertation have addressed critical challenges in model validation, it is still a grand challenge to promote a generic model validation methodology. Continuous researches and technical developments are needed to make the model validation framework feasible and effective. The rest of this section presents possible future researches needed to improve the proposed model validation framework.

1. The experimental errors such as random and bias errors were not quantified in the calibration process. In practice, it is not feasible to find a true computational model through the model calibration procedure because the unknown errors are highly dependent on the current knowledge of experimental researchers or the quality of experimental devices. For example, it is impossible to obtain the experimental random error in the case of destructive testing such as 3-point bending failure and dent failure test.

2. The choice of the calibration model (Eqs. (1)-(3)) should be problem-dependent. If prior knowledge of a model error form (e.g. linear form or nonlinear form) is given,

it is beneficial to consider the model error (e) in the calibration process; however, in many cases it is not easy to figure out the model error form before the model calibration. Should the inappropriate model error form be used in the model calibration process, the calibrated model can be severely misrepresented. To eliminate risk associated with the unknown model form, model error is ignored in this dissertation. A method to extract the appropriate model error in the calibration process will be further investigated.

3. In this dissertation, the distribution type candidates of unknown model variables were decided based on the best of the experts' knowledge. The effect of different distribution types on model validation results needs to be further studied. In addition, a guideline of deciding unknown random variables among many model input variables needs to be developed.

4. A situation in which "component" and "subsystem" data are available but "system" data are not, or vice versa frequently occurs in the model validation process of engineered systems. To address this situation, a systematic validation process to allocate validation resources including experiments needs to be further developed.

5. A statistical table that considering a significance level, a number of experimental data, low and upper bounds of area metric needs to be provided as a reference for validity evaluation, so that engineers in various fields can easily perform the proposed hypothesis test for validity check.

References

[1] AIAA, "Guide for the verification and validation of computational fluid dynamic simulations," American Institute of Aeronautics and Astronautics, Guide G-077-98, 1998.

[2] ASME, P. T. C., "Guide for Verification and Validation in Computational Solid Mechanics," 2006, ASME, New York, NY.

[3] Oberkampf, W. L. and Trucano, T. G., 2002, "Verification and validation in computational fluid dynamics," Progress in Aerospace Sciences, Vol.38, No.3, pp.209-272.

[4] Thacker, B. H., et al., 2004, "Concepts of Model Verification and Validation," LA-14167, Los Alamos National Lab., Los Alamos, NM (US).

[5] Logan, R. W. and Nitta, C. K., 2002, "Verification & validation (V&V) methodology and quantitative reliability at confidence (QRC): basis for an investment strategy," Lawrence Livermore National Laboratory, UCRL-ID-150874, Vol.12, pp. 30.

[6] Babuska, I. and Oden, J. T., 2004, "Verification and validation in computational engineering and science: basic concepts," Computer Methods in Applied Mechanics and Engineering, Vol.193, No.36-38, pp.4057-4066.

[7] Oberkampf, W. L., 2006, "What are validation experiments?," Experimental Techniques, Vol.25, No.3, pp.35-40.

[8] Kaner, C., Falk, J. L., and Nguyen, H. Q., 1999, Testing computer software, John Wiley & Sons, Inc. New York, NY, USA.

[9] Roache, P. J., 1998, "Verification of codes and calculations," AIAA journal, Vol.36, No.5, pp.696-702.

[10] Oberkampf, W. L. and Barone, M. F., 2006, "Measures of agreement between computation and experiment: validation metrics," Journal of Computational Physics, Vol.217, No.1, pp.5-36.

[11] Ferson, S., Oberkampf, W. L., and Ginzburg, L., 2008, "Model validation and predictive capability for the thermal challenge problem," Computer Methods in Applied Mechanics and Engineering, Vol.197, No.29-32, pp.2408-2430.

[12] Rebba, R. and Cafeo, J., 2008, "Probabilistic analysis of a static frame model," Computer Methods in Applied Mechanics and Engineering, Vol.197, No.29-32, pp.2561-2571.

[13] Cho, J. C. and Jung, B. C., 2007, "Prediction of tread pattern wear by an explicit finite element model," Tire science and Technology, Vol.35, No.4, pp.276-299.

[14] Datta, B. N., 2005, "Finite element model updating and partial eigenvalue assignment in structural dynamics: recent developments on computational methods," Mathematical Modeling and Analysis, pp. 15-27.

[15] Modarres, M., Kaminskiy, M., and Krivtsov, V., 1999, "Reliability engineering and risk analysis: a practical guide," CRC Press.

[16] Hills, R. G., Dowding, K. J., and Swiler, L., 2008, "Thermal challenge problem: Summary," Computer Methods in Applied Mechanics and Engineering, Vol.197, No.29-32, pp.2490-2495.

[17] Brandyberry, M. D., 2008, "Thermal problem solution using a surrogate model clustering technique," Computer Methods in Applied Mechanics and Engineering, Vol.197, No.29-32, pp.2390-2407.

[18] Higdon, D., et al., 2008, "A Bayesian calibration approach to the thermal problem," Computer Methods in Applied Mechanics and Engineering, Vol.197, No.29-32, pp.2431-2441.

[19] Hills, R. G. and Dowding, K. J., 2008, "Multivariate approach to the thermal challenge problem," Computer Methods in Applied Mechanics and Engineering, Vol.197, No.29-32, pp.2442-2456.

[20] Liu, F., et al., 2008, "A Bayesian analysis of the thermal challenge problem," Computer Methods in Applied Mechanics and Engineering, Vol.197, No.29-32, pp.2457-2466.

[21] McFarland, J. and Mahadevan, S., 2008, "Multivariate significance testing and model calibration under uncertainty," Computer Methods in Applied Mechanics and Engineering, Vol.197, No.29-32, pp.2467-2479.

[22] Rutherford, B. M., 2008, "Computational modeling issues and methods for the regulatory problem in engineering Solution to the thermal problem," Computer Methods in Applied Mechanics and Engineering, Vol.197, No.29-32, pp.2480-2489.

[23] Babuska, I. and Tempone, R., 2008, "Static frame challenge problem: Summary," Computer Methods in Applied Mechanics and Engineering, Vol.197, No.29-32, pp.2572-2577.

[24] Chleboun, J., 2008, "An approach to the Sandia workshop static frame challenge problem: A combination of elementary probabilistic, fuzzy set, and worst scenario tools," Computer Methods in Applied Mechanics and Engineering, Vol.197, No.29-32, pp. 2500-2516.

[25] Babuska, I., Nobile, F., and Tempone, R., 2008, "A systematic approach to model validation based on Bayesian updates and prediction related rejection criteria," Computer Methods in Applied Mechanics and Engineering, Vol.197, No.29-32, pp.2517-2539.

[26] Grigoriu, M. D. and Field, R. V., 2008, "A solution to the static frame validation challenge problem using Bayesian model selection," Computer Methods in Applied Mechanics and Engineering, Vol.197, No.29-32, pp.2540-2549.

[27] Pradlwarter, H. J. and Schueller, G. I., 2008, "The use of kernel densities and confidence intervals to cope with insufficient data in validation experiments," Computer Methods in Applied Mechanics and Engineering, Vol.197, No.29-32, pp.2550-2560.

[28] Paez, T. L. and Red-Horse, J., 2008, "Structural Dynamics Challenge Problem: Summary," Computer Methods in Applied Mechanics and Engineering, Vol.197, No.29-32, pp.2660-2665.

[29] Ghanem, R. G., Doostan, A., and Red-Horse, J., 2008, "A probabilistic construction of model validation," Computer Methods in Applied Mechanics and Engineering, Vol.197, No.29-32, pp.2585-2595.

[30] Hasselman, T. and Lloyd, G., 2008, "A top-down approach to calibration, validation, uncertainty quantification and predictive accuracy assessment," Computer Methods in Applied Mechanics and Engineering, Vol.197, No.29-32, pp.2596-2606.

[31] Horta, L. G., et al., 2008, "NASA Langley's approach to the Sandia's structural dynamics challenge problem," Computer Methods in Applied Mechanics and Engineering, Vol.197, No.29-32, pp. 2607-2620.

[32] McFarland, J. and Mahadevan, S., 2008, "Error and variability characterization in structural dynamics modeling," Computer Methods in Applied Mechanics and Engineering, Vol.197, No.29-32, pp.2621-2631.

[33] Zang, C., Schwingshackl, C. W., and Ewins, D. J., 2008, "Model validation for structural dynamic analysis: An approach to the Sandia Structural Dynamics Challenge," Computer Methods in Applied Mechanics and Engineering, Vol.197, No.29-32, pp.2645-2659.

[34] Campbell, K., 2006, "Statistical calibration of computer simulations," Reliability Engineering and System Safety, Vol.91, No.10-11, pp.1358-1363.

[35] Xiong, Y., et al., 2009, "A better understanding of model updating strategies in validating engineering models," Computer Methods in Applied Mechanics and Engineering, Vol.198, No.15-16, pp.1327-1337.

[36] Calvi, A., 2005, "Uncertainty-based loads analysis for spacecraft: Finite element model validation and dynamic responses," Computers and Structures, Vol.83, No.14, pp.1103-1112.

[37] Kennedy, M. C. and O'Hagan, A., 2001, "Bayesian calibration of computer models," Journal of the Royal Statistical Society, Series B, Statistical Methodology, pp.425-464.

[38] Bayarri, M. J., et al., 2007, "A framework for validation of computer models," Technometrics, Vol.49, No.2, pp.138-154.

[39] Higdon, D., et al., 2004, "Combining field data and computer simulations for calibration and prediction," SIAM Journal on Scientific Computing, Vol.26, pp.448-466.

[40] Apley, D. W., Liu, J., and Chen, W., 2006, "Understanding the effects of model uncertainty in robust design with computer experiments," Journal of Mechanical Design, Vol.128, pp.945.

[41] Fonseca, J. R., et al., 2005, "Uncertainty identification by the maximum likelihood method," Journal of Sound and Vibration, Vol.288, No.3, pp.587-599.

[42] Kleijnen, J. P. C., 1986, "Statistical tools for simulation practitioners," Marcel Dekker, New York, NY.

[43] Gep, B., Hunter, W. G., and Hunter, J. S., 2005, "Statistics for Experimenters: Design, Innovation and Discovery," Wiley Series in Probability and Statistics, Second edition. Hoboken, New Yersey, USA.

[44] Sacks, J., et al., 1989, "Design and analysis of computer experiments," Statistical science, Vol.4, No.4, pp.409-423.

[45] Montgomery, D. C., 2001, "Design and analysis of experiments," John Wiley & Sons. Inc., New York.

[46] Welch, W. J., et al., 1992, "Screening, predicting, and computer experiments," Technometrics, Vol.34, No.1, pp.15-25.

[47] Morris, M. D., Mitchell, T. J., and Ylvisaker, D., 1993, "Bayesian design and analysis of computer experiments: use of derivatives in surface prediction," Technometrics, Vol.35, No.3, pp.243-255.

[48] Youn, B.D., et al., 2011, "A hierarchical framework for statistical model calibration in engineering product development," Computer Methods in Applied Mechanics and Engineering, Vol.200, No.13-16, pp.1421-1431.

[49] Varghese, P. and Braswell, N., 1996, "Statistical tolerance analysis using FRPDF and numerical convolution," Computer-Aided Design, Vol.28, No.9, pp.723-732.

[50] Lin, C. Y., et al., 1997, "Study of an assembly tolerance allocation model based on Monte Carlo simulation," Journal of Materials Processing Technology, Vol.70, No.1, pp.9-16.

[51] Sobol, I. M., 1998, "On quasi-Monte Carlo integrations," Mathematics and Computers in Simulation, Vol.47, No.2-5, pp.103-112.

[52] Wu, Y. T., 1994, "Computational methods for efficient structural reliability and reliability sensitivity analysis," AIAA journal, Vol.32, No.8, pp.1717-1723.

[53] Bjerager, P., 1988, "Probability integration by directional simulation," Journal of Engineering Mechanics, Vol.114, No.8, pp.1288-1302.

[54] Do Hyun Jung, B. C. L., 2002, "Development of a simple and efficient method for robust optimization," International Journal for Numerical Methods in Engineering, Vol.53, No.9, pp.2201-2215.

[55] Rahman, S. and Rao, B. N., 2001, "A perturbation method for stochastic meshless analysis in elastostatics," International Journal for Numerical Method in Engineering, Vol.50, pp.1961-1991.

[56] Yamazaki, F., Shinozuka, M., and Dasgupta, G., 1988, "Neumann expansion for stochastic finite-element analysis," Journal of Engineering Mechanics, Vol.114, No.8, pp.1335-1354.

[57] Simpson, T. W., et al., 2001, "Kriging models for global approximation in simulation-based multidisciplinary design optimization," AIAA journal, Vol.39, No.12, pp.2233-2241.

[58] Friedman, J. H., 1991, "Multivariate adaptive regression splines," The annals of statistics, Vol.19, No.1, pp.1-67.

[59] Wang, G. G. and Shan, S., 2007, "Review of metamodeling techniques in support of engineering design optimization," Journal of Mechanical Design, Vol.129, pp.370.

[60] Fang, H. and Horstemeyer, M. F., 2006, "Global response approximation with radial basis functions," Engineering Optimization, Vol.38, No.4, pp.407-424.

[61] Mullur, A. A. and Messac, A., 2005, "Extended radial basis functions: more flexible and effective metamodeling," AIAA journal, Vol.43, No.6, pp.1306-1315.

[62] Jin, R., Chen, W., and Simpson, T. W., 2001, "Comparative studies of metamodelling techniques under multiple modelling criteria," Structural and Multidisciplinary Optimization, Vol.23, No.1, pp.1-13.

[63] Clarke, S. M., Griebsch, J. H., and Simpson, T. W., 2005, "Analysis of support vector regression for approximation of complex engineering analyses," Journal of Mechanical Design, Vol.127, pp.1077.

[64] Rahman, S. and Xu, H., 2004, "A univariate dimension-reduction method for multi-dimensional integration in stochastic mechanics," Probabilistic Engineering Mechanics, Vol.19, No.4, pp.393-408.

[65] Youn, B. D., Choi, K. K., and Yi, K., 2005, "Performance moment integration (PMI) method for quality assessment in reliability-based robust design optimization," Mechanics Based Design of Structures and Machines, Vol.33, No.2, pp.185-213.

[66] Xu, H. and Rahman, S., 2004, "A generalized dimension-reduction method for multi-dimensional integration in stochastic mechanics," International Journal for Numerical Method in Engineering, Vol.61, pp.1992-2019.

[67] Rao, M. D., 2003, "Recent Applications of Viscoelastic Damping for Noise Control in Automobiles and Commercial Airplanes," Journal of Sound and Vibration, Vol.262, No.3, pp.457-474. doi:10.1016/S0022-460X(03)00106-8

[68] Wins, D. J., Modal Testing: Theory, Practice and Application, Research Studies Press, Bal dock, Hertfordshire, UK, 2000.

[69] Lall, A. K., Nakra, B. C., and Asnani, N. T., 1983, "Optimum Design of Viscoelastically Damped Sandwich Panels," Engineering Optimization, Vol.6, No. 4, pp.197-205.

[70] Lifshitz, J. M., and Leibowitz, M., 1987, "Optimal Sandwich Beam Design for Maximum Viscoelastic Damping," International Journal of Solids and Structures, Vol.23, No.7, pp.1027-1034.

[71] Marcelin, J. L., Trompette, P., and Smatic, A., 1992, "Optimal Constrained Layer Damping with Partial Coverage," Finite Elements in Analysis and Design, Vol.12, No.3, pp.273-280.

[72] Baz, A., and Ro, J., 1995, "Optimum Design and Control of Active Constrained Layer Damping," Journal of Mechanical Design, Vol.117, No.2, pp.135-144. doi:10.1115/1.2836447.

151

[73] Nakra, B. C., 1998, "Vibration Control in Machines and Structures Using Viscoelastic Damping," Journal of Sound and Vibration, Vol.211, No.3, pp.449-465.

[74] Zheng, H., Cai, C., and Tan, X. M., 2004, "Optimization of Partial Constrained Layer Damping Treatment for Vibrational Energy Minimization of Vibrating Beams," Computers and Structures, Vol.82, Nos.29-30, pp.2493-2570. doi:10.1016/j. compstruc.2004.07.002

[75] Kim, T. W., and Kim, J. H., 2004, "Eigensensitivity Based Optimal Distribution of a Viscoelastic Damping Layer for a Flexible Beam," Journal of Sound and Vibration, Vol.273, Nos.1-2, pp.201-218. doi:10.1016/S0022-460X(03)00479-6

[76] Zheng, H., and Cai, C., 2004, "Minimization of Sound Radiation from Baffled Beams Through Optimization of Partial Constrained Layer Damping Treatment," Applied Acoustics, Vol.65, No.5, pp.501-520. doi:10.1016/j.apacoust. 2003.11.008.

[77] Lee, D. H., 2008, "Optimal Placement of a Constrained-Layer Damping for Reduction of Interior Noise," AIAA Journal, Vol.46, No.1, pp.75-83. doi:10.2514/1.30648.

[78] Lee, D. H., and Hwang, W. S., 2004, "Layout Optimization of an Unconstrained Viscoelastic Layer on Beams Using Fractional Derivative Model," AIAA Journal, Vol.42, No.10, pp.2167-2170. doi:10.2514/1.7482.

[79] Kareem, A., and Sun, W. J., 1990, "Dynamic response of structures with uncertain damping," Engineering Structures, Vol.12, pp.2-8.

[80] Kareem, A., and Gurley, K., 1996, "Damping in structures: its evaluation and treatment of uncertainty," Journal of Wind Engineering and Industrial Aerodynamics, Vol.59, Nos.2-3, pp.131-157. doi:10.1016/0167-6105(96)00004-9.

[81] Li, J., and Chen, J., 2005, "Dynamic response and reliability analysis of structures with uncertain parameters," Internal Journal for Numerical Method in Engineering, Vol.62, No.1, pp.289-315. doi:10.1002/nme.1204.

[82] Soize, C., 2005, "A comprehensive overview of a non-parametric probabilistic approach of model uncertainties for predictive models in structural dynamics," Journal of Sound and Vibration, Vol.288, No.3, pp. 623-652. doi:10.1016/j.jsv. 2005.07.009.

[83] ITP sensors and automation: Low-cost vibration power harvesting for wireless sensors. [cited 2011 5 May]; Available from: http://www1.eere.energy.gov/ industry/ sensors_automation/pdfs/kcf_vibrationpower.pdf.

[84] Glynne-Fones, P., and White, N.M., 2001, "Self-powered Systems: A review of Energy Sources," Sensor Review, Vol.21, pp. 91-97.

[85] Paradiso, J. A., and Starner, T., 2005, "Energy Scavenging for Mobile and Wireless Elctronics," IEEE Pervasive Computing, Vol. 4, No. 1, pp. 18-27.

[86] Roundy, S, Wright, P. K. and Rabaey, J. M., 2005, "Energy scavenging for wireless sensor networks: With special focus on vibrations," Springer.

[87] Glynne-Jones, P., Beeby, S. P. and White, N. M., 2001, "Towards a piezoelectric vibration-powered microgenerator," IEE Science, Measurement and Technology, Vol.148, No.2, pp.68-72.

[88] Sterken, T., Baert, K., Van Hoof, C., Puers, R., Borghs, G., Fiorini, P., Mcp, I. and Leuven, B., 2004, "Comparative modelling for vibration scavengers," Proc. IEEE Sensors.

[89] Silk, M. G., 1984, "Ultrasonic transducers for nondestructive testing," Adem Hilger Ltd.

[90] Leland, E. S., Lai, E. M. and Wright, P. K., 2004, "A self-powered wireless sensor for indoor environmental monitoring," Proc. WNCG Conference, Austin, TX.

[91] Roundy, S., Wright, P. K. and Rabaey, J., 2003, "A study of low level vibrations as a power source for wireless sensor nodes," Computer Communications, Vol.26, No.11, pp.1131-44.

[92] Sodano, H. A., Park, G. and Inman, D. J., 2004, "Estimation of electric charge output for piezoelectric energy harvesting," Strain, Vol.40, No.2, pp.49-58.

[93] Chen, S. N., Wang, G. J. and Chien, M. C., 2006, "Analytical modeling of piezoelectric vibration-induced micro power generator," Mechatronics, Vol.16, No.7, pp.379-87.

[94] Elvin, N., Elvin, A. and Choi, D. H., 2003, "A self-powered damage detection sensor," The Journal of Strain Analysis for Engineering Design, Vol.38, No.2, pp.115-24.

[95] Goldschmidtboeing, F. and Woias, P., 2008, "Characterization of different beam shapes for piezoelectric energy harvesting," Journal of Micromechanics and Microengineering, Vol.18m No.10, pp.104013.

[96] Roundy, S., Leland, E. S., Baker, J., Carleton, E., Reilly, E., Lai, E., Otis, B., Rabaey, J. M., Wright, P. K. and Sundararajan, V., 2005, "Improving power output for vibration-based energy scavengers," IEEE Pervasive Computing, Vol.4, No.1, pp.28-36.

[97] Zheng, B., Chang, C. and Gea, H. C., 2007, "Topology optimization for piezoelectric energy harvesting devices," Proc. 7th WCSMO Conference, Seoul, Korea.

[98] Umeda, M., Nakamura, K. and Ueha, S., 1997, "Energy storage characteristics of a piezo-generator using impact induced vibration," Japanese Journal of Applied Physics, Vol.36, pp.3146-51.

[99] Sodano, H. A., Inman, D. J. and Park, G., 2005, "Generation and storage of electricity from power harvesting devices," Journal of Intelligent Material Systems and Structures, Vol.16, No.1, pp.67.

[100] Sodano, H. A., Inman, D. J. and Park, G., 2005, "Comparison of piezoelectric energy harvesting devices for recharging batteries," Journal of Intelligent Material Systems and Structures, Vol.16, No.10, pp.799.

[101] Sodano, H. A., Lloyd, J. and Inman, D. J., 2006, "An experimental comparison between several active composite actuators for power generation," Smart Materials and Structures, Vol.15, No.5, pp.1211-6.

[102] Granstrom, J., Feenstra, J., Sodano, H. A. and Farinholt, K., 2007, "Energy harvesting from a backpack instrumented with piezoelectric shoulder straps," Smart Materials and Structures, Vol.16, No.5, pp.1810-20.

[103] Analog temperature sensor. [cited 2011 5 May]; Available from: http://www.ambiosystems.com/index.php/Sensors/Analog-temperature-sensor/Detailed-product-flyer.html.

[104] Shenck, N. S. and Paradiso, J. A., 2001, "Energy scavenging with shoe-mounted piezoelectrics," IEEE Micro, Vol.21, No.3, pp.30-42.

[105] Mateu, L. and Moll, F., 2005, "Optimum piezoelectric bending beam structures for energy harvesting using shoe inserts," Journal of Intelligent Materials and System Structures, Vol.16, No.10, pp.835.

[106] Anton, S. R. and Sodano, H. A., 2007, "A review of power harvesting using piezoelectric materials (2003-2006)," Smart Materials and Structures, Vol.16, No.3, pp.1

[107] Sodano, H. A., Inman, D. J. and Park, G., 2004, "A review of power harvesting from vibration using piezoelectric materials," The Shock and Vibration Digest, Vol.36, No.3, pp.197.

[108] Shen, D., S.Y. Choe, and D.J. Kim, 2007, "Analysis of Piezoelectric Materials for Energy Harvesting Devices under High-g Vibrations," Japanese Journal of Applied Physics, Vol.46, pp.6755-6760.

[109] Lefeuvre, E., Badel, A., Richard, C., and Guyomar, D., 2007, "Energy Harvesting using Piezoelectric materials: Case of random vibrations," Journal of Electroceramics, Vol.19, pp.349-355.

[110] Adhikari, S., Friswell, M. I., and Inman, D. J., 2009, "Piezoelectric energy harvesting from broadband random vibrations," Smart Materials and Structures, Vol.18, pp.115005.

[111] Soliman, M. S. M., Abdel-Rahman, E. M., and El-Saadany, E. F., 2008, "A wideband vibration-based energy harvester," Journal of Micromechanics and Microengineering, Vol.18, pp.115021

[112] Ottman, G.K., et al., 2002, "Adaptive piezoelectric energy harvesting circuit for wireless remote power supply," IEEE Transactions on Power Electronics, Vol.17, No.5, pp.669-676.

[113] Ottman, G.K., H.F. Hofmann, and G.A. Lesieutre, 2003, "Optimized piezoelectric energy harvesting circuit using step-down converter in discontinuous conduction mode," IEEE Transactions on Power Electronics, Vol.18, No.2, pp. 696-703.

[114] Der Kiureghian, A. and Ke, J. B., 1988, "The stochastic finite element method in structural reliability," Probabilistic Engineering Mechanics, Vol.3, No.2, pp.83-91.

[115] Grigoriu, M., 1983, "Stochastic Finite Element Analysis of Simple Beams," Journal of Engineering Mechanics, Vol.109, pp.1203.

[116] Liu, W. K., Belytschko, T., and Mani, A., 1986, "Random field finite elements," International Journal for Numerical Methods in Engineering, Vol.23, No.10, pp.1831-1845.

156

[117] Turk, M. and Pentland, A., 1991, "Eigenfaces for recognition," Journal of cognitive neuroscience, Vol.3, No.1, pp.71-86.

[118] Missoum, S., 2008, "Probabilistic optimal design in the presence of random fields," Structural and Multidisciplinary Optimization, Vol.35, No.6, pp.523-530.

[119] Youn, B. D. and Xi, Z., "An Effective Random Field Characterization for Probability Analysis and Design," Proceedings of 49th AIAA/ASME/ASCE/AHS/ASC Structures, Structural Dynamics, and Materials Conference, April, 2008, Schaumburg, IL.

[120] Buranathiti, T., et al., 2006, "Approaches for model validation: methodology and illustration on a sheet metal flanging process," Journal of Manufacturing Science and Engineering, Vol.128, pp.588.

[121] Angus, J. E., 1994, "The Probability Integral Transform and Related Results," Society for Industrial and Applied Mathematics Review, Vol.36, No. 4, pp.652-654.

[122] Youn, B. D., Xi, Z., and Wang, P., "The Eigenvector dimension-reduction (EDR) method for sensitivity-free uncertainty quantification," Structural and Multidisciplinary Optimization, doi:10.1007/s00158-007-0210-7.

[123] Cho, J. C. and Jung, B. C. Jung, "Prediction of Tread Pattern Wear by Explicit FEM," 25th Annual Meeting and Conference on Tire Science and Technology, Akron, Ohio, USA, Sep. 2006.

[124] Hofstetter, K., et al., 2006, "Sliding behaviour of simplified tire tread patterns investigated by means of FEM," Computers and Structures, Vol.84, No.17-18, pp.1151-1163.

[125] Dowding, K. J., Pilch, M., and Hills, R. G., 2008, "Formulation of the thermal problem," Computer Methods in Applied Mechanics and Engineering, Vol.197, No.29-32, pp.2385-2389.

[126] Eldred, L. B., Baker and, W. P., Palazotto A. N., 1995, "Kelvin-voigt vs. fractional derivative model as constitutive relations for viscoelastic material," AIAA Journal, Vol.33, pp.547-550.

[127] Jung, B. C., Lee, D. H. and Youn, B. D., 2009, "Optimal Design of Constrained-Layer Damping Structures Considering Material and Operational Condition Variability," AIAA Journal, Vol. 47, No. 12, pp. 2985-2995.

[128] Lee, S. and Youn, B., 2011, "Designing Energy Harvesting Skin Structure Utilizing Outdoor Unit Vibration," Smart Materials and Structures, Vol.20, pp.057001.

[129] Lee, S. and Youn, B., 2011, "A New Piezoelectric Energy Harvesting Design Concept; Multimodal Energy Harvesting Skin," IEEE Transactions on Ultrasonics, Ferroelectrics, and Frequency Control, Vol.58, No.3, pp.629-645.

[130] Piezo systems product catalog. (cited 2011 40 April) Available from http://www.piezo.com/prodbg1brass.html.

[131] Roundy S. and Wright P.K., 2004, "A piezoelectric vibration based generator for wireless electronics," Smart Materials and Structures, Vol.13, pp.1131-1142.

[132] Analog temperature sensor. [cited 2011 6 May]; Available from: http://www.ambiosystems.com/index.php/Sensors/Analog-temperature-sensor/Detailed-product-flyer.html.

[133] Lee, S., Youn, B.D., and Jung, B.C., 2009, "Robust segment-type energy harvester and its application to a wireless sensor," Smart Materials and Structures, Vol.18, pp.095021.

[134] Analog temperature sensor. [cited 2011 6 May]; Available from: http://www.ambiosystems.com/index.php/Sensors/Analog-temperature-sensor/Detailed-product-flyer.html.